Identification of Novel Components in a cGMP-dependent Signaling Pathway Mediating Sensory Axon Bifurcation

Dissertation

der Mathematisch-Naturwissenschaftlichen Fakultät

der Eberhard Karls Universität Tübingen

zur Erlangung des Grades eines

Doktors der Naturwissenschaften

(Dr. rer. nat.)

vorgelegt von

Alexandra Lisa Martina Böttcher

aus Friedrichshafen

Tübingen

2023

Gedruckt mit Genehmigung der Mathematisch-Naturwissenschaftlichen Fakultät der Eberhard Karls Universität Tübingen.

Tag der mündlichen Qualifikation:	19.03.2024
Dekan:	Prof. Dr. Thilo Stehle
1. Berichterstatter/-in:	PD Dr. Hannes Schmidt
2. Berichterstatter/-in:	Prof. Dr. Robert Feil
3. Berichterstatter/-in:	PD Dr. Andrea Wizenmann

ABSTRACT

Axonal branching mechanisms play a critical role in establishing neuronal circuitry that is the basis for a functional nervous system. A cyclic guanosine monophosphate (cGMP)-dependent signaling pathway mediates axon bifurcation in murine somatosensory neurons. Known parts of this cascade are the extracellular ligand C-type natriuretic peptide (CNP), which binds its transmembrane receptor guanylyl cyclase B (GC-B) thus activating the production of the second messenger cGMP, which in turn activates its effector, the cGMP-dependent kinase I (cGKI). Other components that are essential for the process of axon bifurcation remain elusive. This work aimed to uncover novel putative cGKI substrates and GC-B interactors to gain better mechanistic understanding of the axon bifurcation process. The identification of such components could also provide a basis for new pharmacological approaches given the importance of cGMP-dependent signaling pathways in health and disease.

A mass-spectrometric (MS) phosphoproteome analysis was performed on the murine melanoma cell line B16F10 as well as on embryonic dorsal root ganglion (DRG) tissue after stimulation of cGKI activity with 8Br-cGMP and CNP, respectively. Both analyses lead to the discovery of many significantly regulated phosphorylation sites on putative direct or indirect cGKI substrates. Seven candidates were detected in both screening experiments: apoptotic chromatin condensation inducer in the nucleus (Acin1), glutamine-dependent carbamoyl-phosphate synthase-aspartate carbamoyltransferase-dihydroorotase fusion protein (Cad), cytoplasmic linker protein-associating protein 1 (Clasp1), collapsin response mediator protein 1 (Crmp1), microtubule-associated protein 1B (Map1b), mammalian enabled protein (Mena), and E3 ubiquitin-protein ligase NEDD4-like (Nedd4l).

The transcription of these cGKI substrate candidates was shown in both B16F10 cells and embryonic DRG tissue by RT-PCR. For Acin1, Clasp1, Crmp1, Map1b, and Mena, an expression analysis was performed to investigate the subcellular location in DRG cells as well as the tissue distribution pattern of these candidates. Acin1 showed only a minor presence outside of nuclei and could be found ubiquitously in the analyzed transversal embryo sections. The other candidates were present mostly in the cytosolic fraction, coinciding with cGKI; and to a smaller extent in the membrane fraction, coinciding with GC-B. Immunostaining of transversal embryo sections revealed the location of these four candidates in somata and axons of DRG neurons and some additional areas of the spinal cord, including the dorsal root entry zone (DREZ).

Aiming to verify the direct phosphorylation of Clasp1, Map1b, and Mena at the identified sites by cGKI, an analogue sensitive kinase (ASK) assay was performed on 3xFLAG-tagged constructs of the wildtype (WT) proteins as well as mutants with an alanine (A) substitution at the putatively modified serine (S) residue. An ASK-variant of cGKIα could modify WT Mena and to a significantly lesser extent MenaS637A. Consequently, Mena is a direct phosphorylation substrate of cGKI and S637 is among the modified sites. While results for Map1b remained inconclusive, phosphorylation of Clasp1 by cGKIα-ASK could be shown as well, although no preferential modification of Clasp1S646 was apparent.

cGKI can interact via an N-terminal leucine zipper (LZ) domain with certain substrates that likewise contain such a domain. This can lead to a more stable substrate binding than other transient interactions with phosphorylation targets. Axon tracing of a mouse model expressing a mutant variant of cGKIα with an altered LZ domain affecting substrate binding but not kinase activity led to the discovery of an impairment in sensory axon bifurcation. In mouse embryos of this genotype, merely 23% of all investigated DRG axons entering the DREZ exhibited bifurcation. The remaining 77% of DRG axons instead completed a turn to grow along the rostro-caudal axis of the spinal cord. While a deletion of cGKI would lead to a near absolute absence of bifurcation, the substantial reduction of growth cone splits caused by disruption of the LZ domain indicates the integral nature of interactions via this domain.

Tissue of a GC-B reporter mouse line with an N-terminal hemagglutinin tag was used for pull-down assays to analyze GC-B interactors that co-immunoprecipitated with this enzyme. An MS analysis was performed on heart tissue of adult mice as well as DRG tissue of embryos, both leading to the discovery

of putative GC-B interactors in the cytoskeletal compartment. While in heart tissue GC-B consistently interacted with a microtubule-associated protein, in DRG tissue significant interactions with four cytoskeleton-associated proteins as well as two tubulin monomer isoforms were detected. This suggests a function of GC-B as a possible anchoring point for cytoskeletal components and might be a starting point for uncovering a protein complex directing the cGMP-dependent signaling pathway in growth cones of somatosensory neurons to specific subcellular locations, thus mediating axon bifurcation.

Taken together, both phosphoproteomic screens for GKI substrates and interactome studies for GC-B have led to the identification of new components of the cGMP-dependent pathway, including several cytoskeleton-associated elements in DRG neurons. Some of the identified cGKI phosphorylation sites have yet to be verified in future research, and their involvement in the process of axon bifurcation needs to be studied. While none of the candidate cGKI substrates investigated here contain an LZ domain, such substrates seem to play a critical role *in vivo* and might be the subject of future research efforts. Furthermore, they or other proteins might provide a scaffold to link GC-B and cGKI. Considering the known role of cGMP-dependent pathways in many (patho-)physiological contexts, the discovery of novel putative cGKI substrates is of more general interest in the field of cGMP research even beyond the process of somatosensory axon bifurcation.

ZUSAMMENFASSUNG

Axonale Verzweigungsmechanismen spielen eine entscheidende Rolle beim Aufbau neuronaler Schaltkreise, die die Grundlage für ein funktionierendes Nervensystem bilden. Ein zyklisches Guanosinmonophosphat (cGMP) abhängiger Signalweg vermittelt die Axonverzweigung in somatosensorischen Neuronen der Maus. Bekannte Bestandteile dieser Kaskade sind der extrazelluläre Ligand C-Typ natriuretisches Peptid (CNP), der an seinen Transmembranrezeptor Guanylylzyklase B (GC-B) bindet und so die Produktion des sekundären Botenstoffs cGMP aktiviert, der seinen Effektor, die cGMP-abhängige Kinase I (cGKI), aktiviert. Weitere wesentliche Komponenten des Prozesses der Axonverzweigung sind noch nicht bekannt. Ziel dieser Arbeit war es, neue potenzielle cGKI-Substrate und GC-B-Interaktoren zu ermitteln, um ein besseres mechanistisches Verständnis des Axonverzweigungsprozesses zu erlangen. Die Identifizierung solcher Komponenten könnte außerdem eine Grundlage für neue pharmakologische Ansätze bilden angesichts der Bedeutung, die cGMP-abhängige Signalwege in der (Patho-)Physiologie haben.

Eine massenspektrometrische (MS) Phosphoproteomanalyse wurde an der murinen Melanomzelllinie B16F10 sowie an embryonalem DRG-Gewebe (dorsal root ganglion; Spinalganglion) nach Stimulation der cGKI-Aktivität mit 8Br-cGMP bzw. CNP durchgeführt. Beide Analysen führten zur Entdeckung vieler signifikant regulierter Phosphorylierungsstellen an potenziellen direkten oder indirekten cGKI-Substraten. Sieben Kandidaten wurden in beiden Screening-Experimenten entdeckt: “apoptotic chromatin condensation inducer in the nucleus” (Acin1), “glutamine-dependent carbamoyl-phosphate synthase-aspartate carbamoyltransferase-dihydroorotase fusion protein” (Cad), “cytoplasmic linker protein-associating protein 1” (Clasp1), “collapsin response mediator protein 1” (Crmp1), “microtubule-associated protein 1B” (Map1b), “mammalian enabled protein” (Mena), und “E3 ubiquitin-protein ligase NEDD4-like” (Nedd4l).

Die Transkription dieser cGKI-Substratkandidaten wurde sowohl in B16F10-Zellen als auch in embryonalem DRG-Gewebe durch RT-PCR nachgewiesen. Für Acin1, Clasp1, Crmp1, Map1b und Mena wurde eine Expressionsanalyse durchgeführt, um die subzelluläre Lokalisation in DRG-Zellen sowie das Verteilungsmuster dieser Kandidaten im Gewebe zu untersuchen. Acin1 zeigte nur eine geringe Präsenz außerhalb der Zellkerne und war in den analysierten transversalen Embryoschnitten ubiquitär vorhanden. Die anderen Kandidaten waren hauptsächlich in der zytosolischen Fraktion zu finden, was sich mit cGKI deckt, und in geringerem Maße in der Membranfraktion, in der GC-B vorliegt. Die Immunfärbung transversaler Embryoschnitte ergab, dass diese vier Kandidaten in Somata und Axonen von DRG-Neuronen und einigen zusätzlichen Bereichen des Rückenmarks, einschließlich der DREZ (dorsal root entry zone; Eintrittsort der Hinterwurzel in das Rückenmark), zu finden sind.

Um die direkte Phosphorylierung von Clasp1, Map1b und Mena an den identifizierten Stellen durch cGKI zu überprüfen, wurde ein analogsensitiver Kinase (ASK) Assay an 3xFLAG-markierten Konstrukten der Wildtyp (WT)-Proteine sowie an Mutanten mit einer Alanin (A)-Substitution an dem mutmaßlich modifizierten Serin (S)-Rest durchgeführt. Eine ASK-Variante von cGKIα konnte WT-Mena und in signifikant geringerem Ausmaß MenaS637A modifizieren. Folglich ist Mena ein direktes Phosphorylierungssubstrat von cGKI und S637 ist eine der modifizierten Stellen. Während die Ergebnisse für Map1b nicht schlüssig waren, konnte die Phosphorylierung von Clasp1 durch cGKIα-ASK ebenfalls nachgewiesen werden, wobei jedoch keine bevorzugte Modifikation von Clasp1-S646 erkennbar war.

cGKI kann über eine N-terminale Leuzin-Zipper (LZ)-Domäne mit bestimmten Substraten interagieren, die ebenfalls eine solche Domäne enthalten. Dies kann zu einer stabileren Substratbindung führen als bei anderen transienten Interaktionen mit Phosphorylierungszielen. "Axon Tracing" eines Mausmodells, bei dem cGKIα mit einer mutierten LZ-Domäne exprimiert wird, welche die Substratbindung, nicht aber die Kinaseaktivität beeinträchtigt, zeigte einen Verzweigungsfehler. In Mausembryonen dieses Genotyps wiesen lediglich 23% aller untersuchten DRG-Axone, die in die DREZ eintreten, eine Verzweigung auf. Die restlichen 77% der DRG-Axone vollzogen stattdessen eine Wendung, um entlang der rostro-

kaudalen Achse des Rückenmarks zu wachsen. Während eine Deletion von cGKI zu einem fast völligen Fehlen von Gabelungen führt, zeigt die erhebliche Reduktion der Wachstumskegelspaltungen durch die Störung der LZ-Domäne die Wichtigkeit von Interaktionen über diese Domäne.

Gewebe einer GC-B-Reporter-Mauslinie mit einem N-terminalen Hämagglutinin-Tag wurde für Pull-down-Assays verwendet, um GC-B-Interaktoren zu analysieren, die mit diesem Enzym co-immunpräzipitieren. Eine MS-Analyse wurde an Herzgewebe von erwachsenen Mäusen sowie an DRG-Gewebe von Embryonen durchgeführt, was in beiden Fällen zur Entdeckung von potenziellen GC-B-Interaktoren im Zytoskelett-Kompartiment führte. Während GC-B im Herzgewebe konsistent mit einem Mikrotubuli-assoziierten Protein interagierte, wurden im DRG-Gewebe signifikante Interaktionen mit vier Zytoskelett-assoziierten Proteinen sowie mit zwei Tubulin-Monomer-Isoformen nachgewiesen. Dies unterstreicht die Bedeutung von GC-B als Verankerungspunkt für Komponenten des Zytoskeletts und könnte ein Anhaltspunkt für die Entdeckung eines Proteinkomplexes sein, der den cGMP-abhängigen Signalweg in den Wachstumskegeln somatosensorischer Neuronen zu bestimmten subzellulären Orten lenkt und so die Axonverzweigung steuert.

Insgesamt haben sowohl Phosphoproteom-Screens für GKI-Substrate als auch Interaktom-Studien für GC-B zur Identifizierung neuer Komponenten des cGMP-abhängigen Signalwegs geführt, darunter mehrere mit dem Zytoskelett assoziierte Elemente in DRG-Neuronen. Einige der identifizierten cGKI-Phosphorylierungsstellen müssen in zukünftigen Studien noch verifiziert werden, und ihre Beteiligung am Prozess der Axonverzweigung muss noch untersucht werden. Zwar enthält keines der hier untersuchten cGKI-Substratkandidaten eine LZ-Domäne, doch scheinen solche Substrate *in vivo* eine entscheidende Rolle zu spielen und könnten Gegenstand künftiger Forschungsbemühungen sein. Außerdem könnten sie oder andere Proteine ein Bindeglied zwischen GC-B und cGKI darstellen. In Anbetracht der bekannten Rolle von cGMP-abhängigen Signalwegen in vielen (patho-)physiologischen Zusammenhängen ist die Entdeckung neuartiger potenzieller cGKI-Substrate von allgemeinem Interesse auf dem Gebiet der cGMP-Forschung, auch über den Prozess der somatosensorischen Axonverzweigung hinaus.

CONTENT

1 INTRODUCTION

The fascinating complexity of the nervous system has long inspired the research of scientists, yet we are only at the beginning of dissecting this intriguing network. The basic pattern of neuronal circuitry is laid out during embryonic and early postnatal development. This process is critical for establishing connectivity and thus proper functioning of the mature brain. The characteristic morphologies of neuronal trajectories are shaped by guidance cues and axon branching patterns, a subtype of which is axon bifurcation. The process of axon bifurcation of somatosensory neurons in mouse embryos requires the second messenger cyclic guanosine monophosphate (cGMP). This molecule is also integral in a myriad of other physiological functions, most prominently perhaps vasodilation in the cardiovascular system. cGMP is the focus of extensive research due to its importance in health and disease, and it is the target of several drugs in use today [1–4]. A better understanding of the molecular mechanisms of axonal growth, guidance, and branching might also provide insights into developmental disturbances that cause neurological diseases.

In this thesis I investigated the role of cGMP signaling during axon bifurcation, a crucial step during the development of the projection pattern of somatosensory neurons in mouse embryos. Some components of this specific signaling pathway are already known: the cGMP generator guanylyl cyclase B (GC-B), the GC-B ligand C-type natriuretic peptide (CNP), and the cGMP effector cGMP-dependent kinase I (cGKI) [5–7]. Others however, especially substrates of cGKI, interactors of GC-B, and the growth cone remodeling process preceding its split during bifurcation have yet to be uncovered (Figure 1-1).

Therefore, this thesis aimed to discover novel components of the cGMP-dependent signaling pathway that regulates somatosensory axon bifurcation in mouse embryos. I investigated new connections to the established enzymes of the cascade and searched for putative substrates of cGKI as well as interactors of GC-B.

The first chapter comprises an introduction to the thesis and an overview of the topics axon navigation (Section 1.1), the somatosensory system and its development (Section 1.2), as well as the cGMP signaling pathways (Section 1.3). It concludes with a summary of the aims of this work (Section 1.4). The subsequent chapters detail the materials and methods used for all conducted experiments included in this work (Chapter 2) and present the results obtained in those studies (Chapter 3). The last chapter discusses the data in context of current research, gives the limitations of the conducted research as well as an outlook into future possibilities and considerations (Chapter 4).

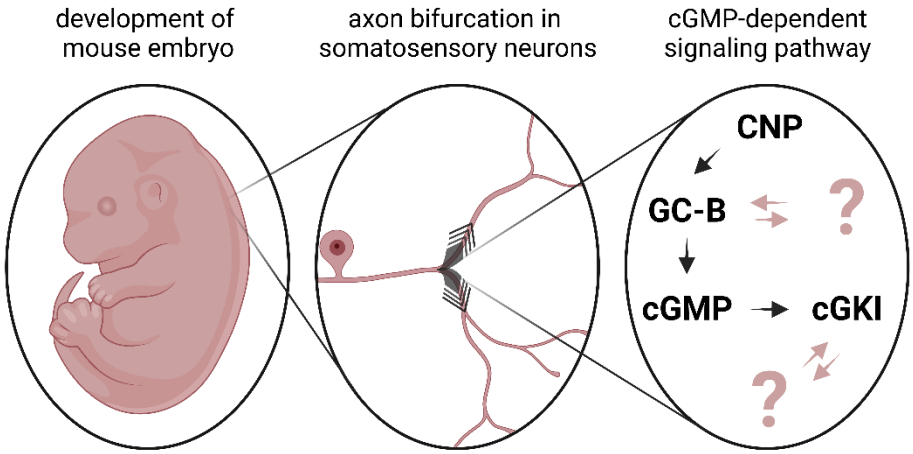

Figure 1-1 ***Overview.***

During the development of the nervous system in mouse embryos, the central axonal afferents of somatosensory neurons undergo a branching pattern called bifurcation. This process is regulated by a cGMP-dependent signaling pathway involving the cGMP generator GC-B (a transmembrane receptor), its extracellular ligand CNP, and the cGMP effector cGKI. The discovery of novel interactors of GC-B and substrates of cGKI are the focus of this thesis.

1.1 AXON NAVIGATION

For neuronal circuits to be established the information transmitting appendage of a neuron – the axon – needs to accurately navigate to its target during development and form a connection. This process takes place during embryonic and early postnatal development. Axonal navigation and pathfinding lead by the growth cone and steered by extracellular guidance cues are governed by cytoskeleton dynamics. General parts of the cytoskeleton are described in the following section, which provides a basis for the subsequent section introducing growth cone dynamics. Many guidance cues and their receptors have already been identified, but the intracellular pathways translating those cues into responses of the growth cone are still unknown, making it the subject of extensive research to date.

1.1.1 The cytoskeleton

There are three types of cytoskeletal filaments – intermediate filaments, actin filaments, and microtubules. A core function of intermediate filaments is the structural integrity of cells and cell-cell contacts [8]. On the other hand, actin filaments and microtubules play critical roles in axon navigation and are explained in more detail in the following paragraphs.

1.1.1.1 Cytoskeleton filaments

1.1.1.1.1 Actin filaments

Besides their involvement in axon navigation, actin filaments are integral for various processes involving movement, such as cell migration and muscle contraction. Actin filaments can indirectly connect with elements of the extracellular matrix via transmembrane proteins (e.g., integrins) and thus facilitate cell movement and anchoring. In cooperation with myosin, actin is part of contractile structures that participate in many cellular transport processes and, most notably, builds the fundamental element of muscles [8].

Actin monomers can combine into polarized polymers called actin filaments. These can further assemble into higher order structures like actin bundles that are more stable than the individual polymers. The polarized actin filaments can grow by addition of an adenosine triphosphate (ATP)-associated actin monomer to the plus-end. Towards the minus-end, associated ATP is hydrolyzed. The resulting adenosine diphosphate (ADP)-actin is prone to detach from the minus-end [9].

1.1.1.1.2 Microtubules

Next to axon outgrowth and growth cone dynamics, microtubules are crucial in several other processes of eukaryotic cells. Importantly, during mitosis they form the mitotic spindle, which separates the chromosomes. Microtubules also form tracks throughout cells that motors can utilize to transport organelles, vesicles, and other structures thereby contributing fundamentally to cell organization and polarity. Together with motors, microtubules also form the cores of cilia and flagella [8,10–12].

Similar to actin filaments, microtubules are polarized structures with a plus-end and a minus-end. Microtubules are made up of hetero-dimers of α- and β-tubulin. Several different isoforms of both monomers exist with different spatiotemporal expression patterns. Instead of ATP, tubulin dimers associate with guanosine triphosphate (GTP) and are added to the plus-ends of protofilaments, which in turn form rigid, hollow tubes called microtubules. This structure makes microtubules more stable but also less flexible than actin filaments. Following hydrolysis of GTP to guanosine diphosphate (GDP), the tubulin dimer can dissociate from the minus-end of microtubules. Unlike actin filaments, microtubules display a growth pattern called dynamic instability with polymers randomly switching between growth (i.e., addition of GTP-tubulin as described above) and shortening (i.e., detaching of protofilaments at the plus-end, also called catastrophe event). Thus, microtubules can experience periods of growth, pausing, and shrinkage. These patterns are influenced by the availability and local concentration of tubulin dimers as well as the presence of microtubule-associated proteins (MAPs). Different isoforms of the tubulin monomers that could be incorporated in a specific sequence may influence the association with different MAPs and thus downstream signaling pathways [9,13,14].

1.1.1.2 Cytoskeleton-binding proteins

The dynamics of both actin filaments and microtubules are influenced by distinct sets of cytoskeleton-binding proteins as well as some crosslinking proteins that can interact with both types of filaments. The following paragraphs describe their different classes as well as give some examples with a focus on their importance for axon navigation.

1.1.1.2.1 Actin-binding proteins

Nucleation factors are actin-binding proteins that create new plus-ends for growth. This is aided by monomer-binding proteins like profilin, that transports new building blocks to the plus-end of growing filaments. Capping proteins that bind to the plus-end of actin filaments can have both a growth inhibitory effect by blocking the addition of new monomers to the growing filament, or a growth supporting effect by stabilizing the plus-end and preventing disassembly. Antagonists of these capping proteins can have similarly opposing effects. Severing proteins like ADF/cofilin affect disassembly of actin filaments by promoting the removal of GDP-actin from the minus-end of filaments. Another set of actin-binding proteins are stabilizing proteins that are involved in assembling actin filaments into higher order structures like bundles or in anchoring them to specific regions of the membrane [9].

1.1.1.2.2 Examples

Ena/Vasp proteins are a conserved family of actin binding proteins that regulate the assembly of the actin filament network. They can associate with the plus-end of actin filaments and antagonize filament capping, thereby promoting growth. Members of this family that occur in mammals are mammalian enabled protein (Mena), vasodilator-stimulated phosphoprotein (Vasp), and Ena-Vasp-like protein (Evl). All family members share the following conserved domains: an N-terminal Ena/Vasp homology (EVH) 1 domain, a proline-rich central region, and a C-terminal EVH2 domain. The EVH1 domain of these proteins can in turn bind to proline-rich regions thus driving subcellular localization and complex formation [15]. Ena/Vasp proteins are critical for several physiological processes, for example, fibroblast migration, axon guidance and neuronal migration, and T-cell migration [16,17]. The Mena-140 (~140kDa) isoform is expressed in developing and adult neuronal tissue where it plays a role in axon guidance among others [18] and has a known tyrosine (Y) phosphorylation site [19]. Murine Vasp contains three phosphorylation sites at serine (S) 153, S235, and threonine (T) 274. Of these sites, Mena contains the first two, and Evl only the first. Phosphorylation of S153 in Vasp affects a change in apparent molecular mass during gel electrophoresis from 46 to 50 kDa. Similarly, Mena and Evl also exhibit this shift when phosphorylated at the respective position [16,19–21].

Collapsin response mediator proteins (Crmps) are a family of cytosolic phosphoproteins that are involved in axon guidance but also other developmental processes of the nervous system like synapse maturation. Phosphorylation events at their C-terminal regions regulate their interactions with other proteins. Crmp1 for example, has been shown to interact with actin as well as the actin-binding protein Evl. It can interact with microtubules as well. Enzymatic functions of Crmps are still being investigated [22,23].

Rho GTPases are another important family of proteins that influence actin cytoskeleton dynamics. They integrate a myriad of signals and coordinate the activation of a range of factors that affect actomyosin contraction and actin filament polymerization and disassembly. They are all a kind of molecular switch that is activated when the bound GDP molecule is replaced by a GTP molecule. Prominent examples include RhoA, Rac, and Cdc42, which are involved in filopodia formation and growth cone steering. The exact effect often depends on the combination of upstream regulators and downstream effectors that are present in a spatially specific manner in the growth cone [8,9].

1.1.1.2.3 Microtubule-associated proteins and crosslinkers

MAPs can be classified by their function or their location of binding. The functional categories include stabilization, destabilization, linkers to other microtubules or parts of the cytoskeleton, and interactions with other proteins or cell structures. Members of these categories might be either lattice-binding or end-binding proteins. The GDP-tubulin body – or lattice – of microtubules can be stabilized by proteins like

MAP tau (Mapt), Map1b, doublecortin, and others. Most stabilizers also have some bundling activity supporting the association of microtubules into higher order structures. Cytoskeletal integrators also include bigger scaffolding proteins like APC that binds to actin filaments as well. Destabilizing proteins have diverse ways of affecting microtubules. Stathmin (Stmn), for example, sequesters tubulin dimers, thus preventing them from being added to the growing end. Other destabilizers like some members of the kinesin family actively cause depolymerization at the tip, while severing proteins like katanin cut microtubules into smaller pieces by extracting tubulin dimers from the lattice. So-called capping proteins adhere to either the plus- or minus-end of the microtubule and can promote or prevent dimer association or dissociation, respectively. For example, calmodulin-regulated spectrin-associated proteins (CAMSAPs) stabilize the minus-end of microtubules by preventing depolymerization. Plus-end tracking proteins (+TIPs) comprise a network of MAPs that track the growing end of microtubules that is made of GTP-tubulin – the GTP-cap. +TIPs include conserved polymerization-promoting proteins such as end-binding protein (EB) 1, which is sometimes referred to as the master +TIP, as most other +TIPs bind it instead of directly associating to the microtubule. Other proteins that interact with microtubules include motors like kinesin and dynein, which use them as tracks for intracellular transport, cytoplasmic linker proteins (CLIPs), that anchor organelles to microtubules, or proteins that are involved in signal transduction, translation, or other metabolic processes. The activity and localization of many MAPs is regulated by their phosphorylation state. For example, the glycogen synthase kinase 3 (GSK3), a constitutively active kinase that in turn can be inhibited via phosphorylation, is involved in many cytoskeletal dynamic processes [10,17,24–26].

1.1.1.2.4 Examples

Microtubule and actin filament structures interact with each other via crosslinkers. Some can be associated directly with both types of cytoskeletal filaments, like microtubule-actin crosslinking factor 1. Others go a more indirect route, like the actin filament binding protein drebrin, which also interacts with the microtubule +TIP network. Other examples of MAPs implicated in microtubule-actin crosstalk are the stabilizers Map1b and Mapt which have both been reported to regulate EB binding to the microtubule plus-end. Their activity seems to be dependent on phosphorylation status, with Map1b also being affected by S-nitrosylation [14,17,27].

There are two mammalian CLIP-associating proteins (Clasps) with several isoforms that differ at the N-terminus with differential expression patterns. Conserved structures include the C-terminal region that can interact, as the name suggests, with CLIPs, but also the Golgi apparatus, and the cell cortex. The mid-section of Clasps contains conserved regions rich in S and arginine (R) residues. These are responsible for the interaction of Clasps with the microtubule-lattice as well as other proteins like other +TIPs. The microtubule binding-activity of Clasps might be regulated via phosphorylation possibly by GSK3. In general, Clasps have a stabilizing effect and inhibit catastrophe events. It has been suggested that the binding localization, which might be regulated via phosphorylation state, could have opposing effects, with +TIP-binding leading to microtubule stabilization and thus axon elongation, while lattice-binding is associated with slower growth cone advance. Additionally, Clasp1 and Clasp2 might have opposing functions during neuronal differentiation, as Clasp1 has been associated with the stimulation of neurite extension and Clasp2 with its inhibition [12–14,27,28].

The components of the cytoskeleton described above all play critical roles in axon navigation, as they influence the dynamic shape of the structure at the growing tip of developing axons – the growth cone. Thus, understanding the regulation of these proteins is of interest when studying axonal growth, guidance, and branching patterns.

1.1.2 Growth cone dynamics

The textbook diagram of a neuron consists of the cell body – or soma – and two types of appendages. Many, typically rather short dendrites extend from the soma to form synapses to other axons and receive information. This information, in the form of ion currents, travels through the soma and reaches the long wire-like extension called the axon. Axons grow out of the soma as neurites during development, headed

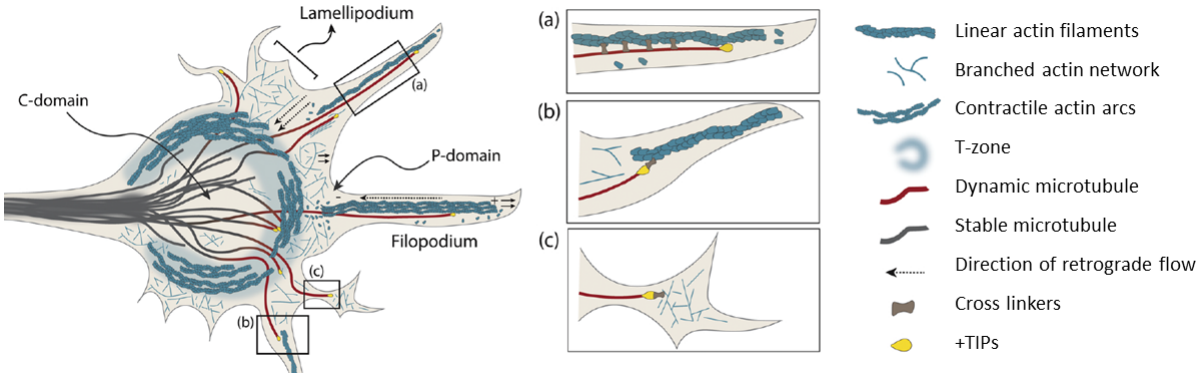

Figure 1-2 ***Cytoskeletal elements of the growth cone.***

The growth cone consists of different areas with the central domain (C-domain) closest to the axon shaft, which is surrounded by the transition zone (T-zone), and the peripheral domain (P-domain) comprising filopodia and lamellipodia-like veils. Each contains characteristic features of the cytoskeleton [29].

by a pathfinding structure called the growth cone. Dynamic changes in the growth cone are influenced by two systems: the cytoskeleton, and the membrane. Localized cytoskeleton remodeling generated by environmental guidance cues builds the basis for axon navigation. The membrane engulfing the cytoskeleton must change with it in a dynamic manner regulated by endo- and exocytosis – the extraction of vesicles from, and incorporation into, the plasma membrane. The structure of the axonal growth cone as shown in Figure 1-2 is divided into three sections. Bundled unidirectional microtubules emanate from the axon shaft into the central domain (C-domain) of the growth cone, along with organelles, vesicles, and central actin bundles. The central stable microtubule bundles are confined to the C-domain by actomyosin contractile structures – so-called actin arcs – which make up the transition zone (T-zone). Beyond the T-zone, the peripheral domain (P-domain) begins, dominated by filamentous actin structures. Tight parallel bundles of unbranched filamentous actin form protruding filopodia dynamically probing their surroundings. Filopodia are embedded in a mesh-like filamentous actin network that gives structure to the lamellipodia-like veils making up the webbing between the filopodia. Along the filamentous actin bundles sporadic pioneer microtubules dynamically explore this region as well [9,29].

During axon extension, the growth cone undergoes repeating steps of protrusion, engorgement, and consolidation. During protrusion the whole P-domain extends, as filamentous actin bundles are anchored to the substrate enabling polymerization and extension of the leading edge. Without anchoring, actin filaments exhibit a dynamic called treadmilling, where polymerization at the plus-end, and depolymerization at the minus-end occur at the same rate and the filament continuously moves towards the center of the growth cone. Exploratory microtubules can be recruited to filopodia by filamentous actin bundles. Engorgement of the T-zone by relaxing actin arcs and invasion of microtubules towards the direction of outgrowth follows. The growth cone neck compacts into a new segment of axon shaft, consolidating the direction of travel. Microtubules in the C-domain are stabilized by actin and an array of MAPs. Microtubules play a dual role in these processes of axon extension. During protrusion, pioneering microtubules aid in exploration thanks to their capacity for dynamic instability. The stable, bundled C-domain microtubules on the other hand are essential for steering as they move toward the area of new growth during the engorgement phase. The following consolidation of the new segment fixes the direction of the axon shaft. Interactions with actin are crucial during these processes, as on the one hand actin arcs prevent premature invasion of the growth cone periphery and on the other hand, filamentous actin bundles guide pioneering microtubules in the P-domain. Filamentous actin bundles can also capture the plus-end of a microtubule and reroute it back towards the C-domain via treadmilling [9,29,30].

There are three main classes of guidance cues that influence axon pathfinding. Adhesive substrate-bound cues are extracellular factors that the axon can grow on. They are made up of cell adhesive molecules and the extracellular matrix. Repellent substrate-bound cues (e.g., slits and ephrins) are their counterpart. The third class of guidance cues are the diffusible chemotrophic cues, a diverse group of molecules. Among them are the prominent guidance cue families of netrins and semaphorins, but they also include

morphogens, growth factors, neurotransmitters, and secreted transcription factors. Whether one of those cues is attractive or repulsive depends on the specific receptors and internal signaling of the growth cone. Guidance cues do not only affect the steering of the growth cone but can also evoke branching and arborization [9,26].

Intracellular pathways leading to specific growth cone behaviors are widely studied and several principal factors that can affect cytoskeleton dynamics and thus growth cone navigation have been identified. Several ubiquitous second messengers such as calcium, cyclic adenosine monophosphate (cAMP), and cGMP have been shown to play a role. Calcium transients in the growth cone of extending axons can regulate their outgrowth and guidance. Their amplitude, localization, and source are integral for which action will be taken. While a global increase of calcium might slow down axon extension, smaller, localized transients can have vastly different effects. Additionally, calcium is involved in (de-)phosphorylation events that regulate cytoskeleton dynamics that likely affect growth cone motility. The cyclic nucleotides cAMP and cGMP seem to work in concert, with their relative levels rather than their absolute concentrations being of consequence, for example via asymmetric gradients across the growth cone. Cyclic nucleotide and calcium signaling might be linked via cyclic nucleotide-gated (CNG) channels. While cell culture experiments clearly suggest that cGMP is involved in the regulation of the cytoskeleton, and thus growth cone dynamics, the downstream effectors are still unknown. As cytoskeleton binding proteins like the ones described above regulate cytoskeleton dynamics, they are also involved in growth cone dynamics. Another group of enzymes heavily implicated in axon growth, guidance, and branching are GTPases, which are critical for actin filament and microtubule dynamics [26,31–35].

Among dynamic patterns exhibited by growth cones and axons are not only pathfinding but also branching and synapse formation. Many factors regulating axon branch formation have been described already, but the mechanisms that induce branching at specific points of axonal trajectories *in vivo* remain poorly understood. To find common such mechanisms, it is helpful to study model systems. The somatosensory system, which is introduced in the following section, is studied as a model for different axon branching patterns.

1.2 THE SOMATOSENSORY SYSTEM

This chapter gives an overview of the physiology as well as development of the somatosensory system. It is used as a model system for different patterns of axon branching, as bifurcation, interstitial branching, and terminal arborization are all observable in the stereotypically organized central projections of developing somatosensory neurons.

1.2.1 Physiology of the somatosensory system

The somatosensory system is responsible for the perception of specific senses. Among those are conscious somatosensation including pain (nociception), itch (pruriception), and touch (mechanosensation), as well as unconscious proprioception which describes head and body position and movement. The somatosensory system has both peripheral and central components. In the periphery, skin, muscles, tendons, and internal organs are innervated. There, the sensory modalities are picked up by specialized receptors or end organs and then the information is carried to the central nervous system (CNS) by first-order neurons. In these specialized so-called pseudo-unipolar neurons, the signal travels from the origin, along the axon, past the soma, and into the CNS. Somata of these neurons are bundled outside of the CNS in groupings called ganglia that are located along the spinal cord and hindbrain. Dorsal root ganglion (DRG) neurons form synaptic connections to second-order neurons in the spinal cord, while cranial sensory ganglion (CSG) neurons do so in the hindbrain.

After that point, the pathway differs depending on the type of first-order neuron. Cutaneous (nociceptive, pririceptive, and mechanoreceptive) collaterals terminate in specified layers of the dorsal horn where they arborize and connect to dorsal horn neurons. The axons of most of these neurons cross the midline and form synapses with third-order neurons in the thalamus, which in turn innervate the primary sensory

cortex. Proprioceptive collaterals on the other hand go further ventral, where they arborize and connect to the ipsilateral cerebellum via spinocerebellar tracts [36].

1.2.2 Embryonic development of the somatosensory system

The somatosensory system develops during the embryonic and early postnatal phase. After establishment of the initial pattern of neurite outgrowth directed via appropriate guidance cues, the network is further refined by pruning of inactive connections [37].

The anatomy of the neuronal network that builds the somatosensory system does not only rely on growth cone pathfinding but also involves axon branching. This enables an axon to make contacts with multiple targets, which is integral for the correct computation and distribution of information. In general, new branches can be formed by splitting of the growth cone (bifurcation) or budding of collaterals from the stem axon (interstitial branching) [38]. Disruption of correct branching patterns leads to severe neurodevelopmental disorders in humans [39]. The projection of first-order neurons of the murine somatosensory system into the CNS can serve as a model to study axon branching, as both bifurcation and interstitial branching as well as terminal arborization can be observed in these neurons in a simple and stereotyped manner (Figure 1-3).

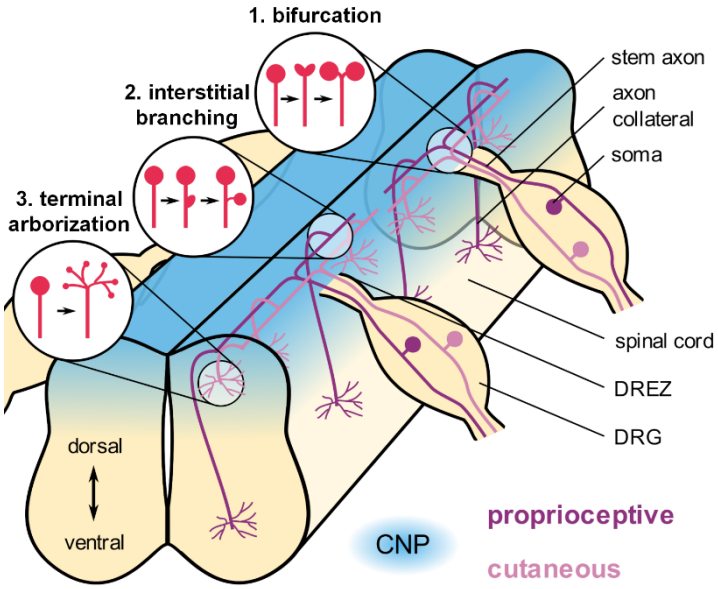

Figure 1-3 ***Somatosensory axon branching patterns.***

When somatosensory axons develop, they undergo different kinds of branching. First, they bifurcate at the DREZ, second, they sprout collaterals via interstitial branching, and third, they arborize in their respective termination fields [42].

Murine afferent axons reach the dorsal root entry zone (DREZ) between embryonic day 10.5 (E10.5) and E13.5, at which point they bifurcate into two stem axons that extend over several segments along the rostro-caudal plane within the developing dorsal funiculus, commonly referred to as the oval bundle of His. After a waiting period of at least one to two days, budding of numerous ventrally directed collaterals (interstitial branching) occurs. Collaterals terminate and arborize depending on their modality as described above with cutaneous collaterals terminating in the dorsal horn and proprioceptive collaterals reaching more ventral areas of the spinal cord [37,40,41].

The second messenger cGMP plays a vital role for the processing of distinct sensations in adulthood [42]. Additionally, a cGMP-dependent signaling cascade controls the bifurcation of DRG neurons at the DREZ as observed *in vivo* in embryonic mice. Both are detailed below, after a general introduction to the cGMP signaling pathway.

1.3 The cGMP signaling pathway

The second messenger molecule cGMP plays a pivotal role in modulating numerous physiological processes. Notably, it influences vasodilation, phototransduction, calcium homeostasis, and neurotransmission. cGMP is synthesized by GCs through the conversion of GTP. These GCs function as the generators of cGMP, initiating its production in response to specific molecular signals. The molecules' degradation is catalyzed by phosphodiesterases (PDEs). Some PDEs not only degrade cGMP but also function as cGMP effectors, as their activity can be regulated by cGMP itself. Effectors also include CNG ion channels, which can be modulated by cGMP, altering cellular excitability and ion flux. Lastly, cGKs are another type of cGMP effector, as they are activated by cGMP, leading to phosphorylation of specific

target proteins and subsequent signaling cascades. The major components of the cGMP signaling pathway are shown in Figure 1-4 and further described in this chapter.

1.3.1 cGMP generators

cGMP generators encompass two principal categories, namely soluble guanylyl cyclases (sGCs) and particulate guanylyl cyclases (pGCs). sGCs exist as heterodimers, with the β1 subunit capable of associating with either the α1 subunit (forming GC1) or the α2 subunit (forming GC2). These enzymes are physiologically stimulated by nitric oxide and carbon monoxide, with the proposed receptor for these gases being the heme group that binds to the β1 subunit [43]. Pharmacologically, sGCs can be regulated by nitric oxide-releasing nitrates or stimulators and activators. Stimulators (e.g., riociguat) interact with intact sGC molecules, eliciting their activation, while activators (e.g., cinaciguat) act on heme-free sGC molecules that are NO-insensitive. The sGC stimulator riociguat, for example, finds clinical use in the management of pulmonary hypertension. Ongoing research in this field continues to yield numerous developments, including (pre-)clinical trials for potential new or repurposed drugs [2,44].

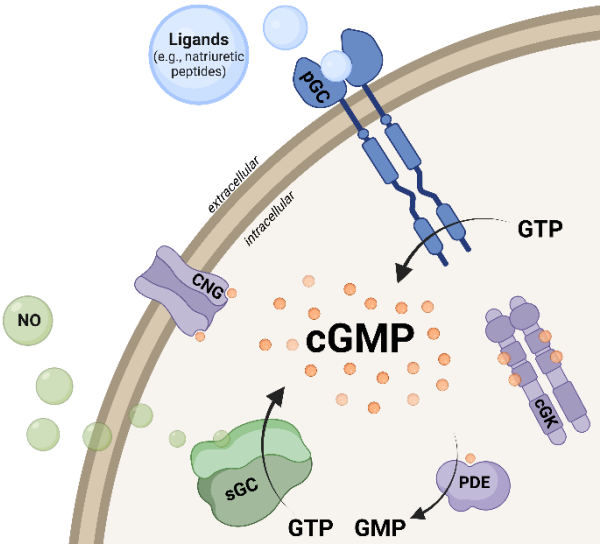

Figure 1-4 ***Prominent cGMP signaling pathway components.***

The molecule cGMP is generated from GTP by sGCs or pGCs, which are activated, among others, by nitric oxide and natriuretic peptides, respectively. The degradation of cGMP back to GMP is catalyzed by PDEs, some of which are also regulated by cGMP. Other effectors of cGMP include CNGs and cGKs.

pGCs constitute a family of seven members in mammals, denoted as GC-A to GC-G. The monomers of these homodimeric enzymes consist of an extracellular ligand binding domain, transmembrane domain, kinase homology domain (KHD), dimerization site, and finally, the GC domain. The GC domain catalyzes the reaction of a GTP molecule to cGMP and pyrophosphate. Physiologically, GTP is divalently bound to a magnesium ion. Among the pGC subtypes, GC-A and GC-B are receptors for natriuretic peptides such as atrio-natriuretic peptide (ANP), B-type natriuretic peptide (BNP), and CNP. GC-C functions as the receptor for guanylin, uroguanylin, and heat-stable enterotoxin. Notably, the pharmacological agent linaclotide, an analog of heat-stable enterotoxin, acts as a ligand for GC-C and finds clinical application in the treatment of irritable bowel syndrome with constipation. Although GC-D and GC-G are pseudogenes in humans, they serve as receptors for carbon dioxide/bicarbonate in mice. GC-E and GC-F operate under the regulatory influence of calcium ions, thereby participating in signal transduction processes within retinal rods and cones [3,45–47].

Furthermore, the scavenger receptor, while devoid of the intracellular GC domain, can bind natriuretic peptides. This receptor, widely expressed throughout various tissues, may facilitate the internalization and subsequent degradation of natriuretic peptides, among other potential effects.

GC-B is expressed in fibroblasts, chondrocytes, brain tissue, lung tissue, vascular smooth muscle cells, and the uterus. The structure and function of GC-B is shown in Figure 1-5. Like GC-A, GC-B contains three intramolecular disulfide bonds and is highly glycosylated on asparagine residues. An N-terminal glycosylation is required for the correct formation of the GC domain [46–48]. The activation of the enzymatic activity of the GC domain requires both extracellular ligand binding and phosphorylation of the seven regulatory S/T residues of the KHD. The precise mechanism of phosphorylation and dephosphorylation of the GC-B KHD *in vivo* which could shed a new light on the regulation of its enzymatic activity is still unknown. There is evidence that a member of the phosphoprotein phosphatase family might be responsible for dephosphorylation and thus inactivation of GC-B in a regulatory manner during oocyte maturation in ovarian follicles [49,50] as well as during long bone growth [48,51].

Both CNP and GC-B are stimulators of long bone growth, which is illustrated by some human genetic diseases. Several homozygous loss-of-function mutations of the gene that encodes GC-B have been identified in human patients that cause acromesomelic dysplasia type maroteaux (AMDM), a rare form of short-limbed dwarfism. Individuals with one normal and one abnormal allele display normal limb proportions but are substantially shorter than the average person from their respective populations [52]. Chromosomal mutations that increase CNP concentrations on the other hand are associated with Marfanoid-like skeletal overgrowth [53,54]. Achondroplasia, a prevalent form of dwarfism, is caused by a gain-of-function mutation in a negative regulator of bone growth – fibroblast growth factor receptor 3 (FGFR3). As CNP/GC-B/cGMP signaling is found to inhibit the function of FGFR3, a CNP analog – vosoritide – was recently approved in the EU for treatment of achondroplasia [55].

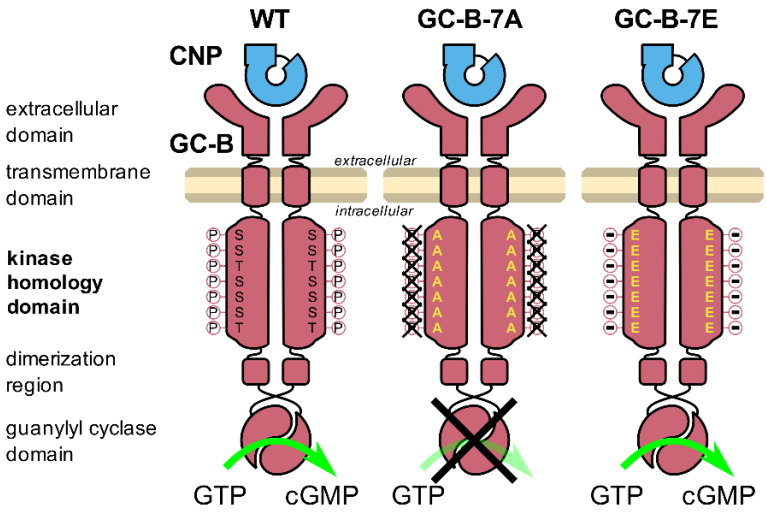

Figure 1-5 ***Structure and enzymatic activity of GC-B in mice of different genotypes.***

GC-B consists of an extracellular domain, a transmembrane domain, a KHD, a dimerization region, and a GC domain. The extracellular domain can bind its ligand CNP in all pictured genotypes. If the seven S/T residues of the KHD are phosphorylated in the WT form of GC-B, binding of CNP leads to the activation of the GC domain which catalyzes the production of cGMP from GTP. This is not possible in GC-B-7A mice where all seven regulatory S/T residues of the KHD are substituted by A. GC-B-7E mice express a phosphomimetic variant of GC-B with E substitutions, where GC activity is activated by CNP binding [42].

In addition to long bone and vertebrae growth, CNP/GC-B signaling is also involved in axonal bifurcation as described below, as well as resumption of meiosis in the ovarian follicle [56].

1.3.2 cGMP degraders

PDEs are responsible for breaking down cGMP to guanosine monophosphate (GMP) through hydrolyzation. In mammalian cells, there are eleven PDE families, with eight of them capable of degrading cGMP. Some PDEs have selectivity for cGMP (PDE1A, PDE1B, PDE5, PDE6, and PDE9), while others can hydrolyze both cGMP and cAMP (PDE1C, PDE2, PDE3, PDE10, and PDE11). The activity of certain PDEs is regulated through allosteric binding of cAMP or cGMP. Additionally, the phosphorylation state of specific PDEs can modulate their enzymatic activity. Of clinical relevance, the pharmacological inhibition of PDE5 by sildenafil, vardenafil, and tadalafil is used in the treatment of erectile dysfunction and pulmonary arterial hypertension [3].

1.3.3 cGMP effectors

cGMP acts through various effectors to mediate its physiological functions. The classical effectors of cGMP include CNG channels and cGKs. Additionally, PDE2 and PDE3 also function as effectors as their activity is regulated by cGMP through allosteric mechanisms.

CNG channels are activated by the intracellular binding of cyclic nucleotides. Upon activation, these channels open, allowing the influx of calcium and sodium ions. CNG channels play a central role in the signal transduction pathways involved in vision and olfaction. These channels exist as heterotetramers with different compositions in rod photoreceptors, cone photoreceptors, and olfactory neurons [57,58].

cGKs are encoded by two genes, Prkg1 and Prkg2, which give rise to three enzyme isoforms: cGKIα, cGKIβ, and cGKII. All cGK isoforms form homodimers through a leucine zipper (LZ) domain located at the N-terminus of the monomers. Each monomer also contains two cGMP binding sites that, upon binding, activate the kinase activity of cGKs. cGKII can anchor to the plasma membrane, which may

impact its activity and function [3]. cGK substrates in general include ion channels, G-proteins and associated regulators, and cytoskeleton associated proteins [59] and the discovery of new phosphorylation targets is an ongoing process [60,61]. It has been shown that the site of phosphorylation of a large number of substrates conforms to the consensus sequence R/K-R/K-X-S*/T* containing R and/or lysine (K) residues, with X being any amino acid and the asterisk marking the phosphorylated residue [62].

The two cGKI isoforms cGKIα and cGKIβ are produced by alternative mRNAs and differ in about 100 N-terminal residues. These segments contain the LZ domain which directs homodimerization and interacts with anchoring proteins. Essential components of signaling pathways can be linked together in anchoring complexes leading to compartmentalization and thus better spatiotemporal control of signaling. This can also be critical for a kinase to reach its phosphorylation targets. In growth cones, it is possible that most cGKI is associated with subcellular compartments in the C-domain like the endoplasmic reticulum (ER) and other vesicular structures, with only a small fraction of the kinase in the P-domain. Possible anchoring structures responsible for this localization are yet to be discovered [35,63,64].

cGKIα specifically is redox-sensitive and oxidation can directly activate its kinase activity independent of cGMP. Oxidation causes the formation of an interprotein disulfide bond between two cysteine residues that are on adjacent chains in the homodimeric complex [65].

1.3.4 cGMP signaling in the somatosensory system

In adulthood, cGMP signaling is integral to pain processing in the somatosensory system. BNP/GC-A signaling is involved in the processing of the itch sensation in the spinal cord via a distinct population of sensory neurons. On the other hand, cGMP produced via CNP/GC-B signaling might be involved in processing of pain and the regeneration of injured peripheral nerves. While GC1 and GC2 are not expressed in sensory neurons themselves, they might still play differential roles in the processing of neuropathic and inflammatory pain respectively as they can be found in distinct populations of interneurons in the spinal dorsal horn [42].

The cGMP effector cGKI is expressed in sensory neurons with high expression levels in nociceptive neurons [66], cGKIα being the major isoform [67]. A cGMP-independent activation of cGKI by oxidation might play a role not only in nerve repair after injury, but also in the processing of neuropathic pain [65,68]. Possible substrates of cGKI in sensory neurons include CRP4, αMLC, IP3RI, and Vasp [66,69]. Other effectors of cGMP that might play a role in the somatosensory system are not yet well defined but might include PDE2A, the major type of PDE expressed in sensory neurons [42].

Many *in vitro* experiments showed the involvement of cGMP in axon guidance of somatosensory neurons [70]. This was observed for mouse, chick, and rat embryonic DRG neurons [5,71–75]. However, not only cGMP itself but rather the ratio between cGMP and cAMP might play a role [76,77], especially considering that cGMP-activated PDE2A, which hydrolyzes both cGMP and cAMP, was found to be the predominant PDE in embryonic mouse DRG neurons [78]. One of the effectors of cGMP in this context might be cGKI, the activation of which could lead to an efflux of calcium [75] – a second messenger shown to be involved in growth cone steering, as described above [31]. Further effectors of cGMP in this context might by the microtubule cytoskeleton [33] or CNG channels [34].

A cGMP-dependent signaling cascade controls the bifurcation of DRG neurons at the DREZ, as observed *in vivo* in mice. CNP is released by precursor cells in the dorsal region of the embryonic spinal cord and binds to the transmembrane receptor GC-B, which generates cGMP. The activation of cGKIα by cGMP leads to the phosphorylation of yet unknown substrates that bring about the bifurcation of the axon via an unknown mechanism. CNP is present in the spinal dorsal horn only during embryonic development between E9 and E17 forming a rostro-caudal gradient. GC-B and cGKIα are expressed in all neurons of CSGs and DRGs, with GC-B being detected as early as E9 and cGKIα at E10. cGKIα can be found in somata and growing axons of sensory neurons, thus also labeling the DREZ and entire dorsal

funiculus at E14. However, the expression of GC-B but not cGKI declines at more advanced developmental stages.

The absence for either CNP, GC-B, or cGKI results in a loss of somatosensory axon bifurcation at the DREZ (Figure 1-6). Instead, the axons randomly turn in either a rostral or caudal direction, which results in a reduced area of the dorsal funiculus as well as a reduced number of collaterals due to the lower number of longitudinal stem axons. This causes a decreased synaptic input to second-order neurons, while the synaptic transmission itself is unchanged. The development of collaterals as well as the gross anatomy of the spinal cord and spinal ganglia also remain unaffected. This observed bifurcation error in the embryonic development of the somatosensory system in the absence of CNP, GC-B, or cGKI persists into adulthood. Physiologically, mice with such a bifurcation error in somatosensory neurons have normal motor balance and coordination while nociception is impaired on the levels of electrophysiology and behavior. Additionally, sensory feedback control in the auditory and mesencephalic trigeminal system is impaired. It is unknown if the same branching errors occur in humans with a deficiency in GC-B. For example, no tests to determine neurological deficits in AMDM patients have been performed [5–7,42,79–81].

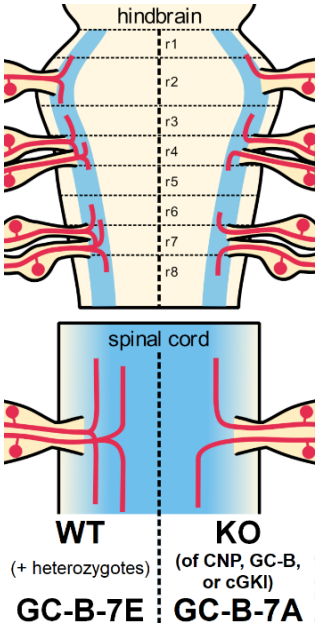

Figure 1-6 ***Different bifurcation phenotypes of DRG and CSG neurons and of MTNs in the spinal cord and hindbrain of different genotypes.***

Bifurcation can be observed at the DREZ and in the hindbrain of WT and GC-B-7E mice. When knocking out CNP, GC-B, or cGKI, or rendering GC-B inactive via alanine substitutions in the KHD in GC-B-7A mice, bifurcation is disrupted [42].

In addition to all neurofilament positive DRG neurons, CSG neurons and mesencephalic trigeminal neurons (MTNs) express both GC-B and cGKIα. CNP is present not only in the spinal cord but also in the hindbrain, primarily at the entry points of sensory afferents in rhombomeres 2, 4, and 6. Central axons of CSG neurons as well as MTNs bifurcate in the hindbrain analogous to the axons of DRG neurons via GC-B induced cGMP signaling (Figure 1-6) [82,83].

In a mouse model that expresses a mutated GC-B protein with alanine (A) substitutions in the KHD (GC-B-7A mice), no phosphorylation can take place and the GC domain is inactive, even in the presence of CNP (Figure 1-5). The somatosensory axon bifurcation phenotype of these animals mirrors that of GC-B-knock-out (KO) mice with a total lack of T-shaped branching at the DREZ (Figure 1-6) [84]. Animals expressing a phosphomimetic variant of GC-B that substitutes seven glutamate (E) residues in the KHD however (GC-B-7E mice; Figure 1-5), do not differ from wildtype (WT) animals with respect to sensory axon bifurcation (Figure 1-6). GC-B is not constitutively active in these animals and produces no cGMP in absence of its ligand CNP [84,85].

While the CNP/GC-B/cGKI signaling has been established as essential for somatosensory axon bifurcation *in vivo*, the downstream mechanism remains elusive. Not least because growth cone splitting in response to CNP cannot be observed *in vitro*, which poses a challenge to experimental approaches. Studies have suggested that GSK3 [80], microtubule dynamics [33,86], and S-palmitoylation [35] might play a role in the regulation of axon branching, which might also be connected to the activation of cGKIα in DRG neurons.

1.4 The aim of this work

A cGMP-dependent signaling pathway regulates the axon bifurcation that can be observed in somatosensory neurons during the development of mouse embryos (Figure 1-1). To gain a better mechanistic understanding of axonal growth, guidance, and branching, the work presented in this thesis aimed to further dissect this CNP-induced cGMP signaling cascade. First, phosphoproteomic screening for novel

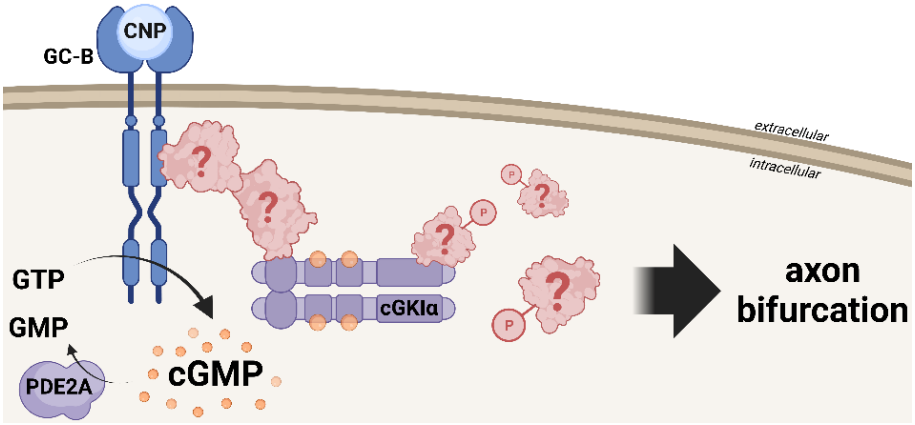

Figure 1-7 ***A cGMP signaling pathway regulates axon bifurcation in somatosensory neurons during murine embryonic development.***

Known players of this pathway are the extracellular ligand CNP, its receptor GC-B, and cGMP effector cGKIα. The aim of the present work was to discover novel components of the cascade that leads to axon bifurcation. Specifically, cGKIα substrates and GC-B interactors were investigated.

substrates of cGKI was applied to expand the known cGMP signaling pathway downstream and investigate possible molecular mechanisms that lead to growth cone splitting. Second, interactors of GC-B were screened to find possible regulators of the signaling cascade via GC-B (de-)phosphorylation and develop a hypothetical membrane anchoring complex that integrates the cytoskeleton as well as cGKI and its targets (Figure 1-7).

Bifurcation of axons is preceded by a growth cone split. The cytoskeleton with its associated network of proteins regulates growth cone dynamics and thus will participate in the mechanical process of splitting the growth cone. MAPs and actin-binding proteins represent likely candidates for cGKI substrates or indirect downstream targets, as their activity is oftentimes regulated by (de-)phosphorylation. The effects of this specific cGMP signaling cascade might be determined by subcellular compartmentalization within the growth cone. Thus, it is possible that a complex of enzymes, substrates, and scaffolding proteins is anchored to the membrane via the local source of cGMP the membrane receptor GC-B. Additionally, GC-B itself can be inactivated in a reversible manner by dephosphorylation. This represents an opportunity to regulate the onset and termination of the axon bifurcation process in question.

In order to validate newly discovered substrates of cGKI in general, the kinase's presence and activity should be confirmed in appropriate cellular or animal models (Section 3.1). In the present work, a murine melanoma cell line as well as several transgenic mouse lines were investigated. Additionally, the potential future use of chick embryos to conduct studies on somatosensory axon bifurcation was considered, and work was started to confirm the presence of the same cGMP-dependent signaling pathway in DRG neurons in these animals.

A phosphoproteome study was performed on both a murine melanoma cell line as well as DRG tissue of mouse embryos to screen for putative cGKI phosphorylation substrates (Section 3.2). As labeling techniques stable isotope labeling by amino acid in cell culture (SILAC) (Section 2.4.1) and stable isotope dimethyl labeling (SIDL) (Section 2.4.2) were used for the cell line and the tissue samples, respectively. The presence of a cGKI consensus sequence, an LZ domain, and a kinase activity domain as well as the cell compartment of candidates were annotated. cGKI is likely to phosphorylate substrates at a consensus sequence and interact with proteins that contain an LZ domain or occur within the same subcellular compartment. Whether a potential substrate contains a kinase or phosphatase domain is of interest considering downstream effects of cGKI activation.

To validate the possibility of phosphorylation of putative substrates by cGKI, several approaches were used (Section 3.3). An expression analysis was done to confirm the presence of both the transcript and protein in the tissue of interest. The subcellular and tissue distribution of candidates was analyzed.

Verification of the phosphorylation of the identified candidate proteins by cGKI was done in an *in vitro* assay with an analogue-sensitive mutant of cGKIα.

Axon tracing studies were performed on mouse models with cGMP signaling mutations to investigate their somatosensory axon bifurcation phenotype (Section 3.4). Mouse lines lacking established cGKI substrates were studied to determine the direct necessity of those substrates in the bifurcation process. Additionally, a cGKIα mutant with a disrupted LZ interaction capability was studied likewise to confirm the involvement of LZ domain interactors of cGKIα in sensory axon bifurcation.

To identify novel interactors of GC-B, pull-down experiments were performed with different murine tissues that exhibit high GC-B expression (Section 3.5). Interaction studies were performed on adult heart tissue and embryonic DRG tissue of mice expressing a hemagglutinin (HA)-tagged GC-B protein. To identify relevant interactors of GC-B, characteristics like kinase or phosphatase activity, the presence of an LZ domain, and the cell compartment were considered. The aim was to identify candidate proteins that regulate the activity of GC-B via (de-)phosphorylation, and interactors that might act as a link between GC-B and cGKI in a hypothetical protein complex, or interactors anchoring this hypothetical complex to the cytoskeleton.

Before presenting and discussing the acquired data in subsequent chapters, the following chapter details materials and methods of the experimental approaches selected to achieve the aims described above.

2 MATERIALS AND METHODS

2.1 MATERIALS

All chemicals used for the experiments shown in this thesis are listed in Table 2-1 alphabetically by the in-text notation given in the first column. Other reagents and ready-made media are similarly listed in Table 2-2. Self-prepared buffers and their composition are given in Table 2-4, with all necessary stock solutions listed in Table 2-3. All kits used for the present work are described in Table 2-5. Primary and secondary antibodies are listed in Table 2-6 and Table 2-7, respectively. The first column of each table gives the in-text notation of each material. Prevalent equipment, tools, and software are listed in Table 2-8. Cell lines are described in Table 2-9.

Table 2-1 ***Chemicals.***

*In-text notation**	*Composition/Formula*	*Brand, No.*	*Storage*
2-Mercaptoethanol	C_2H_6OS	Carl Roth, 4227.1	4 °C
6-Aminohexanoic acid	$C_6H_{13}NO_2$	Carl Roth, 3113.2	RT
6-PhEt-ATPγS	Sodium salt, $C_{18}H_{24}N_5O_{12}SP_3$, 10mM aqueous solution of pH 8.5	BioLog, P 026	-80 °C
8-Br-cGMP	Sodium salt, $C_{10}H_{10}BrN_5NaO_7P$	Sigma Aldrich, B 1381	-80 °C
8-pCPT-cGMP	Sodium salt, $C_{16}H_{14}ClN_5NaO_7PS$	Sigma Aldrich, C5438	-80 °C
Acetone	CH_3COCH_3	Sigma Aldrich, 32201-M	RT
Agarose	Biozym LE Agarose	Biozym, 840004	RT
APS	$(NH_4)_2S_2O_8$	Carl Roth, 9592.2	RT
Boric acid	H_3BO_3	CHEMSOLUTE, 2563	RT
Bromophenol blue	$C_{19}H_{10}Br_4O_5S$	Carl Roth, T116.1	RT
Chloroform	$CHCl_3$	Sigma Aldrich, 288306	RT
Citric acid	$HOC(CO_2H)(CH_2CO_2H)_2$	Carl Roth, 6490	RT
CNP	$C_{93}H_{157}N_{27}O_{28}S_3$	Sigma Aldrich, N8768	-80 °C
DAB	Tetrahydrochloride hydrate, $C_{12}H_{14}N_4$	Sigma Aldrich, D5637	RT
DAPI	$C_{16}H_{15}N_5$	Dianova	--
DEPC	$O(COOC_2H_5)_2$	Sigma Aldrich, D5758	RT
DiI	$C_{59}H_{97}ClN_2O_4$	Sigma Aldrich, 468495	4 °C
DMSO	$(CH_3)_2SO$	Carl Roth, 4720	RT
DOC	Sodium salt, $C_{24}H_{39}NaO_4$	Carl Roth, 3484.1	4 °C
DTT	$C_4H_{10}O_2S_2$	Carl Roth, 6908.3	4 °C
EDTA	Disodium salt dihydrate	Carl Roth, X986.2	RT
EtOH	CH_3CH_2OH	Sigma Aldrich, 34852-M	RT
G2P	Disodium salt hydrate	Sigma Aldrich, G9422	RT
Glycerol	$C_3H_8O_3$	Carl Roth, 3783.2	RT
Glycine	NH_2CH_2COOH	Sigma Aldrich, 33226	RT
H_2O_2	Hydrogen peroxide, 30% solution	Carl Roth, 8070.2	4 °C
HCl	Hydrochloric acid, ≥37%, fuming	Sigma Aldrich, 30721	RT
HEPES	Good's buffer	Carl Roth, HN78.3	RT
Isopropanol	$(CH_3)_2CHOH$	Sigma Aldrich, 59300	RT
KCl	Potassium chloride	Carl Roth, P017.3	RT
KH_2PO_4	Potassium dihydrogen phosphate	Merck, 104873	RT
MeOH	CH_3OH	Sigma Aldrich, 32213	RT
$MgCl_2$	Magnesium chloride hexahydrate	Carl Roth, 2189.1	RT
Na_2HPO_4	Disodium hydrogen phosphate	Carl Roth, 4984	RT
NaCl	Sodium chloride	Merck, 1.06404	RT
NaN_3	Sodium azide	Carl Roth, K305.1	RT
NOG	$C_{14}H_{28}O_6$	Sigma Aldrich, O8001	-20 °C
NP40	Nonidet P40 Substitute	Roche, 11754599001	RT
PFA	$(CH_2O)_n$	Carl Roth, 0335.3	4 °C
PMSF	Protease inhibitor	Carl Roth, 6367	--

*In-text notation**	*Composition/Formula*	*Brand, No.*	*Storage*
PNBM	$C_8H_9NO_5S$, Alkylation reagent	abcam, ab138910	-20°C
SDS	$C_{12}H_{25}NaO_4S$	Carl Roth, 4360.2	RT
SF	NaF	Sigma Aldrich, 201154	RT
Sodium citrate	Dihydrate, $Na_3C_6H_5O_7$ x 2 H_2O	Sigma Aldrich, W302600	RT
SOV	Na_3VO_4	Sigma Aldrich, 567540	RT
Sucrose	$C_{12}H_{22}O_{11}$, D-Sucrose	Carl Roth, 4621.1	RT
TEMED	$C_6H_{16}N_2$	Carl Roth, 2367.3	4°C
Thiourea	NH_2CSNH_2	Sigma Aldrich, T8656	RT
Toluene	$C_6H_5CH_3$	Sigma Aldrich, 34866	RT
Tris	$NH_2C(CH_2OH)_3$, Trizma® base	Sigma Aldrich, T1503	RT
Tween® 20	Polyoxyethylene-20-sorbitan monolaurate	Carl Roth, 9127.1	RT
TX100	$C_{33}H_{60}O_{10}$, polyethylene glycol alkyl phenyl ether	Carl Roth, 3051.2	RT
Urea	$CO(NH_2)_2$	Merck, 108487	RT
Xylene cyanole	$C_{25}H_{27}N_2NaO_6S_2$	Carl Roth, A513.1	RT

* *For abbreviations, see List of Abbreviations.*

Table 2-2 ***Reagents, compounds, ready-made media, and additives.***

In-text notation[1]	*Full notation/Composition/Formula*	*Brand, No.*	*Storage*
3X FLAG® Peptide	Synthetic peptide of 23 amino acid residues	Sigma Aldrich, F4799	-20 °C
anti-HA magnetic beads	Pierce™ Anti-HA Magnetic Beads	Thermo Scientific, 88836	4 °C
anti-FLAG magnetic beads	Anti-FLAG® M2 Magnetic Beads (4 % agarose beads bound with the Anti-FLAG M2 mouse monoclonal antibody)	Sigma Aldrich, M8823	-20 °C
Aquatex®	Aqueous mounting agent for microscopy	Sigma Aldrich, 1.08562	RT
Benzonase	Benzonase® Nuclease	Millipore, E1014	-20 °C
BSA	Fraction V	Carl Roth, 8076.4	4 °C
cOmplete	Protease inhibitor cocktail tablets (1 tablet/10 ml)	Roche, 11836170001	4 °C
dNTPs	10 mM each of dATP, dCTP, dGTP and dTTP	NEB, N0447	-20 °C
DMEM + GlutaMAX™-I	Dulbecco's modified eagle's medium (DMEM), high glucose, GlutaMAX™ Supplement, pyruvate	Gibco, 31966	4 °C
DNA ladder	1 Kb Plus DNA Ladder	Invitrogen, 10787018	4 °C
FBS	Heat-inactivated	Gibco, 10270	-20 °C
HBSS	With sodium bicarbonate, sterile filtered	Sigma Aldrich, H9269	4 °C
ImmuMount	Epredia™ ImmuMount™, aqueous mounting medium for immunostaining and frozen sections	Fisher Scientific, 10662815	RT
Mayer's Hematoxylin solution	Hemalum solution acid according to Mayer	Carl Roth, T865.2	RT
Midori Green Advance	DNA/RNA stain	Nippon Genetics, MG04	4 °C
NGS	Blocking reagent, heat-inactivated	Merck, S26	-20 °C
Opti-MEM	Reduced-Serum Medium	Gibco, 31985070	4 °C
Paraffin	Surgipath Paraplast X-tra	Leica, 39603002	[2]
Pen/Strep	100x solution: 10,000 units/ml penicillin and 10,000 µg/ml streptomycin	Gibco, 15140	-20°C
PhI2	Aqueous solution	Sigma Aldrich, P5726	4 °C
PhI3	DMSO solution	Sigma Aldrich, P0044	4 °C
PhosSTOP	Phosphatase inhibitor tablets (1 tablet/10 ml)	Roche, 4906837001	4 °C
PDL	0.1mg/ml, chemically synthesized extracellular matrix	Gibco, A3890401	-20 °C
Powdered milk	Blotting grade, low in fat	Carl Roth, T145.2	4 °C

In-text notation[1]	*Full notation/Composition/Formula*	*Brand, No.*	*Storage*
Protein ladder	PageRuler™ Prestained Protein Ladder, 10 to 180 kDa	Thermo Scientific, 26616	-20 °C
Proteinase K	20 mg/ml	Genaxxon, M3036	-20 °C
Random primers	Random Primer oligonucleotides (mostly hexamers)	Invitrogen, 48190-011	-20 °C
RNase H	Ribonuclease H, 2 U/µl	Invitrogen, 18021014	-20 °C
Rotiphorese Gel 30	ROTIPHORESE®NF-Acrylamide/Bis-solution 30 (Aqueous acrylamide and bisacrylamide stock solution at ratio 29:1)	Carl Roth, A124.1	4 °C
SILAC-DMEM	High glucose, pyruvate, w/o L-Arginine, w/o L-Lysine	PAN-Biotech, P04-02505S1	4 °C
Tissue-Tek	Sakura Finetek™ Tissue-Tek™ O.C.T. Compound	Fisher Scientific, 12351753	RT
TRIzol	TRIzol™ Reagent	Invitrogen, 15596026	RT
Trypan blue	10x solution: 0.4 % trypan blue stain	Gibco, 15250	4 °C
Trypsin/EDTA	10x solution: 0.5 % trypsin and 5mM EDTA	Gibco, 15400	-20 °C

[1] *For abbreviations, see List of Abbreviations.*
[2] *Melt and keep at 56°C.*

Table 2-3 ***Stock solutions.***

In-text notation[1]	*Composition*	*Storage*
3xFLAG peptide stock	5 mg/ml in TBS (IP)	-20 °C
6-PhEt-ATPγS stock	10 mM in H_2O	-80 °C
8Br-cGMP stock	100 mM in H_2O	-80 °C
8pCPT-cGMP stock	25 mM in H_2O	-80 °C
APS stock	20 % in H_2O	-20 °C
CNP stock	100 µM in H_2O	-80 °C
cOmplete stock	10x in H_2O	-20 °C
DAB stock	0.1 % in PBS	-20 °C
DAPI staining solution	0.5 mg/ml in H_2O	-20 °C
DiI stock	5 % in EtOH	-20 °C
DOC stock	10 % in H_2O	-20 °C
DTT stock (1 M)	1 M in H_2O	-20 °C
DTT stock (50 mM)	50mM in H_2O	-20 °C
EDTA (5 mM)	5mM in PBS (sterile)	4 °C
EDTA stock (0.5 M)	0.5M in H_2O (pH 8.0)	RT
EDTA stock (100 mM)	100mM in H_2O	RT
G2P stock	1M in H_2O	-20 °C
HEPES stock (0.5 M)	0.5M in H_2O (pH 7.4)	4 °C
HEPES stock (1 M)	1 M in H_2O (pH 7.9)	4 °C
KCl stock	3 M in H_2O	RT
MgCl2 stock	1 M in H_2O	RT
NaCl stock (1 M)	1 M in H_2O	RT
NaCl stock (3 M)	3 M in H_2O	RT
NP40 stock	10 % in H_2O	4 °C
PhosSTOP stock	10x in H_2O	-20 °C
PMSF stock	100 mM in 100% EtOH	-20 °C
PNBM stock	50 mM in DMSO	-20 °C
SDS (10 %)	10 % in H_2O	RT
SDS (20 %)	20 % in H_2O	RT
SF stock	500 mM in H_2O	-20 °C
SOV stock[2]	100 mM in H_2O (pH 10.0)	-20 °C
Tris-HCl (1 M, pH 6.8)	1 M in H_2O (pH 6.8)	RT
Tris-HCl (1 M, pH 8.0)	1 M in H_2O (pH 8.0)	RT
Tris-HCl (1 M, pH 8.3)	1 M in H_2O (pH 8.3)	RT

In-text notation[1]	*Composition*	*Storage*
Tris-HCl (1 M, pH 8.8)	1 M in H_2O (pH 8.8)	RT
Tris-HCl (50 mM, pH 7.4)	50 mM in H_2O (pH 7.4)	RT
TX100 stock	10 % in H_2O	RT

[1] *For abbreviations, see List of Abbreviations.*
[2] *Activation: Prepare 100 mM solution of SOV in H2O, adjust pH to 10.0 with 1N NaOH or 1N HCl (solution will be yellow), boil until solution is colorless (~ 10 min), cool to RT, readjust pH to 10.0, repeat until pH stable at 10 and remains colorless at RT.*

Table 2-4 ***Buffers, solutions, and media prepared for the use in this thesis.***

In-text notation[1]	*Composition*	*Storage*
ABC solution	1 % Reagent A, 1 % Reagent B, 50 % PBS in TBS-T	fresh[2]
Anode buffer I	300 mM Tris, 20 % MeOH in H_2O (pH 10.4)	RT
Anode buffer II	30 mM Tris, 20 % MeOH in H_2O (pH 10.4)	RT
Antibody dilution buffer (IHC)	5 % NGS in TBS-T	fresh
Antibody dilution buffer (WB)	5 % BSA, 0.05 % NaN_3 in TBS-T	-20 °C
Antigen retrieval solution	10 mM sodium citrate in H_2O (pH 6.0)	RT
Blocking buffer (IF)	1 % NGS, 0.1% TX100 in PBS	-20 °C
Blocking buffer (IHC)	10 % NGS in TBS-T	fresh
Blocking buffer (WB)	5 % powdered milk in TBS-T	fresh
Cathode buffer	30 mM Tris, 40 mM 6-aminohexanoic acid, 20 % MeOH in H_2O (pH 7.6)	RT
Cell lysis buffer	0.67 % SDS, 100 µM PMSF, 1x PhosSTOP, 21 mM Tris-HCl (pH 8.3) in H_2O	fresh
Cytoplasmic extraction buffer (10x)	300 mM HEPES, 30 mM $MgCl_2$, 1.4 M KCl in H_2O	4 °C
DAB staining solution	0.02 % H_2O_2, 50 % DAB stock in PBS	fresh
Denaturation buffer	6 M urea, 2 M thiourea in 50 mM Tris-HCl (pH 8.0)	4 °C
DEPC water	1 % DEPC in H_2O	RT
DNA loading buffer (6x)	0.125 % bromophenol blue, 0.125 % xylene cyanole, 30 % glycerol, 0.3 M Tris, 0.3 M boric acid, 6 mM EDTA in H_2O	4 °C
Elution buffer	300 µg/ml 3xFLAG peptide in TBS (IP)	fresh
Full medium	10 % FBS, 1x Pen/Strep in DMEM + GlutaMAX™-I	4 °C
Hypotonic buffer	10 mM HEPES (pH 7.9), 1.5 mM $MgCl_2$, 10 mM KCl, 100 µM PMSF, 1x cOmplete, 100 mM DTT in H_2O	fresh
Kinase reaction buffer	20 mM HEPES (pH7.4), 25 mM $MgCl_2$, 137 mM NaCl, 0.5 mM DTT, 0.2 % TX100 in H_2O	fresh
Lysis buffer (IP)	1x TBS (IP), 0.5 % NP40, 1 % PhI2, 1 % PhI3, 1x cOmplete in H_2O	fresh
Lysis buffer (PCR)	50 mM KCl, 2 mM $MgCl_2$, 10 mM Tris (pH 8.0), 0.45 % TX100, 0.45 % Tween-20, 0.01 % gelatin in H_2O	4 °C[3]
Lysis buffer (SIDL)	150 mM NaCl, 1 % NP40, 0.25 % DOC, 0.1 % SDS, 25 mM Tris (pH 7.4), 1 mM EDTA, 1 mM SOV, 5 mM G2P, 5 mM SF, 1x cOmplete in H_2O	fresh
Lysis buffer (SILAC)	1 % NOG, 1x cOmplete, 1 mM SOV, 5 mM G2P, 5 mM SF in denaturation buffer	fresh
PBS	135 mM NaCl, 3 mM KCl, 8 mM Na_2HPO_4, 2 mM KH_2PO_4 in H_2O (pH 7.4)	RT[3]
PCR buffer (10x)	500 mM KCl, 100 mM Tris (pH 8.0), 15 mM $MgCl_2$, 2 mM dNTPs in H_2O	-20 °C
Peroxidase blocking solution	6.3 % H_2O_2, 0.9 % MeOH in PBS	fresh
PFA fixative	4 % PFA in PBS	-20 °C
Replenishment buffer	47 mM KCl, 42.2 % glycerol, 0.422 mM EDTA (pH 8.0), 100 µM PMSF, 1x cOmplete, 100 mM DTT in H_2O	fresh
SDS loading dye (5x)	40 % glycerin, 15 % SDS, 0.1 % bromophenol blue, 25 % 2-mercaptoethanol, 320 mM Tris-HCl (pH 6.8) in H_2O	-20 °C
SDS running buffer (10x)	250 mM Tris, 1 % SDS, 1.9 M glycine in H_2O	RT

In-text notation[1]	*Composition*	*Storage*
Separating gel (10 %)	375 mM Tris-HCl (pH 8.8), 0.1 % SDS, 33 % Rotiphorese Gel 30, 0.1 % APS, 0.1 % TEMED in H_2O	fresh
Separating gel (7.5 %)	375 mM Tris-HCl (pH 8.8), 0.1 % SDS, 25 % Rotiphorese Gel 30, 0.1 % APS, 0.1 % TEMED in H_2O	fresh
Serum-free medium	1x Pen/Strep in DMEM + GlutaMAX™-I	4 °C
SILAC medium (heavy)	10 % FBS, 1x Pen/Strep, Lys-8 (L-[$^{13}C_6$, $^{15}N_2$]), Arg-10 (L-[$^{13}C_6$, $^{15}N_4$]) in SILAC-DMEM	4 °C
SILAC medium (light)	10 % FBS, 1x Pen/Strep, Lys-0 (L-[$^{12}C_6$, $^{14}N_2$]), Arg-0 (L-[$^{12}C_6$, $^{14}N_4$]) in SILAC-DMEM	4 °C
Stacking gel	125 mM Tris-HCl (pH 6.8), 0.1 % SDS, 13 % Rotiphorese Gel 30, 0.1 % APS, 0.1 % TEMED in H_2O	fresh
Stripping buffer	2 % SDS, 100 mM 2-mercaptoethanol in 62.5 mM Tris-HCL (pH 6.8)	RT
Sucrose solution	30 % sucrose in PBS	4 °C
TAE	40 mM Tris, 20 mM acetic acid, 1 mM EDTA H_2O (pH 8.0)	RT
TBS (10x, general)	100 mM Tris, 1.5 M NaCl in H_2O (pH 8.0)	RT
TBS (10x, IP)	300 mM Tris, 1.5 M NaCl in H_2O (pH 7.4)	RT
TBS-T	1x TBS (general), 0.1 % Tween-20 in H_2O	RT
Wash buffer (HA IP)	1x TBS (IP), 0.1 % NP40, 1 % PhI2, 1 % PhI3 in H_2O	fresh
Wash buffer (IF)	0.1 % TX100 in PBS	RT
Wash buffer (WB)	1 % powdered milk in TBS-T	fresh
Wash buffer 1 (FLAG IP)	20 mM HEPES (pH 7.9), 20 % glycerol, 100 mM KCl, 100 µM PMSF, 1 mM DTT in H_2O	fresh
Wash buffer 2 (FLAG IP)	20 mM HEPES (pH 7.9), 20 % glycerol, 300 mM KCl, 0.1 % NP40, 100 µM PMSF, 1 mM DTT in H_2O	fresh

[1] *The specific use of buffers with identical names is given in brackets. For abbreviations, see List of Abbreviations.*
[2] *Dilute Reagents A and B (VECTASTAIN® ABC-HRP Kit) 1:50 in PBS, incubate 30min at RT in the dark, dilute 1:1 in TBS-T directly before use.*
[3] *Autoclave before storage.*

Table 2-5 ***Kits and their components.***

In-text notation	*Contents*	*Brand, No.*
Bradford assay kit	Dye reagent concentrate Bovine serum albumin standard	Bio-Rad, 500-0002
Cell compartment kit	Extraction Buffer CE1 Extraction Buffer CE2 Extraction Buffer CE3 Extraction Buffer CE4 Benzonase® Nuclease Protease Inhibitor Solution (100x) QIAshredder	Qiagen, 37502
Lipofectamine™ 3000	Lipofectamine™ 3000 Reagent P3000™ Enhancer Reagent	Invitrogen, L3000015
Pierce™ BCA Protein Assay Kit	Solution A Solution B BSA	Thermo Scientific, 23227
SuperScript™ III kit	SuperScript III RT 5x first-strand buffer 0.1 M DTT	Invitrogen, 18080
Sylgard	SYLGARD™ 184 silicone elastomer kit	Dow
Taq polymerase kit 1	10x PCR buffer 50 mM $MgCl_2$ Taq DNA polymerase	Invitrogen, 10342020
Taq polymerase kit 2	10x PCR buffer 25 mM $MgCl_2$ Taq DNA polymerase	Genaxxon, M3001

In-text notation	*Contents*	*Brand, No.*
Taq polymerase kit 3	10x PCR buffer 5x Q-solution Taq DNA polymerase	Qiagen, 201203
VECTASTAIN® ABC-HRP Kit	Reagent A Reagent B	Vector Laboratories, PK-4000
WesternBright® Sirius® ECL kit	WesternBright® Sirius® Luminol/enhancer solution WesternBright® Peroxide Chemiluminescent Detection Reagent	Advansta, K-12043

Table 2-6 ***Primary antibodies.***

In-text notation[1, 2]	*Host*	*Use & dilution*[2]				*Brand, No.*
α-Acin1	rabbit	WB 1:1,000	IF 1:100			Invitrogen, PA5-17344
α-cGKI	rabbit	WB 1:1,800	IF 1:900			PD Dr. Schmidt
α-cGKIα	guinea pig		IF 1:10,000	IHC	1:10,000	PD Dr. Schmidt
α-Clasp1	rabbit	WB 1:1,000	IF 1:200			Biorbyt, orb304724
α-Crmp1	rabbit	WB 1:1,000	IF 1:200			Invitrogen, PA5-34768
α-FLAG	mouse	WB 1:1,000				Sigma Aldrich, F1804
α-GAPDH	rabbit	WB 1:2,000				CST, 2118
α-GC-B	guinea pig	WB 1:5,000	IF 1:500	IHC	1:500	PD Dr. Schmidt
α-HA	rabbit	WB 1:1,000	IF 1:800			CST, 3724S
α-Histone H3	rabbit	WB 1:10,000				abcam, ab1791
α-Integrin-β1	rabbit	WB 1:1,000				CST, 34971
α-Map1b	rabbit	WB 1:1,000	IF 1:500			Invitrogen, PA5-78052
α-Mena	rabbit	WB 1:500	IF 1:200			Novusbio, NBP1-87914
α-NFH	chick		IF 1:2,500			abcam, ab4680
α-TPE	rabbit	WB 1:12,500				abcam, ab92570
α-Vasp	rabbit	WB 1:1,000	IF 1:400			CST, 3132
α-pS235-Vasp	rabbit	WB 1:1,000				CST, 3114
α-βActin	rabbit	WB 1:5,000				abcam, ab8227

[1] *In-text notation gives the antibody as α-"target".*
[2] *For abbreviations, see List of Abbreviations.*

Table 2-7 ***Secondary antibodies.***

In-text notation[1,2]	*Target*	*Conjugation*[2]	*Use & dilution*[2]		*Brand, No.*
α-Rb-Alexa488	rabbit	Alexa488	IF	1:1,000	JIR, 111-545-144
α-Rb-Biotin	rabbit	Biotin	IHC	1:250	VectorLabs, BA-1000
α-Gp-Biotin	guinea pig	Biotin	IHC	1:1,000	JIR, 106-065-008
α-Gp-Cy3	guinea pig	Cy3	IF	1:500	JIR, 706-165-148
α-Ch-Cy3	chick	Cy3	IF	1:500	JIR, 703-165-155
α-Gp-HRP	guinea pig	HRP	WB	1:10,000	JIR, 706-035-148
α-Rb-HRP	rabbit	HRP	WB	1:10,000	CST, 7074
α-M-HRP	mouse	HRP	WB	1:10,000	Santa Cruz, SC-2055

[1] *In-text notation gives the antibody as α-"target"-"conjugation".*
[2] *For abbreviations, see List of Abbreviations.*

Table 2-8 ***Equipment, tools, and software.***

Name	*Description*	*Brand / Version*
10cm cell culture dish	Petri dish for adhesion cells	Corning
15cm cell culture dish	Petri dish for adhesion cells	Corning
8-well cell culture slide	Glass slide for adhesion cells	MP Biomedicals
Axioskop 20	Brightfield microscope	ZEISS
BioRender	Illustration software	BioRender.com

Name	*Description*	*Brand / Version*
ChemiDoc	Imaging system	BioRad
EOS 750 D	Digital camera	Canon
EOS utility	Image acquisition software	Canon
Epredia™ Polysine adhesion slides	Paraffin section object slides	Fisher Scientific
Epredia™ SuperFrost Plus™ adhesion slides	Frozen section slides	Fisher Scientific
GraphPad Prism	Statistics and graphing software	Version 9.5.1
HM 335 E	Rotary microtome	Microm
HM 505 E	Cryostat	Microm
ImageJ	Image editing software	Version 1.53
LSM 710	Confocal microscope	ZEISS
LSM 980	Confocal microscope	ZEISS
Microsoft Word	Word processor software	Version 2307
Microsoft PowerPoint	Presentation software	Version 2307
Mini-PROTEAN tetra vertical electrophoresis cell	SDS-PAGE gel running chamber	BioRad
Mini-PROTEAN® tetra cell casting module	SDS-PAGE gel casting	BioRad, 1658015
NanoDrop™ 2000	Spectrometer	Thermo Scientific
Neubauer improved chamber	Cell counting chamber	Marienfeld
Stemi 305	Stereo microscope	ZEISS
Stemi 508	Stereo microscope	ZEISS
Super PAP Pen liquid blocker	Water repellent pen	Science Services
T175 cell culture flask	Flask for adhesion cells (175cm^2)	Corning
Trans-Blot® SD semi-dry transfer cell	SDS-PAGE gel blotting chamber	BioRad

Table 2-9 ***Cell lines.***

Name	*Description*	*Reference*
B16F10	Murine melanoma cell line from a C57BL/6J mouse.	[87]
COS7	African green monkey kidney cells.	[88]

2.2 Animals

2.2.1 Mice

All experiments involving animals and animal-derived tissues were performed in accordance with EU directive 2010/63/EU of the German animal protection law TierSchG. The local animal use and care authority (Regierungspräsidium Tübingen) approved all protocols. All mice were kept in a 12 h:12 h light-dark-cycle at 22 °C with 50-60 % humidity and had access to tap water and standard mouse diet *ad libitum*. The mice referred to as WT mice were of the strain C57BL/6N (Charles River Laboratories), which was also the genetic background of all mouse lines used in this study.

2.2.1.1 Transgenic mouse lines

The genotypes of transgenic lines (Table 2-10) were determined with specific polymerase chain reaction (PCR) protocols. Genomic DNA serving as template for the PCR, was either extracted from ear biopsies taken when the mice were weaned (usually at postnatal day 21 (P21)), or a part of the head was used when embryos were dissected. Each tissue sample was incubated in 200 µl PCR lysis buffer supplemented with 2 µl Proteinase K (Genaxxon) overnight at 56 °C. The reaction was inactivated by heating the sample to 95 °C for 5 min. After spinning down remaining debris for 5 min at 16,000×g, the supernatant was used as template for the genotyping PCR. Specific primers were designed for each transgene to distinguish it from the WT allele. These primers are listed in Table 2-11 along with the respective PCR protocol. As cGKI-LZM and mixed lineage kinase-3 (Mlk3)-KO mice and mouse material were kindly provided by Assoc. Prof. Robert Blanton (Tufts Medical Center, Boston, USA), the genotyping was performed by staff at their in-house animal facility.

Table 2-10 ***Genotypes of transgenic mouse lines.***

In-text notation	*Full notation*	*Description*	*Ref.*
cGKI-KO	B6.129-Prkg1$^{tm2.1Naw}$	KO via excision of exon 10 of the *Prkg1* allele after flanking with loxP sites and subsequent Cre-mediated recombination.	[89]
cGKI-LZM	LZM PKGIα	The initial four LZ domain leucine/isoleucine codons in exon 1α of the *Prkg1* allele were replaced by A encoding codons.	[90]
GC-B-HA	HA-Npr2	Endogenous GC-B expresses an extracellular N-terminal HA tag.	[91]
Mlk3-KO	Mlk3	Whole body KO of the Mlk3 gene by deleting exons 2-5.	[92]
SMIβ-rescue	B6.129-Tagln$^{tm2(PRKG1*)Hfm}$	Selective rescue of the cGKIβ coding sequence in smooth muscle cells under SM22α promotor control to recover viability of adult mice.	[93]
Thy1-YFP-H	B6.Cg-Tg(Thy1-YFP)H$^{Jrs/J}$	A small number of sensory neurons endogenously express yellow fluorescent protein (YFP).	[94]
Vasp-KO	B6.129-Vasp^{tm1Mzim}	Interruption of the *Vasp* gene by deleting exons 4 to 11 via targeted integration of a neomycin-resistance cassette in intron 3.	[95]

PCR products were separated according to their size by agarose gel electrophoresis (2 % agarose in 1xTAE, supplemented with 4 µl Midori Green Advance (Nippon Genetics) after mixing the samples with DNA loading buffer. In a separate lane, a 1 kb plus DNA ladder (Invitrogen) was run along with the samples for 60 min at 100 V to determine the size of the PCR products. An image was acquired with ultraviolet (UV) light at a ChemiDoc (BioRad) imaging system.

Table 2-11 ***Genotyping PCR primers, reaction mixes, and programs.***

Genotype	*Primers*	*PCR mix*	*PCR protocol*	*PCR products*
cGKI-L1	Forward: CCT GGC TGT GAT TTC ACT CC WT reverse: GTC AAG TGA CCA CTA TG L1 reverse: AAA TTA TAA CTT GTC AAA TTC TTG	Invitrogen reagents[1] 15.2 µl H_2O 2.50 µl 10x buffer 0.75 µl 50mM $MgCl_2$ 0.50 µl dNTPs 0.30 µl per primer 0.20 µl *Taq* 5.00 µl DNA	5 min @ 95 °C 35 cycles: 30 sec @ 95 °C 30 sec @ 55 °C 30 sec @ 72 °C 10 min @ 72 °C ∞ @ 8 °C	WT: 284 bp L1: 250 bp
GC-B-HA	Forward: CCT GGC CCT CTT CCC CAG GCT C Reverse: GTG CCT CCA CAG CCA GTG CCA C	Genaxxon reagents[2] 14.8 µl H_2O 2.50 µl 10x buffer 1.50 µl 25mM $MgCl_2$ 0.50 µl dNTPs 0.25 µl per primer 0.20 µl *Taq* 5.00 µl DNA	3 min @ 95 °C 35 cycles: 30 sec @ 95 °C 30 sec @ 62 °C 30 sec @ 72 °C 10 min @ 72 °C ∞ @ 8 °C	WT: 270 bp HA: 307 bp
SMIβ-rescue	Forward: CTC AGA GTG GAA GGC CTG CTT WT reverse: CGC AAG GGT TAC TCA CCA CA Rescue reverse: AAC TCC AGC TCC AGC TCG	Self-made reagents[3] 19.4 µl H_2O 2.50 µl 10x buffer 0.30 µl per primer 0.20 µl *Taq* 2.00 µl DNA	5 min @ 95 °C 35 cycles: 10 sec @ 95 °C 30 sec @ 61 °C 30 sec @ 72 °C 5 min @ 72 °C ∞ @ 8 °C	WT: 290 bp Rescue: 195 bp

Genotype	*Primers*	*PCR mix*	*PCR protocol*	*PCR products*
Thy1-YFP-H	IL forward: GTA GGT GGA AAT TGT AGC ATC ATC C IL reverse: CTA CGC CAC AGA ATT GAA AGA TCT YFP forward: TCC TTG AAG AAG ATG GTG CG YFP reverse: AAG TTC ATC TGC ACC ACC	Invitrogen reagents[1] 10.5 µl H_2O 2.50 µl 10x buffer 1.50 µl 50mM $MgCl_2$ 0.25 µl dNTPs 0.2 µl per IL primer 0.4 µl per YFP primer 0.25 µl *Taq* 2.50 µl DNA	3 min @ 95 °C 35 cycles: 30 sec @ 94 °C 30 sec @ 60 °C 60 sec @ 72 °C 5 min @ 72 °C ∞ @ 8 °C	IL: 324 bp YFP: 173 bp
Vasp-KO	KO forward: CGA ATA GCC TCT CCA CCC AAG CGG CCG GAG AAC KO reverse: GGC CAG CAG AAC AGT ATT GGA GAA CAT CCA GG WT forward: TTA GCT TGG TTT GGG GAC TGA ACC AGC CTC CTT TC WT reverse: CAG CCA CTC CCT GGT ACT TCC TTA CCT TGC TCA C	Qiagen reagents[4] 9.2 µl H_2O 2.0 µl 10x buffer 4.0 µl 5x Q-solution 0.4 µl dNTPs 0.6 µl per primer 0.2 µl *Taq* 1.0 µl DNA	5 min @ 95 °C 35 cycles: 1 min @ 95 °C 1 min @ 65 °C 2 min @ 72 °C 10 min @ 72 °C ∞ @ 8 °C	KO: 700 bp WT: 469 bp

2.2.1.2 Timed breeding

For embryos to be dissected on E13.5, a timed breeding was set up with one male and two females from 5:00 pm to 9:00 am of the following day, when possible vaginal plugs could be detected. The plug date was defined as E0.5. Plugged dams were weighed and transferred to a separate cage, so pregnancy could be confirmed by reweighing on E12.5. Only dams with a minimum weight gain of 3 g were considered for preparation of E13.5 embryos the following day.

2.2.2 Chick

Chick embryos were dissected from Lohmann Brown hatching eggs (Artländer Geflügelhof, Quakenbrück, Germany) kindly provided by PD Dr. Andrea Wizenmann (Institute for Clinical Anatomy and Cell Analysis, University Tübingen). Fertilized eggs were incubated in a humidified incubator at 37 °C and used for preparation at E8.

2.3 Analysis of presence and activity of the CNP/GC-B/cGMP/cGKI pathway

The presence and activity of the CNP/GC-B/cGMP/cGKI pathway was investigated in the murine melanoma cell line B16F10 (Section 2.3.1), as well as in mouse and chick embryos (Section 2.3.2). In B16F10 cells, the localization of cGKI before and after stimulation with cGKI-activating compounds (Section 2.3.1.1) was investigated using two methods. The presence of cGKI in different subcellular fractions was detected via western blotting (Section 2.3.1.2), while the subcellular localization of cGKI was visualized by immunofluorescent (IF) staining of cultured cells (Section 2.3.1.3).

To investigate the presence and location of pathway components in the DRG neurons of mouse and chick embryos, embryos were prepared as described in sections 2.3.2.1 and 2.3.2.2, respectively. The dissected embryos were then fixed, embedded, and cut in frozen sections, which could then be processed with an IF staining (Section 2.3.2.3).

2.3.1 Melanoma cell line B16F10

B16F10 cells were kindly provided by Dr. Grießinger and Dr. Kneiling (University Hospital Tübingen). The cells were cultured in full medium at 37 °C and 6 % CO_2. For passaging, the cells were washed with PBS and incubated for 5 min at 37 °C with 1x Trypsin/EDTA (diluted in PBS) until they detached.

Trypsinization was stopped by adding full medium, and the cell suspension was centrifuged for 5 min at 200×g. The supernatant was discarded, and the cell pellet resuspended in fresh full medium for seeding.

The cell number was counted in a Neubauer improved chamber (Marienfeld) after staining dead cells with 1x trypan blue (diluted in PBS). Cells were seeded at 800,000 cells per 10 cm dish (Corning; see 2.3.1.1 and 2.4.1.1), and 2,500 cells per 8-well slide (MP Biomedicals) that had been autoclaved, precoated overnight at 4 °C with PDL (100 µg/ml; Gibco) in a wet chamber, and washed twice with PBS and once with full medium (Section 2.3.1.3).

2.3.1.1 Stimulation of cGKI activity in B16F10 cells

The stimulation of cGKI activity was performed when B16F10 cells reached 70-80 % confluence. The cells were starved in serum-free medium for 3 h at 37 °C before washing twice with pre-warmed PBS and adding the stimulating compounds. Stimulation conditions for each compound are listed in Table 2-12. Compounds were diluted in PBS supplemented with 1xPhosSTOP (Roche). Before further processing (Section 2.3.1.2 and 2.3.1.3), the cells were washed twice with PBS.

Table 2-12 ***B16F10 cell stimulation conditions for 8Br-cGMP and CNP.***

Compound	*Concentration*	*Time*	*Temperature*
8Br-cGMP	0.5 mM	5 min	37 °C
CNP	0.25 µM	10 min	37 °C

2.3.1.2 Analysis of subcellular fractions of B16F10 cells

For the analysis of the subcellular localization of cGKI, B16F10 cells were detached from the 10 cm dish with 5 mM EDTA and transferred to a 1.5 ml tube. Subcellular fractions were produced with the cell compartment kit (Qiagen) following the fractionation protocol for “cultured cell samples” given by the supplier in the “Qproteome Cell Compartment Handbook”.

2.3.1.2.1 Precipitation

The resulting cytosolic, membrane, nuclear, and cytoskeletal fractions were then precipitated with 8 volumes acetone and 1 volume MeOH overnight at -20 °C and centrifuged for 20 min at 4 °C and 2000×g. The pellet was washed twice with ice-cold 80 % acetone and finally air dried before resuspending the precipitated proteins of each fraction in denaturation buffer. Protein concentrations were determined using the Bradford assay kit (BioRad) according to the “Standard Procedure for Microtiter Plates” included in the manufacturer’s instruction manual.

2.3.1.2.2 SDS polyacrylamide gel electrophoresis

0.25 volumes of 5x SDS loading dye were added before they were denatured at 95 °C for 5 min. SDS polyacrylamide gel electrophoresis (SDS-PAGE) to separate the proteins was performed using hand cast gels created with the Mini-PROTEAN Tetra Cell Casting Module (BioRad). The casting cassette was filled with a 10 % separating gel and covered with isopropanol, which was removed after gel polymerization. A 4 % stacking gel was added on top of the separating gel, along with a comb to create loading wells. The fully polymerized hand-cast gel was then ready for SDS-PAGE, which was conducted with the Mini-PROTEAN Tetra Vertical Electrophoresis Cell (BioRad). The electrode assembly and tank were filled with a freshly prepared 1x dilution of 10x SDS running buffer. The samples were loaded alongside a protein ladder (Thermo Scientific), and the gel was run initially at 100 V for 10 min, followed by an additional 60 min at 150 V.

2.3.1.2.3 Semi-dry western blot

Proteins were transferred from the SDS-gel to a polyvinylidene fluoride (PVDF) membrane using a semi-dry western blot (WB) procedure. The Trans-Blot® SD Semi-Dry Transfer Cell (BioRad) was used and a blotting sandwich was assembled from anode to cathode as follows: anode buffer I-soaked Whatman papers, anode buffer II-soaked Whatman papers, pre-incubated PVDF membrane in MeOH, SDS-

gel, and cathode buffer-soaked Whatman papers. The blotting was run for 80 min at 65 mA per gel. Subsequent incubations and washes were performed with constant agitation. After transfer, the membrane was incubated with WB blocking buffer for 1h at room temperature (RT). The membrane was washed three times in TBS-T for 5 min each, followed by overnight incubation at 4 °C with the corresponding primary antibody diluted in WB antibody dilution buffer. After another set of triple washes with WB wash buffer, the membrane was incubated with the HRP-conjugated secondary antibody diluted in WB wash buffer for 2 h at RT. The dilution factors for primary and secondary antibodies can be found in Table 2-6 and Table 2-7, respectively. Finally, the membrane was washed three times in TBS-T for 5 min each. The HRP-coupled secondary antibodies were detected by enhanced chemiluminescence (ECL) using the WesternBright® Sirius® ECL kit (Advansta) as per the manufacturer's instructions on a ChemiDoc imaging system (BioRad).

2.3.1.3 Immunofluorescent staining of B16F10 cells

B16F10 cells on an 8-well slide (Section 2.3.1) were stimulated according to 2.3.1.1 and fixed with PFA fixative for 10 min at RT. After washing twice with PBS, the samples were incubated in IF blocking buffer for 1 h at RT. The slides were washed another three times in PBS before incubating with the primary antibody in IF blocking buffer overnight at 4 °C in a wet chamber and washed three more times in PBS. The secondary antibody was diluted in IF blocking buffer and supplemented with 1:1000 DAPI staining solution. Incubation with the secondary antibody lasted for 2 h at RT in an opaque wet chamber. Before covering the slide with ImmuMount (Fisher Scientific), it was washed 5 times with PBS and dipped in water. IF images were acquired at a confocal laser scanning microscope (LSM) 710 setup (ZEISS) and converted and assembled for figures in the ImageJ (version 1.53) software.

2.3.2 Mouse and chick embryos

2.3.2.1 Preparation of E13.5 mouse embryos

To dissect embryos on E13.5, a timed breeding was set up as described above (Section 2.2.1.2). E13.5 embryo dissection followed previously described methods [96]. Briefly, the pregnant dam was anesthetized by rapid CO_2 flooding until presumed cardiac arrest, followed by cervical dislocation to ensure death. Hysterectomy was performed by opening the abdominopelvic cavity after disinfecting the abdominal area with 70 % EtOH. The bilateral uterine horns were isolated and transferred to a dish containing ice-cold PBS. Under a stereo microscope (Stemi 305 or Stemi 508, ZEISS), the uterine wall was longitudinally incised, and the amniotic sacs were removed from the placenta. Each embryo's amniotic sac was peeled off, the umbilical cord was cut, and the embryo was decapitated. Material from the head was used for genotyping, if necessary, while the torso was further processed for fixation (Section 2.3.2.3), DRG collection (Section 2.4.2.1), or DiI staining of DRG neurons (Section 2.5.4.1).

2.3.2.2 Preparation of E8 chick embryos

The whole chick embryo was removed from the egg and transferred to a dish with PBS after carefully opening the shell at one end. The head was then removed with scissors, and only the torso was used for all following procedures.

2.3.2.3 Immunofluorescent staining of frozen sections

To produce frozen sections for IF staining, both mouse and chick embryos were incubated in PFA fixative for 2 h at 4 °C in an end-over-end rotator. The fixed tissue was then washed three times in PBS for 30min each under the same conditions before being transferred to sucrose solution at least overnight at 4 °C. The fixed embryos were embedded in Tissue-Tek (Fisher Scientific) and placed on dry ice to solidify completely. Embedded embryos were stored at -20 °C until cutting 10µm transversal sections at a cryostat (HM 505 E, Microm) on frozen section object slides (Fisher Scientific).

Before starting the IF staining, the sections were framed with PAP-Pen (Science Services) and blocked with IF blocking buffer for 1 h at RT in a wet chamber. Three washing steps (10 min each in IF wash buffer at 4 °C under constant agitation) were done after the blocking and each antibody incubation. All antibodies and DAPI staining solution were diluted in IF block buffer. Primary antibody incubation was

done overnight at 4 °C in a wet chamber. Then sections were incubated with secondary antibodies and DAPI simultaneously for 2 h at RT in an opaque wet chamber. After the last IF wash buffer wash, the slides were washed one additional time each in PBS and water before covering in ImmuMount (Fisher Scientific). After polymerization of the mounting medium for 24 h at 4 °C in the dark, the edges of the cover slip were sealed with clear nail polish, and, after drying, the sections could be documented at a confocal LSM 710 or 980 setup (ZEISS) and converted and assembled for figures in the ImageJ (version 1.53) software.

2.4 Phosphoproteome analyses of B16F10 cells and murine embryonic DRG

The phosphoproteome analysis of B16F10 cells after SILAC (Section 2.4.1) and of murine embryonic DRG after SIDL (Section 2.4.2) was done in collaboration with Prof. Boris Maček and Dr. Ana Velic (Proteome Center Tübingen, University of Tübingen). Specifically, the sample processing including phosphopeptide enrichment, as well as the mass spectrometric (MS) analysis (Section 2.4.3) of both experiments were performed by Dr. Ana Velic.

During SILAC, stable isotopes of amino acids were integrated into the proteome of proliferating B16F10 cells (Section 2.4.1.1). Groups labeled with isotopes of different mass received different treatments (Section 2.4.1.2), after which the samples were processed and prepared (Section 2.4.1.3) for MS analysis of the phosphoproteome under the different treatment conditions. To perform the same analysis on embryonic DRG neurons, E13.5 DRGs were collected (Section 2.4.2.1), divided into condition groups, treated, and lysed (Section 2.4.2.2). After further processing, the peptides in the samples were chemically labeled with stable isotopes of different mass (Section 2.4.2.3).

2.4.1 Stable isotope labeling by amino acids in cell culture

SILAC can be used to detect differences in protein abundance among samples of proliferating cells. It is a metabolic labeling technique with non-radioactive stable isotopes. Specific amino acids are incorporated *in vivo* into all proteins of cultured cells. Differentiation between conditions can be achieved by

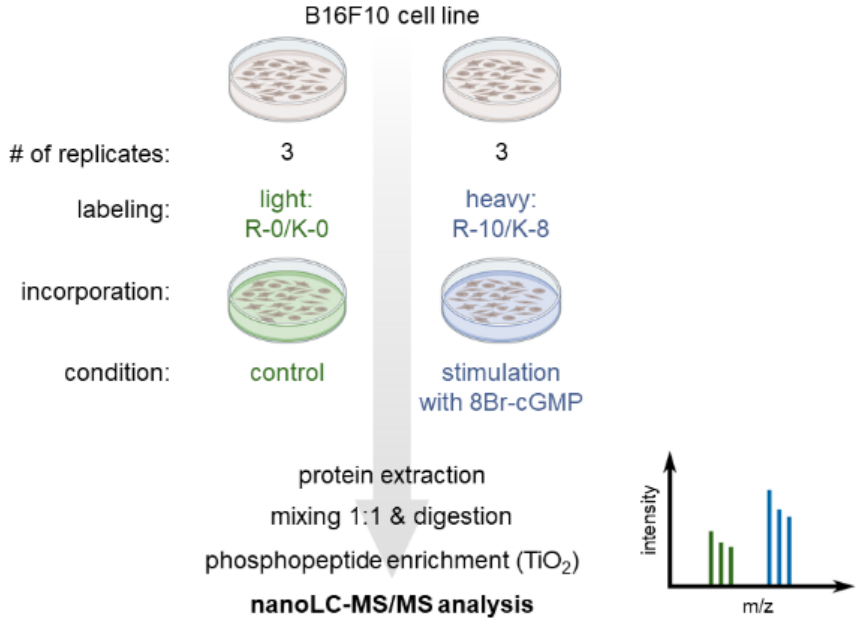

Figure 2-1 ***SILAC workflow.***

Cultured B16F10 cells were separated into three replicates each for two conditions. The cells of the control condition were labeled with light SILAC medium (R-0/K-0) and not stimulated. The cells of the 8Br-cGMP condition were labeled with heavy SILAC medium (R-10/K-8) and stimulated with 8Br-cGMP (0.5 mM, 5 min, 37 °C). After protein extraction samples of each condition were mixed 1:1. All samples then underwent digestion, phosphopeptide enrichment, and nanoLC-MS/MS analysis. An MS spectrum, which can be used to calculate the difference in abundance of specific phosphopeptides in both conditions is represented on the right.

using amino acids of specific mass that are added to the culture medium. Labeled cells can be harvested, mixed, digested, and subsequently measured by nano liquid chromatography with tandem MS (nanoLC-MS/MS). Peptides are identified based on their MS spectra, and ratios of according SILAC pairs can be used for relative quantification.

In the present study, the phosphoproteome of B16F10 cells was analyzed according to the workflow shown in Figure 2-1. The cells were grown in SILAC-DMEM lacking R and K supplemented with 1x Pen/Strep, 10 % FCS and specific stable isotopes of R and K. Light SILAC medium contained K-0 (L-[$^{12}C_6$, $^{14}N_2$]) and R-0 (L-[$^{12}C_6$, $^{14}N_4$]), while heavy SILAC medium contained K-8 (L-[$^{13}C_6$, $^{15}N_2$]) and R-10 (L-[$^{13}C_6$, $^{15}N_4$]). After successful incorporation of the isotopes into the entire proteome of the cultured cells (Section 2.4.1.1), the cells were treated according to their condition, and proteins were extracted (Section 2.4.1.2). Specifically, cells labeled with light isotopes were kept unstimulated as a control condition, and cells with heavy labels were stimulated with 8Br-cGMP. Protein extraction followed with a urea-based lysis buffer. Dr. Velic performed all further processing (Section 2.4.1.3). Proteins of both conditions were mixed equally, digested with trypsin, and phosphopeptides were enriched with TiO_2 beads. Finally, the samples were analyzed with nanoLC-MS/MS (Section 2.4.3) to elucidate which phosphopeptides were more or less abundant after cGKI activity was stimulated.

2.4.1.1 Integration of isotopes

To ensure the incorporation of the isotopes into the entire proteome of the B16F10 cells, they were cultured in light or heavy SILAC medium for 10 days and split every 2-3 days. The incorporation rate for the heavy label was measured at 98.4 % under these conditions. For the experiment presented in this thesis, B16F10 cells were gradually expanded in their respectively labeled SILAC medium until six 80% confluent 10cm dishes per condition were reached on day 10 for stimulation.

2.4.1.2 Stimulation and lysis of B16F10 cells

Before stimulating the B16F10 cells, they were washed twice in SILAC-DMEM and then serum starved in fresh SILAC-DMEM for 3 h at 37 °C. After another wash in SILAC-DMEM, the cells labeled with light isotopes were incubated in SILAC-DMEM alone, while the ones labeled with heavy isotopes were stimulated with SILAC-DMEM supplemented with 0.5 mM 8Br-cGMP for 5 min at 37 °C. To stop the stimulation, the medium was aspirated, and the cells were washed twice with cold PBS. The dishes were then placed on ice, and 500 µl SILAC lysis buffer was added to each. A cell scraper was used to detach the cells from the dish, before transferring them to a 1.5 ml tube. After adding 0.5 µl benzonase (Millipore) and vortexing shortly, the cells were incubated for 10min at RT. The resulting lysate was centrifuged for 15 min at 2800×g, 10 °C, and the supernatant transferred to a new tube, pooling lysates of two 10 cm dishes for one replicate. The samples were precipitated with acetone and MeOH, reconstituted in 500 µl denaturation buffer per replicate, and the protein concentration was determined using the Bradford assay as described above (Section 2.3.1.2.1).

2.4.1.3 Sample processing and phosphopeptide enrichment

The steps described in this section were performed by Prof. Boris Maček and Dr. Ana Velic (Proteome Center Tübingen, University of Tübingen). Samples were further processed and prepared for MS analysis as previously described [97]. Briefly, after mixing the samples 1:1, they were reduced and alkylated before tryptic digestion and purification. Then, phosphopeptides were enriched with TiO_2 beads before nanoLC-MS/MS measurements were performed.

2.4.2 Stable isotope dimethyl labeling by reductive amination

To measure the abundance of specific peptides in different samples of non-proliferating post mitotic cells, a chemical instead of a metabolic labeling technique can be used. In the present study, SIDL by reductive amination was performed. Here, all primary amines in peptides react with formaldehyde to form a Schiff base, which is then rapidly reduced by cyanoborohydride. Depending on the isotopomeric dimethyl reagents used, a different mass is added per label. For the light label, regular formaldehyde and cyanoborohydride are used in the reaction, adding 28 Da per primary amine. For the medium label,

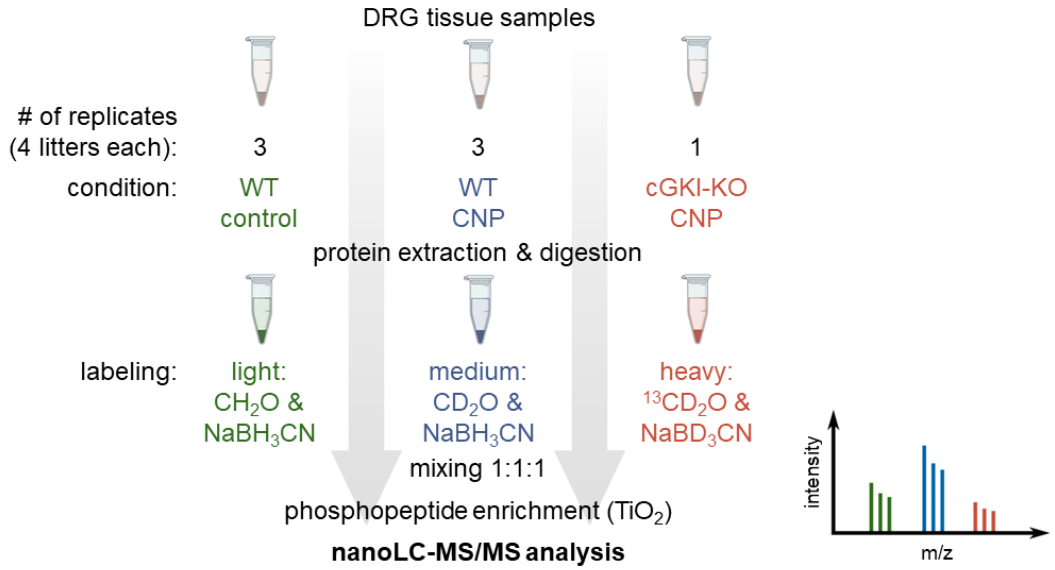

Figure 2-2 ***SIDL workflow.***

DRG tissue samples were collected from E13.5 embryos of WT and cGKI-KO mice. One replicate comprises the DRGs of one litter. Three conditions were compared: WT control, WT CNP, and cGKI-KO CNP. The latter two underwent CNP stimulation (0.25µM, 10min, 37°C). Labeling followed protein extraction and digestion of each replicate with light, medium, and heavy isotopes respectively for the three conditions. The conditions were mixed in equal parts, underwent phosphopeptide enrichment and analyzed via nanoLC-MS/MS. An MS spectrum, which can be used to calculate the difference in abundance of specific phosphopeptides in the conditions is represented on the right.

deuterated formaldehyde and regular cyanoborohydride are used, resulting in an additional 32 Da per primary amine. For the heavy label, deuterated and ^{13}C-labeled formaldehyde and deuterated cyanoborohydride are used, leading to an additional 36 Da per primary amine [98–100].

The workflow of the SIDL experiment performed in this thesis is shown in Figure 2-2. DRG tissue samples were collected from E13.5 mice (Section 2.4.2.1). One replicate required protein from four litters of embryos, assuming an average of eight embryos per litter. Tissue of both WT and cGKI-KO animals was collected and stimulated (Section 2.4.2.2). Three different conditions were compared: WT DRG under control conditions without stimulation (WT control), WT tissue stimulated with CNP (WT CNP), and cGKI-KO tissue stimulated with CNP (cGKI-KO CNP). After the treatment, the proteins of all samples were extracted with a RIPA buffer. Dr. Velic conducted all subsequent steps (Section 2.4.2.3). The proteins were digested with trypsin, chemically labeled according to the scheme shown in Figure 2-2, and mixed in equal parts. To measure the phosphoproteome, an enrichment with TiO_2 beads preceded the nanoLC-MS/MS analysis (Section 2.4.3) by which the mass difference of the labels was used to compare phosphopeptide abundance in the different conditions.

2.4.2.1 Collection of E13.5 DRG

For the collection of E13.5 DRG tissue, embryos were collected as described above (Section 2.3.2.1) and transferred to a 10 cm dish with ice-cold PBS (or labeled 12-well plate in case of cGKI-KO tissue, where genotyping is required). The spinal cord was isolated first as described previously [96]. A wet filter paper was placed in a sylgard dish (10 cm dish coated in a silicone elastomer; SYLGARD™ 184, Dow), on which an embryo torso was positioned with the dorsal side up. All following steps were performed under a stereo microscope (ZEISS). Using two forceps, the skin was carefully opened along the spinal cord from the middle. The DRGs and spinal cord were then detached from the surrounding cartilage by sliding fine forceps with polished tips horizontally, first on one side then on the other after turning the embryo 180°. The spinal cord was completely severed by cutting beneath it with the same forceps and transferred to a small dish with ice-cold HBSS (Sigma Aldrich). The DRGs were cut off along the entire length of the spinal cord using small spring scissors, starting from the top and moving from right to left. After rotating the spinal cord 180°, the same procedure was repeated on the opposite side. All the DRGs were transferred to a tube containing 500 µl HBSS on ice, using forceps.

2.4.2.2 Stimulation and lysis of tissue

The DRGs of one litter collected in HBSS were centrifuged for 5 min at 1500×g, 4 °C. The medium was carefully aspirated, and the pellet resuspended in fresh HBSS supplemented with 1x PhosSTOP and 0.25 µM CNP (without CNP for WT control condition). The DRGs were vortexed briefly and incubated for 10 min at 37 °C on a shaker at 400 rpm. To stop the stimulation, the DRGs were centrifuged again for 5 min at 1500×g, 4 °C, and the supernatant was discarded. The DRGs were lysed in 350 µl of SIDL lysis buffer and homogenized with a plastic stomper. After a 10min incubation on ice, 0.5 µl benzonase was added, the lysate was briefly vortexed and incubated for another 10 min at RT. Finally, the lysate was centrifuged 15 min at 2800×g, 10 °C, and the supernatant was transferred to a new tube. The protein concentration of the sample was measured with the Pierce™ BCA Protein Assay Kit (Thermo Scientific) according to the included company instructions. Until further processing, samples were stored at -80 °C.

2.4.2.3 Sample processing, labeling and phosphopeptide enrichment

The steps described in this section were performed by Prof. Boris Maček and Dr. Ana Velic (Proteome Center Tübingen, University of Tübingen). Samples were further processed and prepared for MS analysis as previously described [100]. After reducing and alkylating the samples, the proteins were precipitated before tryptic digestion, acidification, and desalting. Chemical labeling of the peptides followed on-column with CH_2O and $NaBH_3CN$ for the WT control condition (light), with CD_2O and $NaBH_3CN$ for the WT CNP condition (medium), and with $^{13}CD_2O$ and $NaBD_3CN$ for the cGKI-KO CNP condition (heavy). The samples were then mixed 1:1:1, and phosphopeptides were enriched with TiO_2 beads before nanoLC-MS/MS measurements [100].

2.4.3 MS and data analysis of the phosphoproteome

The steps described in this section were performed by Prof. Boris Maček and Dr. Ana Velic (Proteome Center Tübingen, University of Tübingen). NanoLC-MS/MS analysis of all phosphopeptide samples was performed on an Easy-nLC 1200 ultrahigh-pressure system coupled to the quadrupole Orbitrap mass spectrometer Q Exactive HFX (Thermo Fisher Scientific) via a nanoelectrospray ion source. The raw data of the MS spectra were then processed with the MaxQuant software suite as previously described [97,100].

For the SILAC experiment, three replicates were measured, giving a value each for a specific phosphopeptide intensity, normalized ratio of phosphorylation events from the 8Br-cGMP condition in comparison to the control condition, and significance B.

For the SIDL experiment, only for one replicate were all three conditions (WT control, WT CNP, and cGKI-KO CNP) present. Two additional replicates of the WT conditions were processed, resulting in three replicates total. Each replicate was measured twice, with each measurement giving values of intensity, and ratio for a specific phosphopeptide. During SIDL experiments, both the phosphoproteome and the proteome were measured. Hence, the ratios of CNP compared to control conditions were normalized by proteome data. For each normalized peptide ratio, a significance B value is calculated to determine outliers [101]. In the end, this leads to six values each of intensity, normalized by proteome ratio and significance B for WT CNP vs. WT control as well as two values each for cGKI-KO CNP vs. WT control.

2.4.4 Data processing and presentation

Following the recommendations of Prof. Boris Maček and Dr. Ana Velic, for all MS data a threshold for posterior error probability (PEP) was set to a maximum of 0.05 to filter out false positive phosphorylation events. For the regulation of a phosphopeptide to be considered significant in the present thesis, the significance B value must be ≤ 0.05 in over 50 % of replicates. Means were calculated for the intensity as well as the ratio. The mean ratio must exceed 1.5 to be classified as upregulation, and an upper limit of 0.67 is set for the classification of downregulation. For graphic data presentation, mean intensities were log10 transformed and mean ratios were log2 transformed. Graphs were prepared with the GraphPad Prism software (version 9.5.1).

The database of the UniProt Consortium (uniprot.org) [102] was used to further annotate information for phosphopeptides and the respective proteins, including their cell compartments and functional domains. Additionally, the database was used to complete the sequence of the phosphorylation site, such that the sequence contains the three amino acids preceding the modified residue.

2.5 Analysis of putative cGKI phosphorylation substrates

Several approaches were combined in this thesis to elucidate the validity of putative cGKI phosphorylation substrates found in the phosphoproteome analysis studies described above (Section 2.4). To show the presence of the respective mRNA in B16F10 cells and embryonic DRG neurons, an RT-PCR was performed (Section 2.5.1). The expression patterns of candidate proteins in E13.5 DRGs and the spinal cord were studied both by WB analysis of subcellular fractions as well as by histological analysis of transversal tissue sections of embryos (Section 2.5.2). To validate the putative phosphorylation site *in vitro*, an analogue-sensitive kinase (ASK) assay was performed (Section 2.5.3). Additionally, the bifurcation phenotype of several mouse lines was analyzed to understand the mechanistic involvement of putative cGKI phosphorylation substrates in the sensory axon bifurcation process (Section 2.5.4).

2.5.1 RT-PCR

As a first step of validating the presence of the found putative cGKI phosphorylation substrates (Section 2.4.2) in B16F10 cells and embryonic DRGs, their transcription was analyzed. After extracting RNA, a cDNA library was created by reverse transcription (Section 2.5.1.1). Using this library as template, the presence of the mRNA of the candidates could be determined by PCR with specific primers (Section 2.5.1.2).

2.5.1.1 Creation of cDNA library

2.5.1.1.1 RNA preparation

To inactivate the RNases in the used materials, they were treated with DEPC. Specifically, tubes and tips were submerged in DEPC water and incubated overnight at RT. After decanting the DEPC water for repeated use, all DEPC treated materials as well as DEPC water were autoclaved to destroy the residual DEPC.

The preparation of RNA was performed with RNase-free material. For the B16F10 cell line, material from two T175 flasks (Corning) were collected. For the E13.5 DRGs, tissue from one litter of WT mice was collected as described above (Section 2.4.2.1). After centrifuging for 5 min at 1500×g, 4 °C, the supernatant buffer was removed, and the sample was resuspended in 600 µl TRIzol, homogenized with a potter then filled up to 1600 µl with TRIzol and incubated for 5 min at RT. After adding 320 µl chloroform, the sample was vortexed and centrifuged for 15 min at 10,000×g, 4 °C. While avoiding the interphase, 800 µl of the upper phase were transferred to a new tube and mixed with 660 µl isopropanol. The sample was incubated for 10 min at RT and centrifuged for 10 min at 12,000×g, 4 °C before aspirating the supernatant. The RNA pellet was washed with 1.5 ml of 75 % EtOH, incubated for 5 min at RT, and centrifuged for 5 min at 12,000×g, 4 °C. After aspirating the supernatant once more, the pellet was air-dried shortly at 37 °C, then carefully solved in RNase-free water by pipetting up and down. Before determining the yield at a NanoDrop™ 2000 spectrophotometer (Thermo Scientific), the sample was incubated 5 min at 37 °C and 5 min on ice.

2.5.1.1.2 First-strand cDNA synthesis

A cDNA library was created with the SuperScript™ III kit (Invitrogen) using 8 µg RNA and random primers (Invitrogen) according to the kit instructions. To remove RNA complementary to the cDNA, 1 µl RNase H (Invitrogen) was added and incubated for 20 min at 37 °C. This reaction was inactivated by heating the sample to 70 °C for 15 min.

2.5.1.2 Taq-PCR

The primers for the Taq-PCRs were designed with the help of the Primer3Plus online tool (primer3plus.com) with a product size range of 200-350, minimal and maximal primer sizes of 19 and 21, respectively, as well as minimal and maximal primer GC % of 40 and 60. The mispriming/repeat library was set to "RODENT_AND_SIMPLE". All other settings were kept at the default values. The goal of choosing multiple primer pairs for each candidate was to cover all known mRNA transcripts and thus indicate the existence of any isoform of the respective protein. All used primers as well as the corresponding PCR products are listed in Table 2-13.

Table 2-13 ***Primers for RT-PCR with cDNA library of E13.5 DRGs.***

*Transcript of **	*Primer*	*Sequence*	*PCR product*
Acin1	Forward 1	GGG AAA GAC GAT CAT CCA GA	248 bp
	Reverse 1	AAA CTG CTT CAG GGT TGG TG	
	Forward 2	GCA GAC CAA GTC AGC AAT GA	307 bp
	Reverse 2	AGT CAT CGG CAT GAA GAT CC	
Cad	Forward 1	GTT CTC CTT CTC ACG CTT GG	242 bp
	Reverse 1	GGC TGG CAT AGA GGC TGT AG	
	Forward 2	CCA AGC AGG AGG AGT TTG AG	265 bp
	Reverse 2	TAC ATG CCG TTC TCA GCT TG	
Clasp1	Forward 1	ACT GGG GTT TCC ACA GTC AC	261 bp
	Reverse 1	GCT GGA GAG ATC CTG TCG TC	
	Forward 2	GTG GCA TTC CCC ATT ATC TG	342 bp
	Reverse 2	CTT TTG CTT GCA CAG ATC CA	
Crmp1	Forward 1	CCT GGT GGA GTG AAG ACC AT	300 bp
	Reverse 1	CTC TTC CCG AAC ACC ATC AT	
	Forward 2	GCA TCT CTA CCA GCG TGT CA	237 bp
	Reverse 2	CCT GTA CGC CTT GGA TTG TT	
Map1b	Forward 1	GGG AGT CTG TGG TCA GTG GT	282 bp
	Reverse 1	AAG ATG CAG GTT CTC GGC TA	
	Forward 2	GAC ACG GAC CCC TGA AGT AA	335 bp
	Reverse 2	CTG AGG GGG ACT TCT TTT CC	
Mena	Forward 1	AAC TTT GGC AGC AAA GAG GA	251 bp
	Reverse 1	TTC TGT CGC TGC TGT TCT TG	
	Forward 2	TGG AGG GAA TAC TGG GAG TG	275 bp
	Reverse 2	TGC CGT TCA TTG TGT TTG TT	
Nedd4l	Forward 1	AGA GGA GGG AGA ATC CCG TA	274 bp
	Reverse 1	CAG GAA GTC GTC TCG TGT CA	
	Forward 2	TGA ACG ACT GGA GAC AGC AC	234 bp
	Reverse 2	TGG GTA GTT TTT CGG GAC TG	

** For abbreviations, see List of Abbreviations.*

The Taq polymerase kit 1 (Invitrogen) was used to perform the PCR with a reaction mix according to the kit instructions. The PCR program consisted of an initial denaturation step for 2 min at 94 °C, 35 PCR cycles (30 sec denaturation at 94.5 °C, 30 sec annealing at 55 °C, 30 sec extension at 72 °C), followed by a final extension step for 10 min at 72 °C. The DNA fragments were then run in an agarose electrophoresis and detected by UV light as described above (Section 2.2.1.1).

2.5.2 Expression pattern

After demonstrating the presence of their respective transcripts, the protein expression pattern of the candidates was analyzed. The subcellular location of the candidates was detected in E13.5 DRG tissue samples via WB analysis of subcellular protein fractions (Section 2.5.2.1). The tissue distribution of the proteins was analyzed on transversal sections of E13.5 mouse and E8 chick embryos by IF staining as described above (Section 2.3.2.3) and of E12 mouse embryos by immunohistochemical (IHC) staining (Section 2.5.2.2).

2.5.2.1 Analysis of subcellular fractions of E13.5 DRGs

To determine the subcellular localization of putative cGKI phosphorylation substrates in E13.5 DRGs, subcellular fractions were produced with the cell compartment kit. The DRGs of one litter of WT embryos were collected as described above (Section 2.4.2.1) before following the fractionation protocol for "tissue samples" given by the supplier in the "Qproteome Cell Compartment Handbook". The fractions were separated by SDS-PAGE (Section 2.3.1.2.2) and analyzed via WB (Section 2.3.1.2.3).

2.5.2.2 Histological analysis of E13.5 mouse embryos

For IHC staining, embryos were embedded in paraffin (Leica) after dehydrating the tissue in an increasing EtOH concentration series (70 %, 80 %, 95 %, 100 %) and toluene, then incubating in paraffin at 56 °C overnight. 10 µm sections were cut with a rotary microtome (HM 335 E, Microm) and mounted on paraffin section object slides (Fisher Scientific). Before staining, the sections were rehydrated in toluene and a decreasing EtOH concentration series (100 %, 90 %, 80 %, 70 %, 60 %) and lastly PBS. Sections were framed with PAP-Pen (Science Services), then endogenous peroxidases were blocked by incubation with peroxidase blocking solution for 20 min at RT in a wet chamber. After a washing step with PBS, antigens were unmasked with antigen retrieval solution for 15 min at RT then for 10 min at 92 °C. The solution was left to cool down for 10 min, and, after a washing step in TBS-T, the slides were incubated in IHC blocking buffer for 2 h at RT in a wet chamber. Immunospecific labeling with primary antibodies in IHC antibody dilution buffer was done overnight at 4 °C in a wet chamber. The incubations with antibodies and ABC solution were followed by three washing steps with TBS-T for 5 min each at RT and under constant agitation. Incubation with biotinylated secondary antibody in IHC antibody dilution buffer followed for 2 h at RT in a wet chamber. The ABC solution was prepared by diluting Reagent A and B (VECTASTAIN® ABC-HRP Kit; VectorLabs) 1:50 in PBS, incubating 30 min at RT in the dark, and diluting the resulting mixture 1:1 in TBS-T directly before use. The slides were incubated in ABC solution for 30 min at RT in an opaque wet chamber. DAB staining solution was added, and the slides were incubated at RT until the color developed. Staining was stopped by immersing the slides in tap water. Slices were counterstained with Mayer's Hematoxylin solution (Carl Roth) until a nuclear staining was visible under a stereo microscope. The staining was stopped by immersing the slides in running tap water for 10 min. The sections were covered in Aquatex (Sigma Aldrich) and glass cover slips and let dry overnight at RT. Brightfield images for documentation were acquired at an Axioskop 20 (ZEISS) with an EOS 750 D (Canon) digital camera mounted with a 2.5x lens and controlled with the EOS utility software (Canon).

2.5.3 Validation of putative phosphorylation sites

To validate whether the candidates can be phosphorylated by cGKI *in vitro*, an ASK assay was performed. To confirm the phosphorylation of the candidate proteins at the specific site found during phosphoproteome analysis (Section 2.4), not only the native protein but also a mutant was examined. Here, a point mutation caused an A substitution of the putatively phosphorylated S residue. This *in vitro* validation process is shown in Figure 2-3. In a first step, 3xFLAG-tagged variants of the candidate proteins were produced by transiently transfecting COS7 cells with respective expression vectors. After two days in culture cytosolic proteins were extracted from the transfected COS7 cells (Section 2.5.3.1). Then, the ASK assay was performed with an analogue sensitive mutant of cGKI. Here, cGKI substrates were thiophosphorylated and subsequently transformed to thio-phosphate esters (TPEs) which could be detected via WB analysis (Section 2.5.3.2).

2.5.3.1 Production of 3xFLAG-tagged proteins

COS7 cells were cultured analogous to B16F10 cells as described above (Section 2.3.1). Cells were seeded in 15 cm dishes (Corning) and grown until 60-70 % confluency. Transfection with mammalian expression vectors was performed with Lipofectamine™ 3000 (Invitrogen) according to the provider's instructions. Preparation of cytosolic proteins was performed 48 h after transfection.

A 15 cm dish with transfected COS7 cells was washed twice with PBS, before the cells were subsequently scraped in 2 ml fresh ice-cold PBS and transferred to a tube. All following steps were performed

on ice. The cells were centrifuged for 10 min at 1850×g, 4 °C and the supernatant was discarded. The pellet was resuspended in five volumes of hypotonic buffer and centrifuged again for 5 min at 1850×g, 4 °C. After discarding the supernatant, the cells were replenished with hypotonic buffer up to three volumes of the original pellet. After leaving the cells to swell on ice for 10 min, they were homogenized with a plastic stomper and the nuclei were spun down for 15 min at 3300×g, 4 °C. The supernatant was transferred to an ultracentrifuge tube, and 0.11 volumes of 10x cytoplasmic extraction buffer were added. The sample was then centrifuged for 1 h at 100,000×g, 4 °C, the supernatant was transferred to a new tube, and 0.9 volumes of replenishment buffer was added. The protein lysates were stored at -80 °C until use.

For purification of FLAG-tagged proteins, cytosolic proteins from five 15 cm dishes of transfected COS7 cells were processed with anti-FLAG magnetic beads (Sigma Aldrich). 30 µl of beads were washed twice with FLAG IP wash buffer 1 before adding the lysate and incubating for 1.5 h at 4 °C on an end-over-end rotator. The beads were separated on a magnetic stand and the supernatant was saved as flow through fraction. The beads were washed five times with FLAG IP wash buffer 2 at a volume equivalent to the lysate that was loaded. Between washing steps, beads were separated on a magnetic stand, and the first two supernatants were saved as wash fractions 1 and 2. To elute FLAG-tagged proteins from the beads, they were incubated twice in elution buffer for 1h at 4 °C on an end-over-end rotator. Both elution fractions were saved. All fractions were stored at -20 °C except elution fraction 1, which was stored at -80 °C until use. To confirm the purification of the 3xFLAG-tagged protein, all saved fractions were analyzed via WB (Section 2.3.1.2) at equal volume fractions.

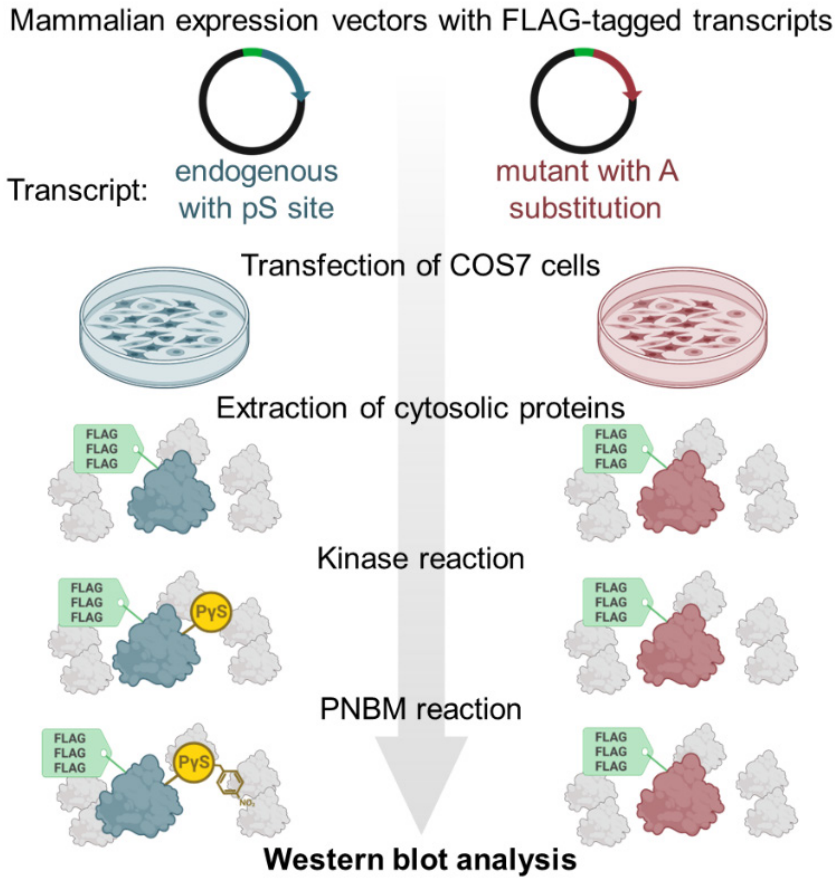

Figure 2-3 ***Workflow for the validation of putative cGKI phosphorylation sites via ASK assay****.*

Mammalian expression vectors with FLAG-tagged transcripts of candidates are transiently transfected into cultured COS7 cells. Two transcripts per candidate were used, one containing the endogenous sequence with the putative pS site, one containing a mutant with an A substitution at that site. Cytosolic proteins of the COS7 cells are extracted and used as input for the kinase reaction with ASK mutant of cGKIα and bulky ATP with an additional gamma-thiol resulting in thio-phosphorylated (PγS) substrates. In a subsequent PNBM reaction these are transformed in to TPEs, which are detectable by antibody.

2.5.3.2 Analogue sensitive kinase assay

To validate specific substrates of cGKI *in vitro*, the ASK assay was used. Generally, ASKs are engineered with a mutation in their ATP binding site that allows them to accept an N6-alkylated ATP without losing their substrate specificity. When using such a bulky ATP with an additional gamma-thiol (A*TPγS) these mutated kinases mediate a thio-phosphorylation in their substrates instead of a phosphorylation. In a subsequent step, thio-phosphates can be alkylated by PNBM to yield TPEs, which can in turn be recognized by a specific antibody [103–105].

A 3xFLAG-tagged ASK mutant of cGKIα (3xFLAG-cGKIα-ASK) was developed by PD Dr. Hannes Schmidt (University of Tübingen), and a respective expression plasmid was kindly provided for this study. For the kinase reaction, isolated cytoplasmic proteins from transfected COS7 cells or purified FLAG-tagged proteins were mixed with the aforementioned 3xFLAG-cGKIα-ASK (produced and purified as described above), 1 mM 6-PhEt-ATPγS, and 1.25 mM 8pCPT-cGMP in kinase reaction buffer in a volume of 18 µl and incubated for 15 min at 30 °C on a shaker at 350 rpm. To stop the kinase reaction, 50 µM EDTA was added. To initiate the transformation of thio-phosphate residues to TPE residues, 2.5 mM PNBM was added and incubated for 2 h at RT.

The samples were analyzed via WB as described above (Section 2.3.1.2.2 and 2.3.1.2.3). To facilitate the separation of bigger proteins, a 7.5 % separating gel was used. The same PVDF membrane was re-incubated several times with different primary antibodies. Between re-incubations, the membrane was stripped by detergent and heat, specifically with stripping buffer for 10 to 30 min at 56 °C. The stripping buffer was washed off with TBS-T three times for 10 min each under constant agitation. The membrane was then re-blocked in WB blocking buffer and washed in TBS-T before the next overnight incubation with the primary antibody and subsequent detection by HRP-coupled secondary antibody by chemiluminescence. A densitometric analysis was done on UV images with the ImageJ software (version 1.53) and statistical analysis as well as graphic representation of the results was done with the GraphPad Prism software (version 9.5.1).

2.5.4 Axon tracing

To investigate the involvement of known cGKI phosphorylation substrate Vasp as well as the ability of cGKI to bind substrates in the process of sensory axon bifurcation, tracing studies were performed to evaluate the bifurcation phenotype of several mouse models. Two different techniques were utilized here, as described below.

2.5.4.1 DiI staining of E13.5 DRG neurons in whole mount of spinal cord

Spinal cords of E13.5 embryos were dissected, the DRG neurons were stained with the lipophilic tracer 1,1'-dioctadecyl-3,3,3',3'-tetramethylindocarbocyanine perchlorate (DiI; Sigma Aldrich), and the bifurcation was analyzed as previously described [96]. Briefly, dissected spinal cords of E13.5 mouse embryos (Section 2.3.2.1 and 2.3.2.1) are incubated in PFA fixative for 2 h on ice. For the DiI labeling, glass capillaries were prepared with a micropipette puller to obtain a fine tip, which was dipped in a drop of DiI stock solution under microscopic control. Fixed spinal cords were positioned under a stereo microscope with the ventral side facing up, to cut along the floorplate and open the spinal cord along the entire length. After placing the spinal cord dorsal side up, in an inverted open book formation, on a slide, every second DRG on both sides of the spina cord was carefully pierced with the DiI-covered glass pipette tip. The thus labeled spinal cords were submerged again in PFA fixative and incubated overnight at 4 °C to allow the lipophilic tracer to diffuse along the membrane of axons. For microscopic analysis, spinal cords were mounted in PBS.

2.5.4.2 Imaging of P15 DRG neurons in whole mount of spinal cord

Due to the late activation of the Thy1 promoter, the bifurcation phenotype of DRG neurons from Vasp-KO mice transgenically expressing a Thy1-YFP-H reporter was analyzed at P15. A small fraction of DRG neurons in these reporter mice are labeled with YFP, which enables the analysis of individual sensory axons [94]. The spinal cords from P15 mice were incubated in PFA fixative for 2 h at RT before being washed in PBS, mounted, and examined as previously described [6].

2.5.4.3 Data acquisition and analysis

Mounted spinal cords were documented at a confocal LSM 710 setup (ZEISS) and images were converted and assembled for figures in the ImageJ (version 1.53) software. Bifurcation events and turns were counted at the microscope by eye and the data was entered into the GraphPad Prism software (version 9.5.1) to prepare graphs.

2.6 PROTEOME ANALYSIS OF PUTATIVE GC-B INTERACTORS

The proteome analysis of adult heart tissue and E13.5 DRG tissue of GC-B-HA mice to identify putative GC-B interactors was performed in collaboration with Dr. Karsten Boldt and Katrin Junger (Core Facility for Medical Bioanalytics [CFMB], University of Tübingen). Specifically, the on-bead digest and MS analysis were performed at the CFMB (Section 2.6.2).

2.6.1 Tissue lysis and co-immunoprecipitation

The whole heart of adult mice was dissected and washed in PBS, while E13.5 DRG tissue samples were collected as described above (Section 2.4.2.1). After aspirating any medium, the tissue samples were snap frozen in liquid nitrogen and stored at -80 °C until use. The tissue was mixed with IP lysis buffer, homogenized with a plastic stomper, and incubated for 30 min at 4 °C in an end-over-end rotator. The sample was centrifuged three times for 10 min each at 16,000×g, 4 °C, transferring the supernatant to a new tube each time. The protein concentration was determined with the Pierce™ BCA Protein Assay Kit (Thermo Scientific) according to the supplier's instructions. The concentration of the samples was adjusted to the required amount by dilution with IP lysis buffer. Before starting the IP procedure, the Pierce anti-HA magnetic beads (Thermo Scientific) were washed once in IP TBS, once with IP lysis buffer, and twice with HA IP wash buffer. For each washing step, the beads were separated with a magnetic stand. After the last washing step, the beads were ready for the lysate, which was loaded, and the samples were brought to the CFMB on ice, where all further processing was done. For the experiments with adult heart tissue, n=4 technical replicates were measured of lysates from one P95 WT mouse and a pool of three P75 GC-B-HA mice. For the experiments with E13.5 DRG tissue, n=4 biological replicates per genotype were measured of lysates originating from one litter of embryos each.

2.6.2 On-bead-digest, sample preparation, and MS analysis

The steps described in this section were performed by Dr. Karsten Boldt and Katrin Junger (CFMB, University of Tübingen). After a further 30 min to 1h incubation at 4 °C on an end-over-end rotator, the beads were washed three times with IP TBS before starting the on-bead-digest as previously described [106]. The samples were subjected to overnight tryptic digestion followed by alkylation, then desalting via StageTips (Thermo Fisher). MS analysis of the processed samples was performed as previously described [106] on an Ultimate3000 RSLC system coupled to an Orbitrap Fusion Tribrid mass spectrometer (Thermo Fisher) and label-free quantification of MS spectra was performed using the MaxQuant software. The samples were filtered such that each protein was quantified in at least one genotype (GC-B-HA and WT) in over 50 % of samples. For all these proteins, the median label-free quantification intensity was calculated per genotype. Then the difference of these medians – Δ(HA-WT) = median HA - median WT – was calculated, resulting in one value per protein. A positive ΔHA-WT indicates that the protein was enriched in the eluates of the pull-down performed on tissue of GC-B-HA mice and thus a possible interaction with GC-B. A t-test was performed to test for reproducibility and a significance A test was performed to detect outliers of the normal distribution.

2.6.3 Data processing and presentation

Following the recommendation of Dr. Karsten Boldt, both statistical tests (t-test and significance A test) must yield a value of at most 0.05 for the interaction to be considered significant. Additionally, the difference Δ(HA-WT) must exceed a value of 2 for the protein to be classified as putative GC-B interactor. Further information was annotated for each protein using the database of the UniProt Consortium (uniprot.org) [102]. Graphs were prepared with the GraphPad Prism software (version 9.5.1) plotting log10 transformed intensity against the difference of the medians.

3 RESULTS

To further elucidate the cGMP signaling pathway that regulates embryonic DRG axon bifurcation I searched for both cGKI substrates and GC-B interactors. After confirming the presence of the involved pathway components in the respective tissues (Section 3.1), screens for putative cGKI phosphorylation targets were performed on the murine melanoma cell line B16F10 and E13.5 DRGs (Section 3.2). Here, stable isotope labeling and phosphoproteome analysis was done on samples after treatment with cGKI activating compounds and under control conditions. In identifying putative cGKI phosphorylation substrates, distinct characteristics were considered. Among those were the presence of a cGKI consensus sequence, an LZ domain, and a kinase activity domain as well as the cell compartment of candidates. A number of validation experiments were then performed on a selection of candidates to confirm their expression in the area of interest and their phosphorylation by cGKI (Section 3.3). Axon tracing studies were then performed on KO mouse models of known cGKI substrates to investigate their involvement in the bifurcation process of embryonic murine DRG neurons (Section 3.4). Additionally, an LZ mutant of cGKI was studied likewise to confirm the involvement of LZ domain interactors of cGKI in sensory axon bifurcation. Lastly, GC-B interactors were screened for in murine tissue lysates of adult hearts and embryonic DRGs (Section 3.5). Here, Co-IP with an anti-HA pull-down followed by proteome analysis were performed with tissue from mice with HA-tagged GC-B and WT mice as control. To identify relevant interactors of GC-B, characteristics like kinase or phosphatase activity, the presence of an LZ domain, and the cell compartment were considered.

3.1 A cGMP SIGNALING PATHWAY IS PRESENT IN A MURINE MELANOMA CELL LINE AND EMBRYONIC DRGS OF MICE AND CHICK

A CNP-induced signaling cascade regulates axon bifurcation in murine somatosensory neurons via activation of cGKI. To identify novel cGKI substrates, one experimental approach is to perform phosphoproteomic analysis of a cell line after SILAC. Here, I used the murine melanoma cell line B16F10 and, as a first step confirmed the expression of all necessary pathway components in this cell line (Section 3.1.1). GC-B-HA mice and chick embryos represent systems that would open new possibilities for experimental approaches. Thus, I aimed to confirm the expression pattern and tissue distribution of the involved cGMP signaling pathway components that are established in other mouse models in these systems (Section 3.1.2).

3.1.1 B16F10 cell line

In subcellular fractions of cultured B16F10 cells, cGKI was detected by WB analysis only in the fraction containing cytosolic proteins, not in the nuclear or membrane fractions. This was shown both under control conditions as well as after stimulation of cultured cells with 0.25 µM CNP for 10min at 37°C (Figure 3-1A). Similarly, an IF staining of cGKI in cultured B16F10 cells revealed the unchanged localization of the kinase in the cytosol under control conditions as well as after stimulation of the cells. Two stimulation conditions were tested with CNP (0.25 µM, 10 min, 37 °C; Figure 3-1B) and the membrane penetrable cGMP derivate 8Br-cGMP (0.5 mM, 5 min, 37 °C; Figure 3-1C). The subcellular distribution of cGKI was comparable under all investigated conditions. The kinase is found throughout the entire cytosol with no apparent accumulation near the membrane or nucleus. While UniProt lists the cytosol, membrane, and Golgi apparatus as compartments for cGKI (UniProt ID: P0C605), at the present resolution no statement can be made about the presence of cGKI in any organelle.

3.1.2 Embryonic DRGs in mice and chick

In transversal sections of E13.5 mouse embryos, an IF co-staining showed cGKI in NFH-positive cells, with somata in the DRG and axonal projections within the DREZ and the dorsal funiculus of the spinal cord. This was shown for both WT and GC-B-HA mice (Figure 3-2A). Similarly, co-staining of HA and NFH showed the presence of HA-tagged GC-B in DRG neurons of GC-B-HA mice but not in WT mice (Figure 3-2B).

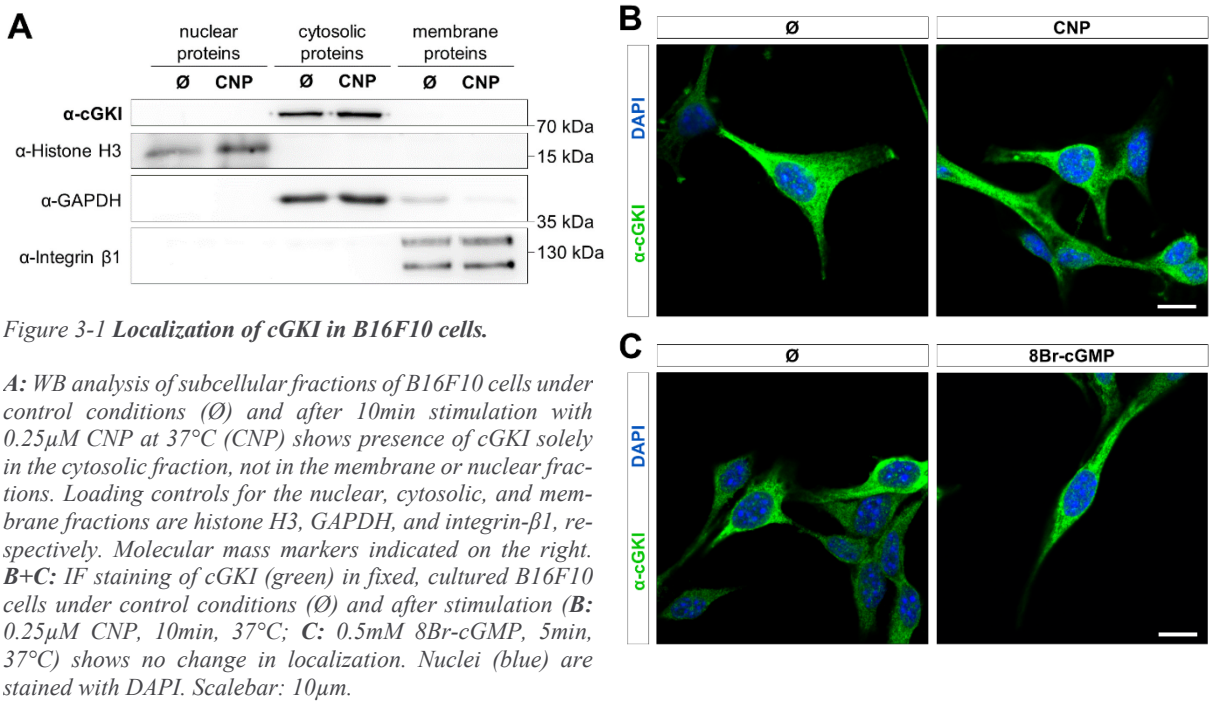

Figure 3-1 ***Localization of cGKI in B16F10 cells.***

A: *WB analysis of subcellular fractions of B16F10 cells under control conditions (Ø) and after 10min stimulation with 0.25µM CNP at 37°C (CNP) shows presence of cGKI solely in the cytosolic fraction, not in the membrane or nuclear fractions. Loading controls for the nuclear, cytosolic, and membrane fractions are histone H3, GAPDH, and integrin-β1, respectively. Molecular mass markers indicated on the right.* ***B+C:*** *IF staining of cGKI (green) in fixed, cultured B16F10 cells under control conditions (Ø) and after stimulation (****B:*** *0.25µM CNP, 10min, 37°C;* ***C:*** *0.5mM 8Br-cGMP, 5min, 37°C) shows no change in localization. Nuclei (blue) are stained with DAPI. Scalebar: 10µm.*

Figure 3-2C shows the presence of the critical cGMP-pathway component cGKI in DRG neurons of E8 chick embryos. Comparable to the distribution in murine samples, transversal sections of E8 chick embryos probed for the cGKI antigen showed an IF signal in cell bodies located in the DRG and axonal projections to the spinal cord, arriving at the DREZ and distributing across the dorsal funiculus.

3.1.3 Summary

The presence and activity of cGMP pathway components was investigated in the murine melanoma cell line B16F10 as well as in chick and GC-B-HA mouse embryos. In B16F10 cells, cGKI is ubiquitously present and its localization in the cytosol before and after stimulation with kinase-activating compounds was unchanged. This makes it an eligible cell line for further experiments to determine novel cGKI substrates via SILAC and MS analysis (Section 3.2.1). The distribution of HA-tagged GC-B in E13.5 mouse embryonic spinal cord and DRGs was analogous to that of cGKI in GC-B-HA mice, while not detectable in WT mice with anti-HA. This makes GC-B-HA mice a valuable addition as GC-B reporter mouse line in various analyses, as HA antibodies are readily available and established as opposed to antibodies against GC-B, which are not commercially available and are not applicable in some setups. Thus, GC-B-HA mice were selected for further experiments to identify novel GC-B interactors via anti-HA pull-down and MS analysis (Section 3.5). The expression of cGKI in E8 chick DRGs and spinal cord was comparable to that of E13.5 mice. This makes a first step in validating the chick system as alternative model to further study DRG neuron bifurcation in the future.

3.2 Phosphoproteome analyses of B16F10 cells and murine embryonic DRGs reveal novel putative cGKI phosphorylation substrates

The MS analysis of the phosphoproteome is an approach to identify novel kinase phosphorylation substrates. To directly compare the activated kinase to a baseline however, the phosphoproteome of both conditions must be labeled appropriately. Here, in collaboration with the Proteome Center Tübingen (University of Tübingen) I utilize two different stable isotope labeling techniques one for a stable cell line and another for acutely dissected tissue with the aim of identifying phosphoproteins downstream of cGKI via MS analysis. As demonstrated, the murine melanoma cell line B16F10 readily expresses the kinase in question. This easily maintained and expanded cell line was labeled via SILAC, then a stimulation condition with the cGMP analog 8Br-cGMP was compared with an unstimulated control condition

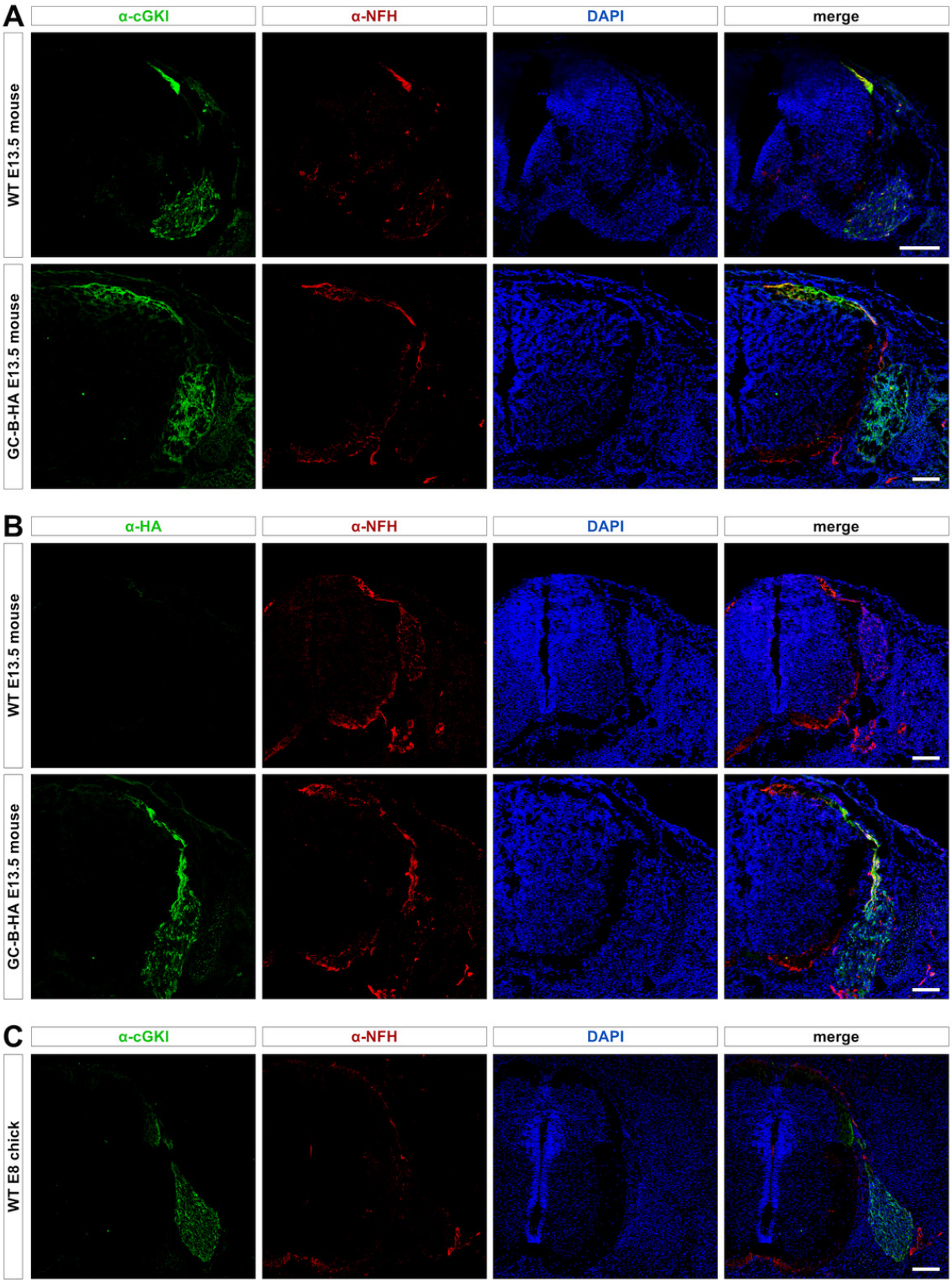

Figure 3-2 ***Localization of cGMP signaling pathway components in mouse and chick embryos.***

A: *IF staining in transversal sections of E13.5 WT and GC-B-HA mice shows presence of cGKI (green) in NFH-positive (red) sensory neurons in DRG with projections to the DREZ and dorsal funiculus.* ***B:*** *IF staining in transversal sections of E13.5 WT and GC-B-HA mice shows presence of HA-tagged GC-B (green) only in NFH-positive (red) neurons in GC-B-HA mice.* ***C:*** *IF staining in transversal sections of E8 chick shows presence of cGKI (green) in NFH-positive (red) sensory neurons in DRG with projections to the DREZ and dorsal funiculus.* ***A-C:*** *Nuclei (blue) are stained with DAPI. Scalebar: 100µm.*

in an MS analysis to identify peptides with a changed phosphorylation status after activation of cGKI (Section 3.2.1). Next, I moved closer to the physiological situation of somatosensory axon bifurcation by investigating acutely dissected murine embryonic DRGs (Section 3.2.2). The stimulation was performed with CNP to mimic the cGMP signaling pathway that controls DRG axon bifurcation during embryonic development. This more elaborate experimental setup also required the use of a different labeling technique for the postmitotic tissue – SIDL. Additionally, the utilization of transgenic mice allowed for the addition of samples from cGKI deficient mice as negative control.

3.2.1 B16F10 cell line

Stimulation of cultured (non-SILAC-labeled) B16F10 murine melanoma cells with 0.5 mM 8Br-cGMP for 5 min at 37 °C resulted in the phosphorylation of the established cGKI target Vasp at S153 and/or S235 (Figure 3-3A). Probing a PVDF membrane in a WB analysis of respective lysates with a phospho-specific antibody for pS235-Vasp revealed Vasp molecules that were phosphorylated at S235. The size shift of the protein band from 45 kDa to 50 kDa indicates an additional phosphorylation at S153 [20]. Thus, the upper protein band signifies Vasp molecules with a phosphorylation at both sites, while the lower one represents Vasp molecules that were phosphorylated only at S235.

After SILAC labeling of B16F10 cells, 6062 phosphopeptides were detected by MS analysis; 5507 of those with PEP $\leq$ 0.05 and valid values for a normalized ratio 8Br-cGMP/control are represented in Figure 3-3B. Statistical analysis revealed 184 significantly regulated phosphopeptides (significance B $\leq$ 0.05 in over 50 % of samples) after stimulation of cGKI activity (0.5 mM 8Br-cGMP, 5 min, 37 °C) in comparison to unstimulated cells as a control condition. Of the significantly changed phosphopeptides, 125 were upregulated with a mean ratio 8Br-cGMP/control $\geq$ 1.5 (Table 3-1), while the remaining 59 were downregulated with a mean ratio 8Br-cGMP/control $\leq$ 0.67 (Table 3-2). Of the proteins corresponding to the significantly downregulated phosphopeptides, MAP/microtubule affinity-regulating kinase 3 (Mark3; S469, mean 8Br-cGMP/control = 0.40) and cyclin-dependent kinase 2 (Cdk2; Y15, mean 8Br-cGMP/control = 0.48) both possess a protein kinase domain. TSC22 domain family protein 4 (Tsc22d4; T223, mean 8Br-cGMP/control = 0.19) contains an LZ domain.

Of the proteins corresponding to the significantly upregulated phosphopeptides, eleven possessed a protein kinase domain (red in Figure 3-3C). Interestingly, one of those proteins – specifically, inhibitor of nuclear factor kappa-B kinase subunit beta (Ikbkb; S672, mean 8Br-cGMP/control = 19.50) – also contained an LZ domain that might interact with the respective region in cGKI. Additionally, Ikbkb is annotated on UniProt to occur in the cytosol and at the intracellular side of the membrane in addition to the nucleus, further increasing the likelihood of its interaction with and phosphorylation by cGKI. Interestingly, S419 of Mark3 (mean 8Br-cGMP/control = 4.31) was among the other upregulated phosphopeptides of proteins that contain a kinase domain, revealing a second phosphorylation site in this kinase that was significantly regulated in B16F10 cells by treatment with 8Br-cGMP.

Screening all significantly regulated phosphopeptides for the cGKI consensus sequence R/K-R/K-X-S*/T* left 61 phosphopeptides, all of which were upregulated. Most of these – 54 – were of proteins that the UniProt consortium annotates as occurring in the cytosol (Figure 3-3B+C). Annotation of compartments also revealed 30 phosphopeptides of proteins found exclusively in the nucleus, one exclusively in other organelles (specifically the ER), and one exclusively in the extracellular space (Figure 3-3B), contrasting the detected subcellular location of cGKI in the cytoplasm of B16F10 cells (Section 3.1.1) and its annotated location in the database.

The established cGKI phosphorylation substrate Vasp could not be identified in the present study, as the respective phosphopeptide containing the S235 site was only detected in one of the three samples. Even though it had a highly significant ratio (8Br-cGMP/control = 14.96; significance B = 1.98×10^{-23}) in one sample, the lack of detection in the other two samples excluded it from the significance requirements of the present study (significance B $\leq$ 0.05 in over 50 % of samples). This failure to detect the respective phosphopeptide at all could be a result of the used digestion method via trypsin, as this severs proteins

after R or K, thus potentially destroying the sought-after peptide that contains such residues directly before and after the phosphorylation site.

Despite not containing Vasp, the dataset of significantly regulated phosphopeptides in B16F10 cells after stimulation with a cGMP analog shown in this section contains many potential novel cGKI substrates or downstream targets in general. To investigate cGKI substrates that might be specifically involved in somatosensory axon bifurcation, a subsequent phosphoproteome study was performed on acutely dissected E13.5 murine DRGs.

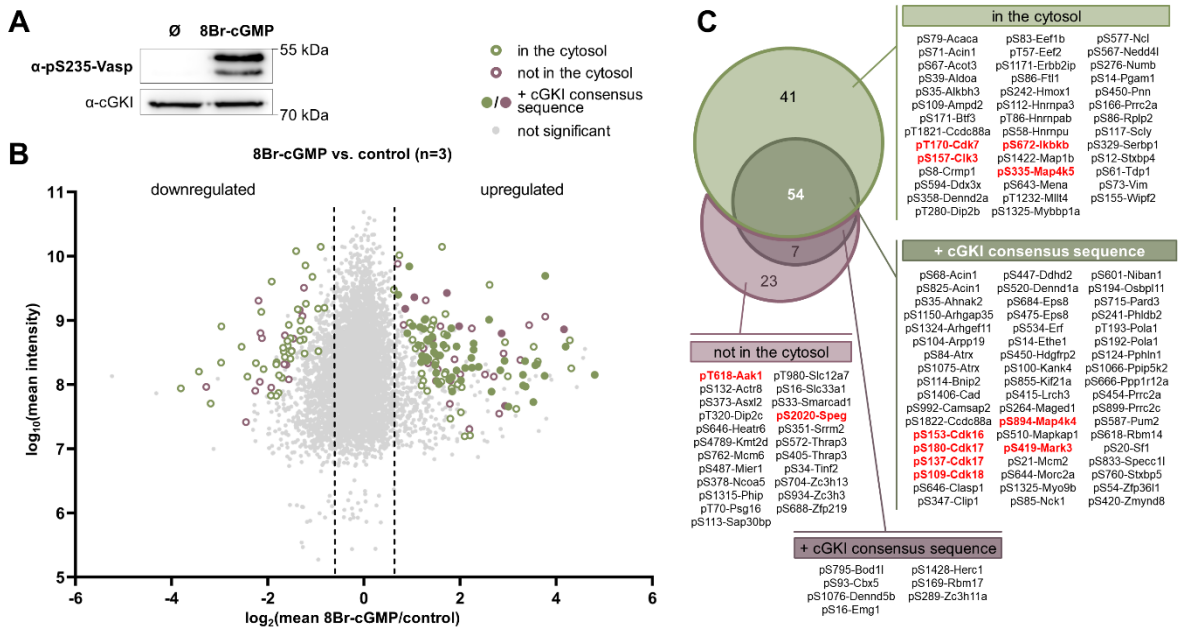

Figure 3-3 ***Phosphoproteomic screen for cGKI phosphorylation substrates in B16F10 cells shows significantly regulated phosphorylation events after stimulation with 8Br-cGMP.***

A: *WB analysis of B16F10 cell lysates under control conditions (Ø) and after 5min stimulation with 0.5mM 8Br-cGMP at 37°C (8Br-cGMP) shows phosphorylation of the known cGKI substrate Vasp at S153 as indicated by the band shift from 45kDa to 50kDa and/or at S235 as probed by a phospho-specific antibody only under stimulation conditions. Loading control is cGKI. Molecular mass markers indicated on the right.* ***B:*** *Log2 transformed ratio of phosphorylation events from 8Br-cGMP (0.5mM, 5min, 37°C) stimulated B16F10 cells in comparison to untreated cells (mean 8Br-cGMP/control) relative to the log10 transformed phosphopeptide intensities are shown. The mean values of three samples are shown. Events are considered significant if over 50% of samples yielded a significance B ≤ 0.05. All other events are considered not significant (light grey circle). Upregulated events are defined as mean ratio of at least 1.5; downregulated events are defined as maximum mean ratio of 0.67. Significantly regulated phosphopeptides of proteins located in the cytosol are shown in green. Significantly regulated phosphopeptides of proteins that do not occur in the cytosol are marked in purple. If the found phosphorylation site is at a cGKI consensus sequence (R/K-R/K-X-S*/T*), the corresponding circle is filled in.* ***C:*** *Venn diagram of the 125 significantly upregulated phosphopeptides, showing overlaps of different compartment categories with the cGKI consensus sequence. If the respective protein contains a kinase activity domain, the result is listed in bold red letters. Results are listed with phosphorylation site and gene name.*

Table 3-1 ***Overview of significantly upregulated phosphorylation events in B16F10 cells after stimulation with 8Br-cGMP.*** *The proteins are listed in descending order of mean ratio 8Br-cGMP/control.*

Protein ID (UniProt)	Gene name	Putative phosphorylation site	cGKI consensus sequence		Mean 8Br-cGMP/control	Compartments[1]
Q64213	Sf1	pS20	RKXS	+	27.88	C, N
B8JJ92	Acin1	pS71	XXXS		19.91	C, M, N
O88351[2,3]	Ikbkb	pS672	XXXS		19.50	C, M, N
B8JJ92	Acin1	pS68	RKXS	+	18.35	C, M, N
E9PZP8	Herc1	pS1428	RRXS	+	17.92	
Q9JIX8	Acin1	pS825	RKXS	+	13.68	C, M, N
Q6PDK2	Kmt2d	pS4789	RXXS		13.68	N
Q9QYH6	Maged1	pS264	RRXS	+	13.55	C, M, N
Q8C4S8	Dennd2a	pS358	RXXS		12.28	C, CS
Q91YM2	Arhgap35	pS1150	RKXS	+	12.13	C, CS, M, N

Protein ID (UniProt)	Gene name	Putative phosphorylation site	cGKI consensus sequence		Mean 8Br-cGMP/control	Compartments[1]
Q6PEV3	Wipf2	pS155	XRXS		11.84	C, CS
O35492[3]	Clk3	pS157	RXXS		11.58	C, CS, N
Q69ZX6	Morc2a	pS644	RKXS	+	11.52	C, N
A0A2I3BRW2	Tinf2	pS34	RXXS		10.83	N
P33609	Pola1	pT193	KRXT	+	10.30	C, N
Q8BVU0	Lrch3	pS415	RRXS	+	10.22	C
P33609	Pola1	pS192	KKXS	+	9.94	C, N
Q9DBR7	Ppp1r12a	pS666	RRXS	+	9.91	C, CS, M, N
Q6P1G0	Heatr6	pS646	XXXS		9.56	
Q03173	Mena	pS643	XXXS		9.01	C, CS, M
Q99NH2	Pard3	pS715	RRXS	+	8.04	C, CS, M
Q8K1E6	Alkbh3	pS35	XRXS		7.96	C, N, O
Q8JZX4	Rbm17	pS169	RKXS	+	7.66	N
P97427	Crmp1	pS8	XKXS		7.65	C, CS, N
Q6ZQB6	Ppip5k2	pS1066	RKXS	+	7.60	C
Q8BZ32	Asxl2	pS373	XXXS		7.49	N
A2RSQ0	Dennd5b	pS1076	RRXS	+	7.28	M
Q9QY06	Myo9b	pS1325	RRXS	+	7.15	C, CS
Q99J27	Slc33a1	pS16	XRXS		7.03	O
Q91W39	Ncoa5	pS378	XRXS		6.50	CS, N
Q80Y98	Ddhd2	pS447	RKXS	+	6.30	C, O
P14873	Map1b	pS1422	RXXS		6.12	C, CS, M
P56212	Arpp19	pS104	RKXS	+	6.08	C
Q04692	Smarcad1	pS33	XRXS		5.74	N
Q8C1B1	Camsap2	pS992	RRXS	+	5.23	C, CS, O
Q61687	Atrx	pS84	RKXS	+	4.87	C, N
Q3UMU9	Hdgfrp2	pS450	RKXS	+	4.86	C, N
Q80U58	Pum2	pS587	RRXS	+	4.76	C, N, O
Q8R2S9	Actr8	pS132	XXXS		4.75	N
E9Q0A3	Arhgef11	pS1324	RKXS	+	4.70	C, M, N
Q8CFI0	Nedd4l	pS567	XXXS		4.62	C, M, O
Q9WVL3	Slc12a7	pT980	XXXT		4.58	M
Q03141[3]	Mark3	pS419	RRXS	+	4.31	C, M
Q99020	Hnrnpab	pT86	XXXT		4.27	C, N
Q7TSC1	Prrc2a	pS166	XRXS		4.10	C, M, N
Q6P9J5	Kank4	pS100	RKXS	+	4.05	C, CS
Q5SNZ0	Ccdc88a	pT1821	XRXT		4.05	C, CS, M, O
P97311	Mcm6	pS762	XXXS		4.01	N
E9Q6J5	Bod1l	pS795	RRXS	+	3.95	N
P14901	Hmox1	pS242	RXXS		3.87	C, N, O
Q08509	Eps8	pS684	RRXS	+	3.80	C, M
Q5SNZ0	Ccdc88a	pS1822	RRXS	+	3.80	C, CS, M, O
D3YXQ6	Psg16	pT70	XXXT		3.70	E
Q8K382	Dennd1a	pS520	RRXS	+	3.58	C, M, O
Q7TSC1	Prrc2a	pS454	RKXS	+	3.56	C, M, N
Q9QZS3	Numb	pS276	RXXS		3.55	C, M, O
Q99M51	Nck1	pS85	RKXS	+	3.53	C, M, N, O
Q8VDD9	Phip	pS1315	RXXS		3.48	N
Q9DBT5	Ampd2	pS109	KXXS		3.48	C
Q8CHP0	Zc3h3	pS934	XXXS		3.45	N
P97820[3]	Map4k4	pS894	RKXS	+	3.43	C
Q922J3	Clip1	pS347	RKXS	+	3.32	C, CS, N, O
Q6NZF1	Zc3h11a	pS289	RKXS	+	3.31	N
Q8BPM2[3]	Map4k5	pS335	RXXS		3.29	C
Q8BG05	Hnrnpa3	pS112	RXXS		3.25	C, N
Q7TPV4	Mybbp1a	pS1325	RXXS		3.25	C, N
Q8VEK3	Hnrnpu	pS58	XXXS		3.25	C, CS, N, O
P99027	Rplp2	pS86	XXXS		3.21	C, O
Q80TH2	Erbb2ip	pS1171	RXXS		3.18	C, M, N

Protein ID (UniProt)	Gene name	Putative phosphorylation site	cGKI consensus sequence		Mean 8Br-cGMP/control	Compartments[1]
Q3UW53	Niban1	pS601	RRXS	+	3.15	C, M
P58252	Eef2	pT57	XRXT		3.08	C, M, N
Q9QZQ1	Mllt4	pT1232	XXXT		3.06	C, M, N
Q3UHJ0[3]	Aak1	pT618	XXXT		3.01	M, O
Q8C2Q3	Rbm14	pS618	RRXS	+	3.00	C, N
Q8K2H1	Pphln1	pS124	RRXS	+	2.95	C, N, O
Q5UAK0	Mier1	pS487	XKXS		2.95	N
Q62407[3]	Speg	pS2020	RXXS		2.90	N
Q8K1N2	Phldb2	pS241	RKXS	+	2.86	C, CS, M
Q61687	Atrx	pS1075	KRXS	+	2.84	C, N
B7ZMZ7	Dip2c	pT320	XXXT		2.83	
Q3TLH4	Prrc2c	pS899	RKXS	+	2.82	C, O
Q9DBJ1	Pgam1	pS14	XXXS		2.81	C, N
P23950	Zfp36l1	pS54	RRXS	+	2.80	C, N, O
Q04899[3]	Cdk18	pS109	RRXS	+	2.75	C, N
Q80TV8	Clasp1	pS646	RRXS	+	2.73	C, CS, O
Q8BJ37	Tdp1	pS61	RXXS		2.73	C, M, N, O
Q9WV89	Stxbp4	pS12	RXXS		2.72	C, O
Q569Z6	Thrap3	pS572	RXXS		2.70	N
Q8K0D0[3]	Cdk17	pS180	RRXS	+	2.68	C, N
O35691	Pnn	pS450	XXXS		2.67	C, N, O
P09405	Ncl	pS577	KXXS		2.62	C, N
Q2KN98	Specc1l	pS833	RRXS	+	2.54	C, CS
A2A485	Zmynd8	pS420	RRXS	+	2.53	C, N, O
Q6IQX8	Zfp219	pS688	XXXS		2.52	N
O70251	Eef1b	pS83	XXXS		2.51	C, O
P29391	Ftl1	pS86	XKXS		2.49	C, E, O
Q8CI95	Osbpl11	pS194	RRXS	+	2.49	C, N, O
Q9DCM0	Ethe1	pS14	RRXS	+	2.47	C, N, O
Q8K400	Stxbp5	pS760	RKXS	+	2.45	C, M
Q569Z6	Thrap3	pS405	XXXS		2.44	N
Q9JLI6	Scly	pS117	XXXS		2.43	C, O
Q8K0D0[3]	Cdk17	pS137	RRXS	+	2.40	C, N
P70459	Erf	pS534	RRXS	+	2.37	C, N
Q02614	Sap30bp	pS113	RXXS		2.36	CS, N
Q64152	Btf3	pS171	XKXS		2.35	C, N
Q9QXL2	Kif21a	pS855	RKXS	+	2.32	C, CS, M
Q03147[3]	Cdk7	pT170	RXXT		2.30	C, CS, N, M
Q3UH60	Dip2b	pT280	XXXT		2.30	C, N
Q04735[3]	Cdk16	pS153	RRXS	+	2.29	C, CS, M, N
Q9QYR7	Acot3	pS67	RXXS		2.28	C, O
Q3URZ6	Ahnak2	pS35	RKXS	+	2.25	C, M
Q8BKH7	Mapkap1	pS510	RRXS	+	2.19	C, M, N, O
P05064	Aldoa	pS39	XXXS		2.10	C, CS, E, M, O
O35130	Emg1	pS16	RRXS	+	2.07	N
Q08509	Eps8	pS475	KRXS	+	2.02	C, M
Q62167	Ddx3x	pS594	XRXS		2.02	C, M, N, O
Q5SWU9	Acaca	pS79	XXXS		1.94	C, CS, O
P97310	Mcm2	pS21	RRXS	+	1.92	C, N
B2RQC6	Cad	pS1406	RRXS	+	1.87	C, N
Q61686	Cbx5	pS93	RKXS	+	1.82	N
E9Q784	Zc3h13	pS704	RXXS		1.77	N
Q9CY58	Serbp1	pS329	KXXS		1.67	C, M, N
O54940	Bnip2	pS114	RKXS	+	1.64	C, N
Q8BTI8	Srrm2	pS351	XXXS		1.63	N
P20152	Vim	pS73	XRXS		1.54	C, CS, M, N, O

[1] Compartments: C: cytosol, CS: cytoskeleton, E: extracellular, M: membrane, N: nucleus, O: organelles
[2] Protein contains LZ domain.
[3] Protein contains kinase activity domain.

Table 3-2 ***Overview of significantly downregulated phosphorylation events in B16F10 cells after stimulation with 8Br-cGMP.*** *The proteins are listed in ascending order of mean ratio 8Br-cGMP/control.*

Protein ID (UniProt)	Gene name	Phosphorylation site	Mean 8Br-cGMP/control	Compartments[1]
Q8BU31	Rap2c	pS151	0.07	C, M
Q9ERL0	Mllt1	pS259	0.09	C, N
Q9WUK4	Rfc2	pS178	0.10	N
P0C7L0	Wipf3	pS161	0.11	C
P11157	Rrm2	pS20	0.13	C, N
Q03173	Mena	pT721	0.13	C, CS, M
Q99M54	Cdca3	pS67	0.17	C
Q8BVE8	Whsc1	pT110	0.18	N
Q9EQN3[2]	Tsc22d4	pT223	0.19	C, N
Q8JZK9	Hmgcs1	pS495	0.21	C
Q69ZS7	Hbs1l	pT229	0.21	
A2A7S8	Kiaa1522	pS959	0.22	
P43274	H1-4	pT18	0.22	N
B7ZMZ7	Dip2c	pT123	0.23	
Q9R1Z8	Sorbs3	pS412	0.23	C, CS, N
P43277	H1-3	pT18	0.23	N
Q8CC35	Synpo	pS488	0.24	C, CS, N
Q80UG5	Sept9	pT143	0.26	C, CS
Q64701	Rbl1	pS640	0.26	N
P09405	Ncl	pT121	0.26	C, N
Q80UG5	Sept9	pT49	0.28	C, CS
Q7TSC1	Prrc2a	pS1145	0.28	C, M, N
Q58A65	Spag9	pT586	0.28	C, M
O35250	Exoc7	pS250	0.29	C, M
O70400	Pdlim1	pS130	0.29	C, CS
Q8CHG7	Rapgef2	pS1079	0.31	C, M
Q8K4B0	Mta1	pS576	0.31	C, N
O70305	Atxn2	pT549	0.31	C
Q61687	Atrx	pS590	0.32	N
Q8CI51	Pdlim5	pS111	0.32	C, CS
Q6PDJ6	Fbxo42	pS365	0.32	
Q8CI51	Pdlim5	pS359	0.33	C, CS
Q6DFV3	Arhgap21	pS610	0.33	C, CS, M
Q8R2M2	Dnttip2	pT342	0.33	N
Q5PSV9	Mdc1	pT1480	0.34	N
Q8K298	Anln	pS180	0.34	C, CS, N
Q0VGY8	Tanc1	pS64	0.35	
Q99PL6	Ubxn6	pS36	0.35	C, CS, M, N
Q8K298	Anln	pS637	0.35	C, CS, N
Q9CW46	Raver1	pT469	0.35	C, N
Q8VDY4	Efcab7	pS212	0.36	M
P26645	Marcks	pT143	0.38	C, CS, M
Q7TQH0	Atxn2l	pS407	0.39	C, M
Q3UH68	Limch1	pS973	0.40	C, CS
Q03141[3]	Mark3	pS469	0.40	C, M
Q5NC05	Ttf2	pS119	0.40	C, N
G3X963	Atad2	pS307	0.40	
P97386	Lig3	pS211	0.41	N
P37913	Lig1	pS51	0.42	N
Q8VD37	Sgip1	pS484	0.42	C, M
Q8K2K6	Agfg1	pS181	0.43	C, N
Q80XU3	Nucks1	pS181	0.43	C, N
Q3UIA2	Arhgap17	pS625	0.43	C, M
Q9QZQ1	Mllt4	pS1510	0.45	C, M, N
P97377[3]	Cdk2	pY15	0.48	C, CS, N
Q8CI51	Pdlim5	pS361	0.52	C, CS
Q04888	Sox10	pT240	0.52	C, N

Protein ID (UniProt)	Gene name	Phosphorylation site	Mean 8Br-cGMP/control	Compartments[1]
Q80UG5	Sept9	pS85	0.54	C, CS
Q99L88	Sntb1	pS86	0.57	C, CS, M

[1] *Compartments: C: cytosol, CS: cytoskeleton, E: extracellular, M: membrane, N: nucleus, O: organelles*
[2] *Protein contains LZ domain.*
[3] *Protein contains kinase activity domain.*

3.2.2 Embryonic DRGs

Stimulation of acutely excised DRG tissue with 0.25 µM CNP for 10 min at 37 °C led to the phosphorylation of Vasp at S153 and/or S235 (Figure 3-4A) in a similar pattern as the stimulation of B16F10 cells with 8Br-cGMP (Figure 3-3A). Figure 3-4A shows a representative WB analysis of one of the samples that was subsequently labeled via SIDL and measured for phosphoproteome.

Three SIDL labeling experiments of DRG lysates were performed, with MS analysis detecting 6277, 4456, and 4607 phosphopeptides with PEP ≤ 0.05 (6346, 4512, and 4648 total, respectively) in each. Most of those were found in several experiments, yielding 7059 unique phosphopeptides overall. Of those, 2212 events gave valid values for the ratio CNP/control normalized by proteome in at least one experiment (Figure 3-4B). Of the 42 significant phosphorylation events (significance B ≤ 0.05 in over 50 % of experiments), 5 were found to be independent from cGKI activity, as shown in Figure 3-4C, and were thus removed from further analysis. Of the remaining 37 events, 12 were not sufficiently up- or downregulated for further consideration, 19 were upregulated with a mean ratio CNP/control ≥ 1.5 (Table 3-3), and 6 were downregulated with a mean ratio CNP/control ≤ 0.67 (Table 3-4). The proteins corresponding to the significantly regulated phosphopeptides found in the MS analysis were further classified by cell compartments and by whether the phosphorylation site corresponded to a cGKI consensus sequence (Figure 3-4B+D). Additionally, serine/threonine-protein kinase doublecortin-like kinase 1 (Dclk1), which was found to be phosphorylated at S332 (mean CNP/control = 3.70) after stimulation with CNP, contained a kinase activity domain; this kinase plays a role in neuronal migration and axon outgrowth [107].

The splicing factor transformer-2 protein homolog alpha (Tra2a) was found to be phosphorylated at T200 (mean CNP/control = 4.48). However, Tra2a is a nuclear protein [108], making its direct interaction with cGKI less likely. Similarly, the nucleoprotein translocated promoter region (Tpr) has been shown to be part of the nuclear pore complex that mediates protein transport to and from the nucleus [109], reducing the probability of a direct phosphorylation by cGKI at S2223 (mean CNP/control = 2.48). While thioredoxin-related transmembrane protein 1 (Tmx1) is active in the ER, the putatively phosphorylated S245 found in the present study is located in its cytoplasmic domain; this transmembrane protein was suggested to play a role in platelet aggregation [110]. High mobility group protein B3 (Hmgb3), which is a chromatin-binding protein regulating renewal and differentiation in hematopoietic stem cells [111], was found to have increased phosphorylation at S135 after CNP stimulation (mean CNP/control = 2.23). In the Arf-GAP domain and FG repeat-containing protein 1 (Agfg1), which plays a role in spermiogenesis [112], a significant phosphorylation event was recorded in E13.5 DRG at S293 after treatment with CNP, while a dephosphorylation of the same protein was found at S181 after treatment of B16F10 cells with 8Br-cGMP (mean 8Br-cGMP/control = 0.43; Table 3-2).

For Map1b, which plays a role in neuronal differentiation and neurite extension [113] three potential phosphorylation sites were identified at S561, which contains the cGKI consensus sequence, and at S1307 and T1928. Additionally, a site with significantly downregulated phosphorylation after treatment with CNP was found at T1277 (mean CNP/control = 0.31). Interestingly, Map1b was also found to be phosphorylated in the phosphoproteome screen of B16F10 cells after treatment with 8Br-cGMP at the additional site S1422 (mean 8Br-cGMP/control=6.12; Table 3-1).

E3 ubiquitin-protein ligase Nedd4l plays a role in ubiquitinoylation and internalization of various ion channels, and S477, which was identified to be phosphorylated in E13.5 DRG tissue after stimulation with CNP, is a known phosphorylation site of serum/glucocorticoid-regulated kinase 1 (Sgk1) [114]. In

the B16F10 phosphoproteome screen after treatment with 8Br-cGMP, a significant upregulation of a phosphorylation site in the same protein but at S567 was found (mean 8Br-cGMP/control = 4.62; Table 3-1). The cytoskeletal protein Stmn1 plays a role in microtubule dynamics, and the phosphorylation found in the present study (S63) is not only located in a cGKI consensus sequence but is also among its known phosphorylation sites at Sl6, S25, S38 and S63 that regulate its affinity to tubulin and thus might be involved in neurite outgrowth [115]. The calcium-binding protein and ER chaperone calnexin (Canx), is another putative cGKI substrate found in the present study in which the specific site that was identified is a known phosphorylation site of the protein. Specifically, S563 is a known phosphorylation site of extracellular signal-regulated kinase 1 (Erk1) among others [116]. Both phosphorylation sites of the 40S ribosomal protein S6 (Rps6) at S235 and S236 found in the present phosphoproteome screen of E13.5 DRG lysates are also known [117].

Interestingly, four peptides were found to be significantly phosphorylated at the same site after stimulation of cGKI activity both in B16F10 cells and E13.5 DRG tissue (Figure 3-4E). Except for the site found in Crmp1, three of those four sites were also located in a cGKI consensus sequence. They belong to the proteins Acin1, Cad, and Clasp1. Acin1 plays a role in alternative RNA splicing and gene expression [118]. Cad has three enzymatic domains lending its name: a glutamine-dependent carbamoyl-phosphate synthase domain (C), an aspartate carbamoyl transferase domain (A), and a dihydroorotase domain (D). The detected phosphorylation site of Cad at S1406 is a known phosphorylation site of protein kinase A (PKA), which downregulates the protein's function in *de novo* pyrimidine biosynthesis [119]. Clasp1 is a MAP that plays a role in developmental and regenerative axon growth [120]. Crmp1, which was found to be expressed in E12 DRG neurons, plays a role in the rearrangement of the actin cytoskeleton [121].

The first 30 amino acid residues of the EVH2 region (221-373) of the Vasp protein (`221 - GLAAA IAGAK LRKV`**`S*`** `KQEEA SGGPL APKAE - 250`) include a known cGKI phosphorylation site of the protein at S235. In the phosphoproteomic screen for cGKI substrates in E13.5 DRG lysates, an equivalent site in the EVH2 region (623-799) of the neural variant of Mena, which plays a role in growth cone remodeling and actin cytoskeleton organization [122] was found at S637 (`623 - GLAAA IAGAK LRKV`**`S*`** `RVEDG SFPGG GNTGS - 652`). The sequence between Vasp and Mena are 100% identical for the first 15 residues of EVH2, including the S in question and its preceding neighbors, which include a cGKI consensus sequence. Interestingly, two significant phosphorylation events of Mena were detected in the phosphoproteome screen of B16F10 cells after treatment with 8Br-cGMP. While they are not at the same site, an increased phosphorylation was found in close proximity at S643 (mean 8Br-cGMP/control = 9.01; Table 3-1). Additionally, a downregulated phosphopeptide was documented in the same screen at residue T721 (mean 8Br-cGMP/control = 0.13; Table 3-2).

As in the previously described study of the murine melanoma cell line B16F10, the known cGKI substrate Vasp was not among the identified regulated phosphopeptides. In this case, however, more information is available as to the cause. The Vasp phosphopeptide is absent in the dataset not due to a lack of phosphorylation but the protein itself was not detected and does also not appear in the proteome dataset for normalization. Possibly, the prevalence of this protein was below the detection threshold for this MS analysis, while high enough to be picked up by WB analysis.

3.2.3 Summary

In collaboration with the Proteome Center Tübingen (University of Tübingen), a phosphoproteome analysis of both B16F10 cells and E13.5 DRGs was performed after stable isotope labeling of the samples. Several promising putative cGKI phosphorylation substrates were determined in response to the stimulation of cGMP signaling in comparison to control conditions. Four phosphopeptides (of Acin1, Cad, Clasp1, and Crmp1) were found to be significantly upregulated in both studies, while no overlap was found in those phosphopeptides that were downregulated after cGKI stimulation. While the known cGKI substrate Vasp was not identified in either study, a member of the same protein family, Mena, was found to be phosphorylated in both B16F10 cells and E13.5 DRG explants at different sites. Similarly, the

phosphorylation status of Agfg1, Map1b and Nedd4l was significantly changed in different sites in both studies. Several of these putative novel cGKI phosphorylation substrates undergo validation by several methods in the experiments presented in the following section.

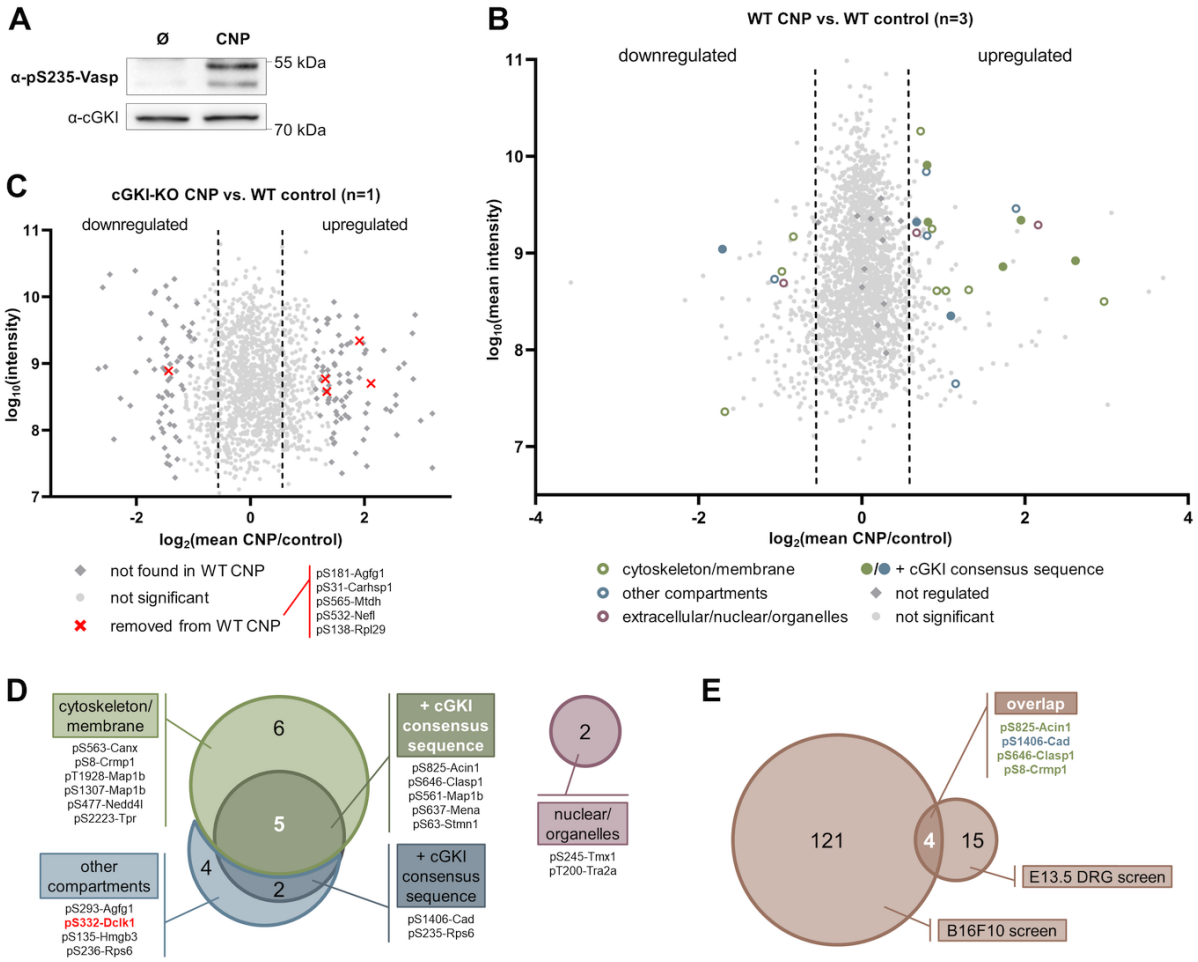

Figure 3-4 ***Phosphoproteomic screen for cGKI phosphorylation substrates in E13.5 DRG lysates shows significantly regulated phosphorylation events after stimulation with CNP.***

A: *WB analysis of E13.5 DRG lysates under control conditions (Ø) and after 10min stimulation with 0.25µM CNP at 37°C (CNP) shows phosphorylation of the known cGKI substrate Vasp at S153 as indicated by the band shift from 45kDa to 50kDa and/or at S235 as probed by a phospho-specific antibody, mostly under stimulation conditions. Loading control is cGKI. Molecular mass markers indicated on the right.* ***B:*** *Log2 transformed ratio of phosphorylation events normalized to the proteome from CNP (0.25µM, 10min, 37°C) stimulated DRGs in comparison to untreated tissue from WT mice (mean CNP/control) relative to the log10 transformed phosphopeptide intensities are shown. The mean values of three samples with two measurements each are shown. Events are considered significant if at least one of the measurements of at least two samples yielded a significance B ≤ 0.05. All other events are considered not significant (light grey circles). Upregulated events are defined as mean ratio of at least 1.5, downregulated events are defined as maximum mean ratio of 0.67. All remaining events are considered not sufficiently regulated (dark grey diamonds). Significantly regulated phosphopeptides of proteins located exclusively in the nucleus, other organelles, or the extracellular space are shown in purple. Significantly regulated phosphopeptides of proteins occurring in the cytoskeletal compartment, and/or the membrane are shown in green. Significantly regulated phosphopeptides of proteins in other compartments are marked in blue. If the found phosphorylation site is at a cGKI consensus sequence (R/K-R/K-X-S*/T*), the corresponding circle is filled in.* ***C:*** *Log2 transformed ratio of phosphorylation events normalized to the proteome of CNP stimulated DRGs from cGKI-KO mice in comparison to untreated tissue from WT mice (mean CNP/control) relative to the log10 transformed phosphopeptide intensities are shown. The mean values of two measurements of the same sample are shown. Events are considered significant if at least one of the measurements yielded a significance B ≤ 0.05. All other events are considered not significant (light grey circles). Upregulated events are defined as mean ratio of at least 1.5; downregulated events are defined as maximum mean ratio of 0.67. If a phosphopeptide showed the same significant regulation in CNP stimulated DRGs of cGKI-KO and WT mice, this event is considered independent of cGKI activity and removed from the phosphoproteomic screen in WT tissue (red cross). All other events do not overlap (dark grey diamonds).* ***D:*** *Venn diagram of the 19 significantly upregulated phosphopeptides, showing overlaps of different compartment categories with the cGKI consensus sequence. If the respective protein contains a kinase activity domain, the result is listed in bold red letters.* ***E:*** *Venn diagram of the 140 significantly upregulated phosphopeptides found in phosphoproteomic screens of B16F10 cells and E13.5 DRGs, four of which were found in both screens.* ***D, E:*** *Results are listed with phosphorylation site and gene name.*

Table 3-3 ***Overview of putative cGKI phosphorylation substrates based on significantly upregulated phosphorylation events in E13.5 DRG tissue after stimulation with CNP.*** *The proteins are listed in descending order of mean CNP/control ratio.*

Protein ID (UniProt)	Gene name	Putative phosphorylation site	cGKI consensus sequence		Compartments[1]	Mean CNP/ control
P97427	Crmp1	pS8[2]	XKXS		C, CS	7.84
Q03173	Mena	pS637	RKXS	+	C, CS, M	6.15
Q6PFR5	Tra2a	pT200	RXXT		N	4.48
P14873	Map1b	pS561	RKXS	+	C, CS, M	3.85
		pT1928	XXXT			1.89
		pS1307	XXXS			1.81
Q9JLM8[3]	Dclk1	pS332	KXXS			3.70
Q9JIX8	Acin1	pS825[2]	RKXS	+	C, M, N	3.31
F6ZDS4	Tpr	pS2223	XXXS		C, CS, N	2.48
O54879	Hmgb3	pS135	XXXS		C, N	2.23
B2RQC6	Cad	pS1406[2]	RRXS	+	C, N	2.12
Q8CFI0	Nedd4l	pS477	RXXS		C, M, O	2.05
Q80TV8	Clasp1	pS646[2]	RRXS	+	C, CS, O	1.75
Q8K2K6	Agfg1	pS293	KXXS		C, N, O	1.75
P54227	Stmn1	pS63	RRXS	+	C, CS	1.74
P62754	Rps6	pS236	RXXS		C, N, O	1.72
		pS235	RRXS	+		1.59
P35564	Canx	pS563	XXXS		C, M, O	1.65
Q8VBT0	Tmx1	pS245	XXXS		O	1.60

[1] *Compartments: C: cytosol, CS: cytoskeleton, M: membrane, N: nucleus, O: organelles*
[2] *The same phosphorylation site was found in B16F10 cell phosphoproteome analysis.*
[3] *Protein contains kinase activity domain.*

Table 3-4 ***Overview of significantly downregulated phosphorylation events in E13.5 DRG tissue after stimulation with CNP.*** *The proteins are listed in ascending order of mean ratio CNP/control.*

Protein ID (UniProt)	Gene name	Putative phosphorylation site	cGKI consensus sequence		Compartments[1]	Mean CNP/ control
Q9D1R9	Rpl34	pS12	RRXS	+	C, O	0.31
P14873	Map1b	pT1277	XXXT		C, CS, M	0.31
Q7TMY8	Huwe1	pS3818	XXXS		C, N, O	0.48
Q80TV8	Clasp1	pS1088	XXXS		C, CS, O	0.51
P59017	Bcl2l13	pS302	XXXS		O	0.51
P10637	Mapt	pT112	XXXT		C, CS, E, M, N	0.56

[1] *Compartments: C: cytosol, CS: cytoskeleton, E: extracellular, M: membrane, N: nucleus, O: organelles*

3.3 Validation of novel putative cGKI phosphorylation substrates

To confirm the validity of the putative cGKI phosphorylation substrates found in the phosphoproteome analysis studies described above, several experiments were performed. The presence of the respective mRNA in B16F10 cells and embryonic DRG neurons was evaluated via an RT-PCR to confirm gene transcription of the candidates. Additionally, the expression patterns of candidate proteins in murine E13.5 DRGs were examined by WB analysis of subcellular fractions and the tissue distribution was investigated in a histological analysis of transversal tissue sections of embryos (Section 3.3.1). The putative specific cGKI phosphorylation sites of several candidates were then further examined *in vitro* with an ASK assay (Section 3.3.2).

3.3.1 Several cGKI substrate candidates are expressed in embryonic DRGs

In a first step to study the presence and expression of several putative cGKI substrates their transcription was confirmed in both B16F10 cells and E13.5 DRGs. All investigated transcripts (Acin1, Cad, Clasp1, Crmp1, Map1b, Mena, Nedd4l) were present in the cDNA library generated from both B16F10 cells and E13.5 DRG tissue, as shown by respective bands of RT-PCR products (Figure 3-5A). The primers for those RT-PCR reactions were chosen to cover all known isoforms of the proteins in question. Thus, no statement can be made about the prevalence of specific isoforms.

As shown above for the B16F10 cell line (Figure 3-1A), cGKI was also expressed only in the cytosolic fraction of E13.5 DRG tissue lysates, along with its known phosphorylation target Vasp, while its source of activating cGMP (GC-B) was found in the membrane fraction (Figure 3-5B). The α-isoform cGKI was found in DRG neurons and their projections to the DREZ and in the dorsal funiculus, as shown by IF staining of E13.5 murine transversal sections (Figure 3-5C-H) as well as IHC staining of E12.5 murine transversal sections (Figure 3-5O). Similarly, IHC staining of GC-B in E12.5 mice revealed expression in neurons located in the DRG projecting to the DREZ and dorsal funiculus (Figure 3-5O). The pattern of IF and IHC staining of mouse embryo transversal sections with anti-Vasp revealed vessel-like structures surrounding the cGKIα-positive cells of the DRGs as well as reaching throughout the spinal cord (Figure 3-5H+N).

Acin1 has several splicing variants that can be found in E13.5 DRG tissue lysates via WB analysis. The total protein at ~220 kDa and the L-isoform (~150 kDa) were only present in the nuclear fraction. The smaller isoforms S-, and S'-Acin1 represent the largest group and, while also detected in the cytosolic and membrane fractions, were mostly present in the nuclear fraction (Figure 3-5B). The primary location in the nucleus was additionally shown in an IF staining of E13.5 mouse embryo transversal sections (Figure 3-5C), where several nuclei of cGKIα-positive DRG neurons also expressed Acin1. This observation was also made in an IHC staining of E12.5 mouse embryo transversal section, in which the brown DAB overlapped with the violet hematoxylin nuclear counterstain (Figure 3-5I). However, in none of these sections is the location of Acin1 exclusive to the nuclei of DRG neurons but rather universal.

The ~170 kDa Clasp1 band was found primarily in the cytosolic fraction and partly in the membrane fraction of E13.5 DRG tissue lysates (Figure 3-5B). The IF staining for this MAP strongly corresponded to that of cGKIα in E13.5 mouse embryo transversal sections. While not exclusively limited to those cells, there was a marked overlap with the DRG neuron projections to the DREZ (Figure 3-5D). Similarly, the IHC staining of E12.5 mouse transversal sections showed a strong signal in DRG neurons and their projections as well as a weaker unspecific universal background of Clasp1-positive cells (Figure 3-5J).

Several bands were observed in the WB analysis of Crmp1 in the cytosolic fraction of E13.5 mouse DRG lysates, with some weaker corresponding bands in the membrane fraction. The major band corresponded with the expected size of the shorter isoform of this protein 62-65 kDa [22] (Figure 3-5B). Like that of Clasp1, the IF staining of Crmp1 showed overlapping signals with cGKIα most intensely in the DRG neurons and their projections to the DREZ in E13.5 mouse embryos (Figure 3-5E). While the corresponding IHC staining of Crmp1 in murine embryos had an even stronger unspecific background signal, the same pattern could still be observed (Figure 3-5K).

Map1b is made up of a heavy (~240 kDa) and a light (~30 kDa) chain. The protein band was found in all three investigated fractions of E13.5 DRG tissue (Figure 3-5B). An overlap with cGKIα expression in E13.5 mouse embryo transversal sections was again observed in DRG neurons and their projections to the DREZ. This MAP also exhibited an IF signal in the tissue surrounding the spinal cord of E13.5 mouse embryos (Figure 3-5F). IHC staining of E12.5 murine tissue additionally showed a strong signal throughout the spinal cord but not the surrounding tissue in a transversal embryo section (Figure 3-5L).

Several isoforms of Mena are expressed in murine E13.5 DRG. The 140 kDa neuronal variant and the smaller 88/80 kDa isoforms [19] were found in both the cytosolic and the membrane fraction after WB analysis (Figure 3-5B). While the IF signal showed a weak universal signal in E13.5 mouse transversal sections, there was a colocalization with cGKIα in the DRG neurons and their projections to the DREZ (Figure 3-5G). An analogous observation was made in an IHC staining of E12.5 mouse embryo transversal sections (Figure 3-5M).

The same antibodies used for the analysis of murine tissue shown in Figure 3-5 were utilized in an IF staining of E8 chick transversal sections (data not shown) to further characterize this model system for possible future experiments. However, this histological analysis was inconclusive, as most

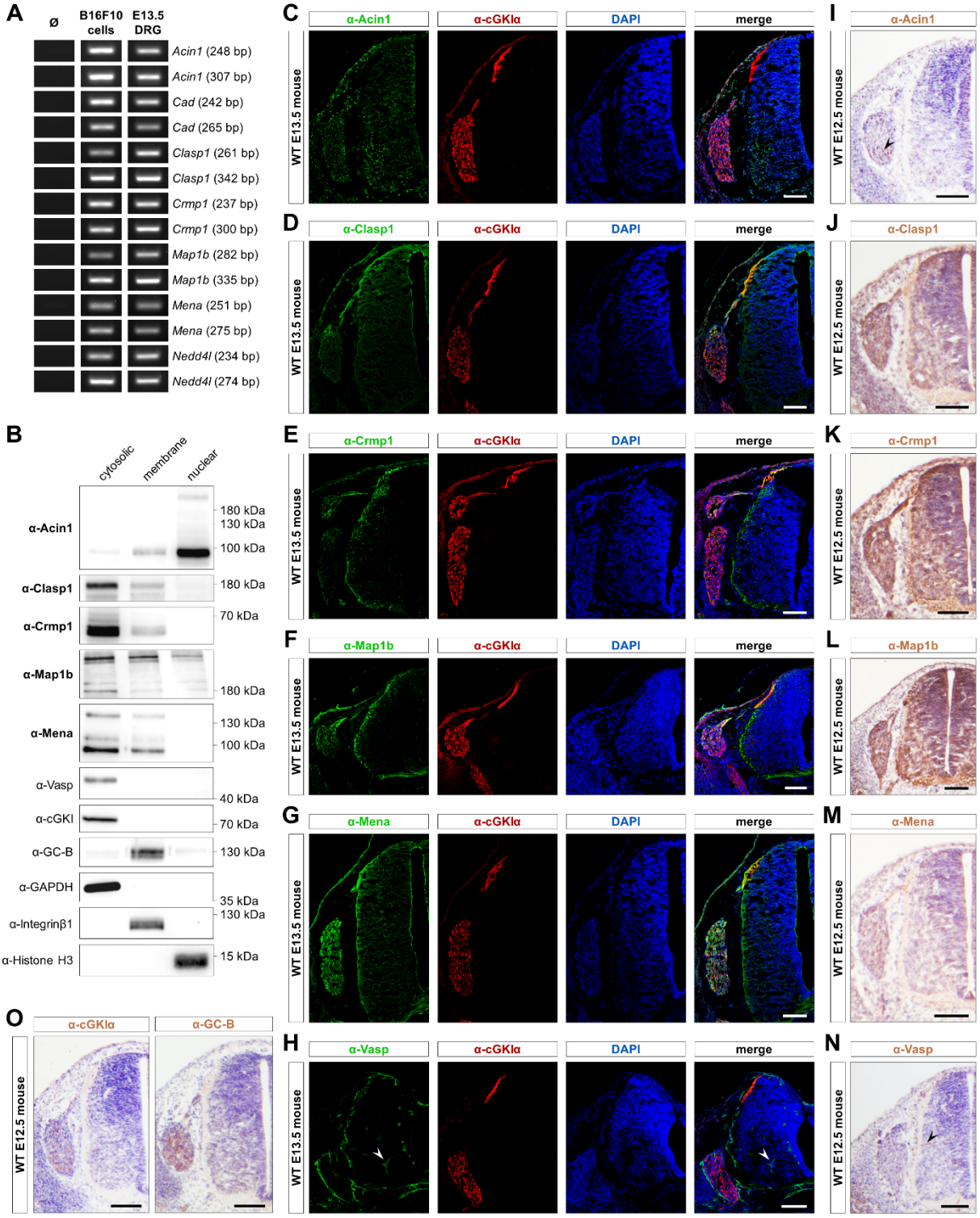

Figure 3-5 ***Select putative cGKI phosphorylation substrates are expressed in E13.5 DRGs.***

A: *RT-PCR analysis of select candidates Acin1, Cad, Clasp1, Crmp1, Map1b, Mena, and Nedd4l in B16F10 cells and mouse E13.5 DRG. Ø is a negative control without template in the reaction mix. The sizes of the PCR amplification products are given in parenthesis.* ***B:*** *WB analysis of select candidates Acin1, Clasp1, Crmp1, Map1b, Mena, known cGKI phosphorylation substrate Vasp, and cGMP-signaling components cGKI and GC-B in subcellular fractions of E13.5 DRG lysates. Loading controls for cytosolic, membrane, and nuclear fractions are GAPDH, integrin-β1, and histone H3, respectively. Molecular mass markers are indicated on the right.* ***C-H****: IF staining in transversal sections of E13.5 spinal cords of WT mice of select candidates Acin1 (**C**), Clasp1 (**D**), Crmp1 (**E**), Map1b (**F**), Mena (**G**), known cGKI phosphorylation substrate Vasp (**H**) (green) and cGKIα (red). Nuclei (blue) are stained with DAPI. Scalebar: 100µm.* ***I-O:*** *IHC staining (brown) of selected candidates Acin1 (**I**), Clasp1 (**J**), Crmp1 (**K**), Map1b (**L**), Mena (**M**), known cGKI phosphorylation substrate Vasp (**N**) and cGMP-signaling components cGKIα and GC-B (**O**). Nuclei (violet) are counterstained with hematoxylin. Scalebar: 100µm.*

antibodies (except anti-Acin1) did not give a signal on this tissue. Beside technical problems, the most probable cause for this could be that the antibodies simply do not recognize the chick protein.

In murine tissue however, all investigated proteins were found to be present in DRG neurons to some extent. The overwhelming localization of Acin1 in the nucleus, however, makes its interaction with and thus phosphorylation by cGKI *in vivo* unlikely. The phosphorylation of three other candidates (Clasp1, Map1b, and Mena) by cGKIα was investigated more closely in an *in vitro* assay presented in the following section.

3.3.2 Mena could be validated *in vitro* as cGKIα phosphorylation substrate via an analogue sensitive kinase assay

To validate the phosphorylation of specific proteins by cGKIα an ASK assay with an analogue sensitive mutant of the kinase was performed on several samples of either purified protein or COS7 cell lysate after transient transfection. The cGKIα-ASK can accept A*TPγS to catalyze a thio-phosphorylation in its substrates. This reaction can be visualized in a WB analysis after alkylating the thio-phosphates to TPEs with PNBM. By utilizing respective A mutants of candidates as negative controls, specific phosphorylation sites could also be evaluated.

An ASK assay of purified 3xFLAG-tagged Vasp showed the expected *in vitro* phosphorylation of this protein by a 3xFLAG-tagged ASK mutant of cGKIα (Figure 3-7B). This kinase also auto-phosphorylated, resulting in an additional protein band in WB analysis when probing for TPE. This reaction occurred only in the presence of 6-PheEt-ATPγS and after transforming thio-phosphate residues to TPE via treatment with PNBM.

An ASK assay of purified 3xFLAG-Mena (neuronal 140 kDa variant) showed *in vitro* phosphorylation of the protein by 3xFLAG-cGKIα-ASK as well as the auto-phosphorylation of the kinase only in the complete reaction mix (Figure 3-6A). When replacing WT Mena with a mutant that included an S637A substitution, the detected TPE band was diminished demonstrating the specificity of the phosphorylation of Mena at S637 by cGKI. The remaining of a band might indicate that the mutant could still be processed by cGKIα-ASK at other S or T residues, resulting in TPE signals. Possibly, Mena could be phosphorylated at S643, which was found in the phosphoproteome screen off B16F10 cells described above, or at S255, which was found to be phosphorylated by PKA [122] and corresponds to the established Vasp phosphorylation site at S153. The auto-phosphorylation of cGKIα-ASK was observed at the same level regardless of which Mena variant was present in the kinase reaction mix; this is indicated by an equally intense TPE band at ~76 kDa. As both Mena variants and cGKIα-ASK are all FLAG-tagged, their presence and equal loading was confirmed by re-probing the PVDF membrane with FLAG antibody after stripping the TPE antibody. Using this method, sizes of the detected TPE bands were also confirmed to correspond with their respective re-detection by FLAG antibody.

COS7 cells showed an endogenous expression of Mena, several other putative cGKI phosphorylation targets (Acin1, Clasp1, Crmp1, and Map1b), as well as the known phosphorylation target Vasp in WB analysis. However, the WT form of cGKI could not be detected (Figure 3-6B). Furthermore, the level of endogenous neuronal variant of Mena in COS7 cells was much lower than that of the smaller variants and could be greatly increased when transiently transfected with a respective expression plasmid (Figure 3-7A).

An ASK assay with a cell lysate containing cytosolic proteins of COS7 cells that were transiently transfected with an expression vector of 3xFLAG-Mena resulted in a visible TPE band for Mena under positive experimental conditions with all reaction components present (Figure 3-6C). Like the ASK assay with purified proteins, the MenaS637A mutant in COS7 cell lysate was thio-phosphorylated by cGKIα-ASK, but less so. Here, the remaining band could also result from endogenously expressed Mena in COS7 cells. Additionally, there were unspecific reactions catalyzed by enzymes present in the lysate, as indicated by the background signal present in the reaction mixes containing lysate, 6-PheEt-ATPγS, and PNBM but no cGKIα-ASK. A densitometry quantification of the TPE signal normalized by FLAG

yielded a significantly higher result for the reaction of 3xFLAG-Mena (mean ± SEM = 0.583 ± 0.034; n = 4) than 3x-FLAG-MenaS637A (mean ± SEM = 0.190 ± 0.051; n = 4) after subtraction of the background (p = 0.0011; t-test; Figure 3-6D).

Analogous experiments were performed with COS7 cells transiently transfected with 3xFLAG-tagged Clasp1 and Map1b and their respective A substituted mutants. For Clasp1 a TPE band could be observed in the reaction mix of the WT variants at the expected height of ~170 kDa, that was distinguishable from the background of the reaction lacking the ASK (Figure 3-7C). This indicates that Clasp1 was thio-phosphorylated by cGKIα-ASK *in vitro*. The same can be observed in the assay of Clasp1S646A however, so no statement can be made about the specificity of that site.

For Map1b, the experiment remained inconclusive. Possibly due to an insufficient amount of the tagged protein in the reaction mix or due to low blotting efficiency of this bigger protein, no TPE band could be observed in any reaction mix at the expected height (Figure 3-7D). Thus, no statement can be made about the *in vitro* phosphorylation of Map1b nor about the validity of the specific phosphorylation site at Map1b-pS561.

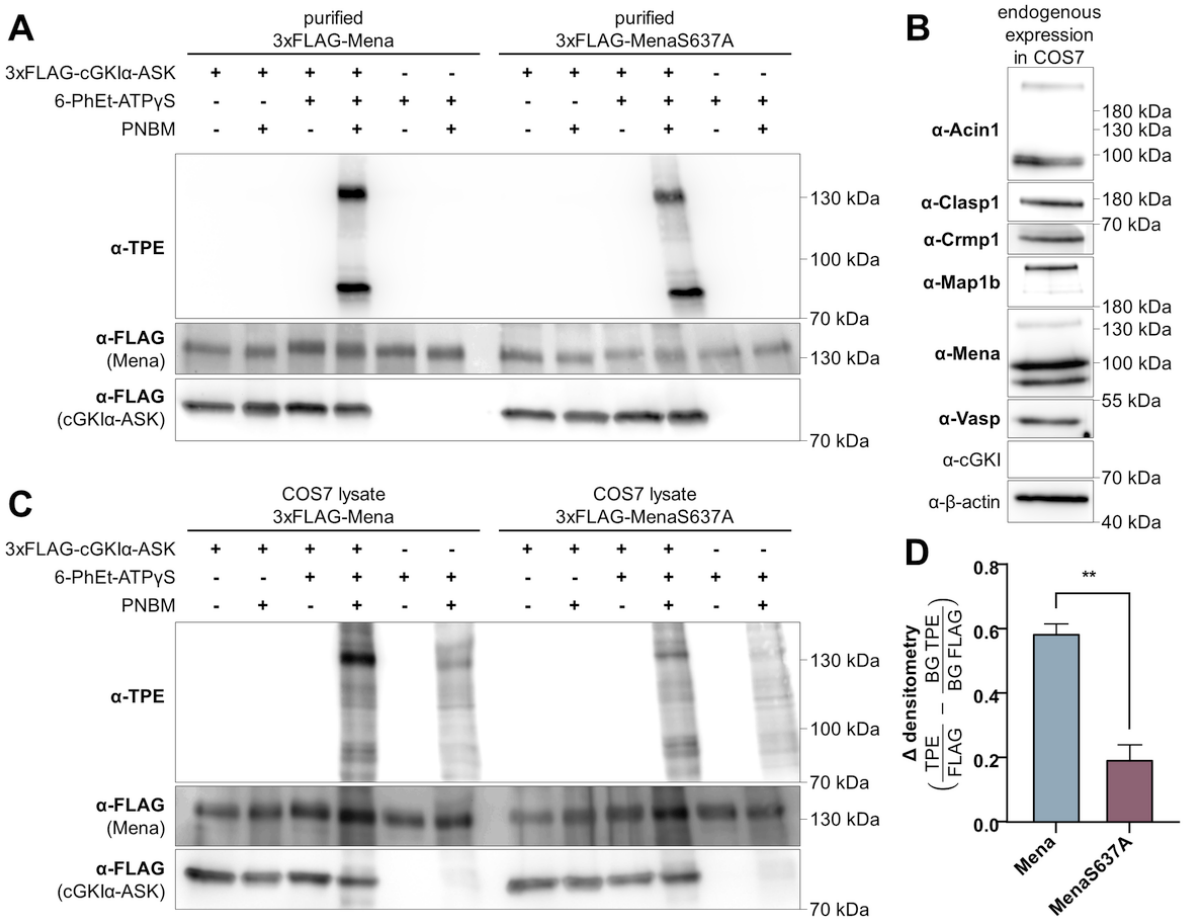

Figure 3-6 ***Mena could be validated in vitro as cGKIα phosphorylation substrate via an analogue sensitive kinase (ASK) assay.***

A*: WB analysis of ASK assay of purified 3xFLAG-Mena and respective alanine mutant 3xFLAG-MenaS637A with 3xFLAG-cGKIα-ASK. PVDF membrane was probed for TPE, stripped, then re-probed for FLAG. Molecular mass markers indicated on the right.* ***B:*** *WB analysis of endogenous expression of select putative cGKI phosphorylation substrates Acin1, Clasp1, Crmp1, Map1b, Mena, known cGKI phosphorylation substrate Vasp, and cGKI. As loading control, β-actin is used.* ***C:*** *WB analysis of ASK assay of COS7 lysate transfected with 3xFLAG-Mena and respective alanine mutant 3xFLAG-MenaS637A with 3xFLAG-cGKIα-ASK. PVDF membrane was probed for TPE, stripped, then re-probed for FLAG. Molecular mass markers indicated on the right.* ***D:*** *Quantification of densitometric analysis of 3xFLAG-Mena and 3xFLAG-MenaS637A thio-phosphorylated by 3xFLAG-cGKIα-ASK. TPE signal normalized by respective FLAG signal. The signal of the last column was subtracted as background (BG). N=4 technical replicates analyzed by one WB each. Values given as mean±SEM. **p=0.0011 (t-test).*

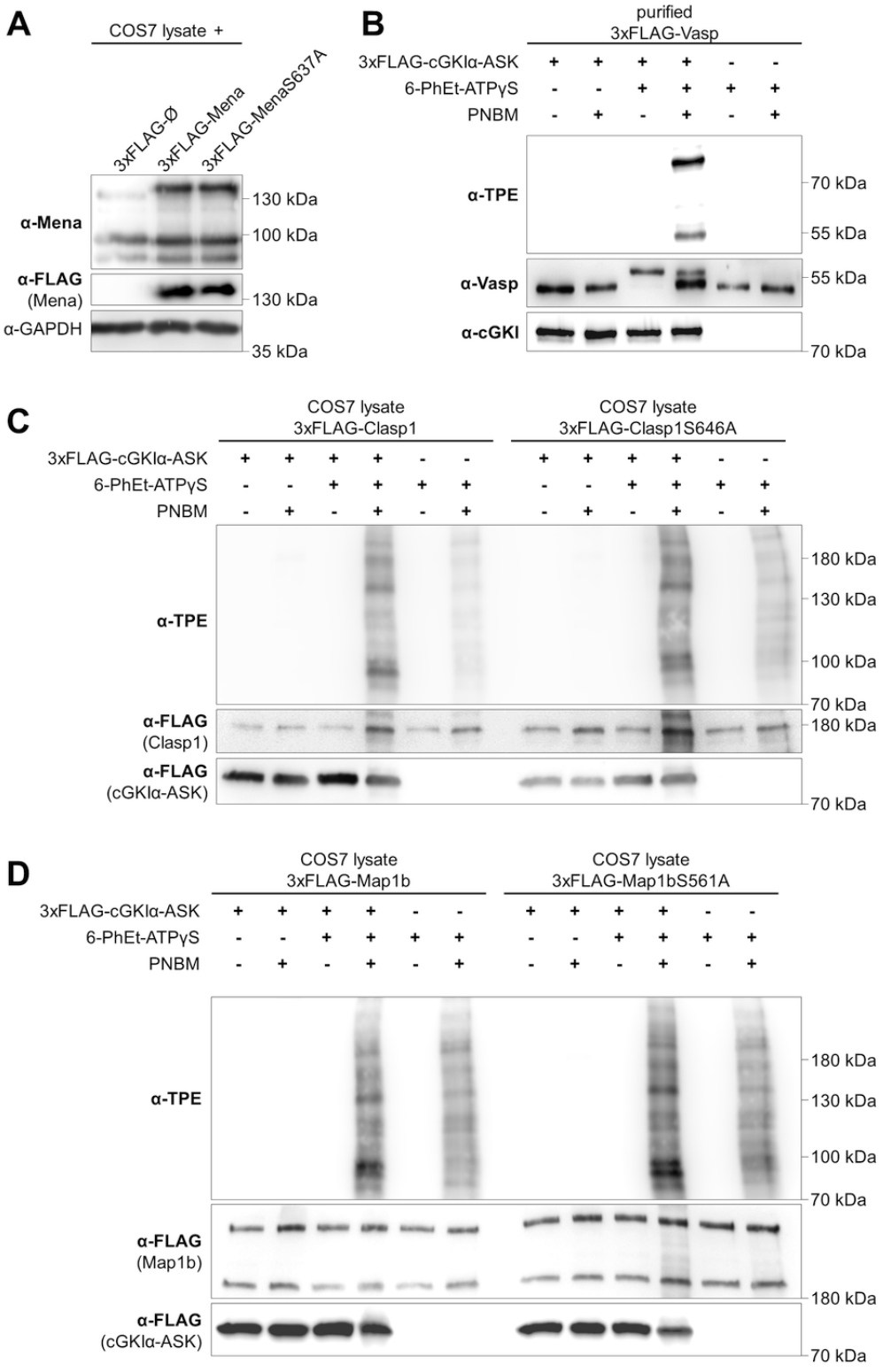

Figure 3-7 ***Clasp1 and Map1b could not be validated in vitro as cGKIα phosphorylation substrate via an analogue sensitive kinase (ASK) assay.***

A: *WB analysis of COS7 whole cell lysates transiently transfected with empty FLAG-tag vector (3xFLAG-Ø) and mammalian expression vectors for 3xFLAG-Mena and 3xFLAG-MenaS637A. GAPDH is loading control.* ***B:*** *WB analysis of ASK assay with purified 3xFLAG-Vasp. ASK samples were loaded twice, one PVDF membrane being probed for TPE, the other divided and the parts probed for cGKI and Vasp, respectively.* ***C:*** *WB analysis of ASK assay of COS7 lysate transfected with 3xFLAG-Clasp1 and respective alanine mutant 3xFLAG-Clasp1S646A, with 3xFLAG-cGKIα-ASK. PVDF membrane was probed for TPE, stripped, then re-probed for FLAG.* ***D:*** *WB analysis of ASK assay of COS7 lysate transfected with 3xFLAG-Map1b and respective alanine mutant 3xFLAG-Map1bS561A, with 3xFLAG-cGKIα-ASK. PVDF membrane was probed for TPE, stripped, then re-probed for FLAG.* ***A-D:*** *Molecular mass markers indicated on the right.*

3.3.3 Summary

All tested putative cGKI substrates transcripts (Acin1, Cad, Clasp1, Crmp1, Map1b, Mena, Nedd4l) were expressed in embryonic DRG neurons to some capacity. While for Cad, and Nedd4l, only the transcription could be shown so far, their tissue distribution and *in vitro* phosphorylation might be tested in the future if suitable antibodies and expression vectors are available. Acin1, while highly phosphorylated at S825 and other sites in both screening experiments presented in this thesis, could mostly be found in the nuclei of both DRG neurons and surrounding tissue. This makes phosphorylation by the cytosolic kinase cGKI *in vivo* less likely. Clasp1, Crmp1, Map1b, and Mena are all present in embryonic DRG cytosolic and membrane fractions in WB analysis and can be found in DRG neuron projections to the DREZ in IF staining.

The phosphorylation of Clasp1, Map1b, and Mena was also tested *in vitro* with an analogue sensitive mutant of cGKIα. Here, the analysis of Clasp1 and Map1b was inconclusive so far, while Mena was shown to be phosphorylated. Additionally, the phosphorylation site of Mena at S637 that was discovered in a phosphoproteome screen of CNP-stimulated E13.5 DRG tissue could be confirmed in this *in vitro* assay. However, the A mutant of this site could still be phosphorylated, indicating other additional cGKIα phosphorylation sites in Mena. The established cGKI substrate Vasp was likewise expressed in DRGs and could be phosphorylated in the ASK assay. In the following section, the bifurcation phenotype of a Vasp-KO and several other mouse models were investigated to further elucidate the signaling pathway involved in this process.

3.4 SOMATOSENSORY AXON TRACING STUDIES

To see the impact of genetic aberrations on the axon bifurcation phenotype of DRG neurons, it is possible to visualize those branching events at both an embryonic stage and postnatally. Here, excised embryonic spinal cords with intact attached DRGs of different transgenic mouse lines were labeled with a lipophilic tracer – DiI – which travels along cell membranes, thus encompassing the axonal projections of marked DRG neurons. At E13.5 all DRG projections of WT mice have undergone bifurcation at the DREZ [37,40,41], which makes this a good reference point of comparing the bifurcation rate of transgenic mice. Presented here, are the axon tracing studies via DiI labeling of three mouse lines compared to the WT. Mlk3 has been found to be a cGKIα phosphorylation substrate as well as an LZ domain interaction partner [123]. Here, the effect of this protein's absence on somatosensory axon bifurcation was investigated with a respective KO mouse model [93]. The effect of a functioning LZ domain of cGKIα on somatosensory axon bifurcation in general was investigated with a cGKI-LZM mouse line [90]. A KO of Vasp was analyzed, as it is a known substrate of cGKI [20], that is expressed in DRG neurons at their time of bifurcation, but its involvement in this process has not been shown. Axon tracing studies at a postnatal stage were performed in the present work via a Thy1-YFP-H reporter mouse line on Vasp-KO mouse models. In mouse models with bifurcation errors, this can be done to show a possible compensation at later developmental stages. All analyses of the cGKI-LZM and the Mlk3-KO mouse lines were performed by the author at in the facilities of Assoc. Prof. Robert Blanton at the Tufts Medical Center (Boston, USA), who kindly provided the animals for these studies.

3.4.1 Knock-out mouse models of Vasp and Mlk3 have normal DRG axon bifurcation

Axon tracing studies of murine embryonic DRG neurons with DiI labeling showed the T-branches resulting from bifurcation of sensory axons after entering the spinal cord at the DREZ in WT animals (Figure 3-8A). Quantification of DiI-labeled DRG neurons in spinal cords of seven animals showed an almost-pure bifurcation phenotype, with 99.2 % of 122 counted axons exhibiting a functioning bifurcation, resulting in the T-shaped branches (Figure 3-8B). Embryos of Vasp-KO (100 % T-branches in 61 counted axons of n = 3 animals) and Mlk3-KO (90.7 % T-branches in 226 counted axons of n = 7 animals) mice had a comparable phenotype with the vast majority of axons bifurcating (Figure 3-8A+B). The involvement of Vasp in axon bifurcation was further investigated using P15 Thy1-YFP-H reporter mice with a heterozygous and homozygous KO of Vasp (Figure 3-8C). In both genotypes most of the counted axons endogenously labeled with YFP had bifurcated. In n = 1 spinal cord of a Thy1-YFP-

H;Vasp$^{WT/KO}$ mouse, 95.7 % of the counted 117 axons bifurcated, while in n = 3 spinal cords of Thy1-YFP-H;Vasp$^{KO/KO}$ mice 98.7 % of the 225 counted axons bifurcated (Figure 3-8D). Analysis artifacts are a probable source of deviation from the expected 100 % of axons bifurcating.

3.4.2 A leucine zipper mutant of cGKIα shows DRG axon bifurcation error

An aberrant bifurcation phenotype was observed in an axon tracing study by DiI labeling of E13.5 DRG neurons of cGKI-LZM mice (Figure 3-8A). The quantification of n=6 spinal cords with 226 counted axons resulted in only 23 % T-branches and 77 % turns (42 % R-turns to the rostral end of the spinal cord and 35 % C-turns to the caudal end; Figure 3-8B). The disrupted bifurcation phenotype of the cGKI-LZM mouse line indicates that a cGKIα LZ domain interacting protein is likely functionally involved in the bifurcation process of murine somatosensory axons.

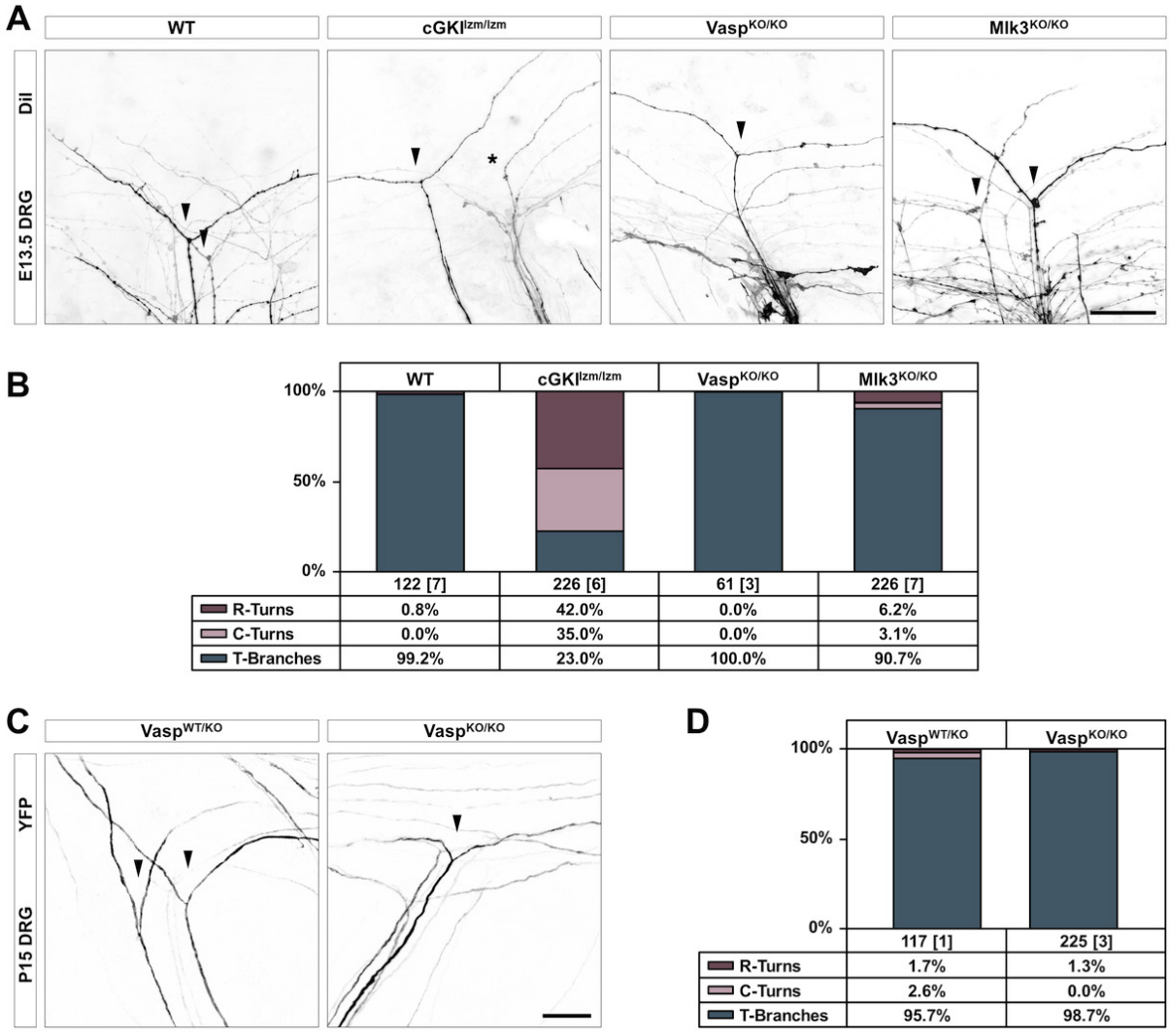

Figure 3-8 ***Axon bifurcation in cGKI-LZM mice is impaired, while it is normal in Vasp-KO and MLK3-KO mice.***

A: *DiI tracing of axon projections in DRG neurons of WT, cGKI-LZM, Vasp-KO, and MLK3-KO mice at E13.5. Axons from WT, Vasp-KO, and MLK3-KO mice nearly always show a T-branch (arrow), while axons from mice with mutated LZ domain in cGKI often fail to bifurcate (asterisk). Scale bar: 50µm.* ***B:*** *Quantification of the bifurcation phenotype of DRG neurons from WT, cGKI-LZM, Vasp-KO, and MLK3-KO embryos showing the percentage of T-branches, rostral turns, and caudal turns. Numbers indicate the number of axons counted with the number of embryos analyzed given in brackets.* ***C****: Axon tracing of DRG axons from P15 Thy-1-YFP-H reporter mice crossed into Vasp-KO mice normal sensory axon bifurcation (arrow) in the dorsal root entry zone. Scale bar: 50µm.* ***D:*** *Quantification of branching errors using Thy-1-YFP-H reporter mice. Numbers indicate the number of axons counted with the number of spinal cords analyzed given in brackets. C, caudal; KO, knock-out; LZM, leucine zipper mutant; R, rostral; WT, wild type.*

3.4.3 Summary

Neither the KO of Vasp nor Mlk3 affected the bifurcation phenotype of DRG neurons *in vivo* in the present axon tracing studies. As other Ena/Vasp protein family members are present in DRG neurons at the time of bifurcation, it is possible they have a compensatory effect. Specifically, Mena, which has been identified as putative cGKI substrate in the present work could play a role here. A KO mouse model of this protein has indeed been investigated and no bifurcation error could be observed [H. Schmidt, unpublished]. Notably, double KO mouse models of Vasp and Mena and even a triple KO of Mena, Vasp, and Evl have successfully been generated by others and their DRG axon bifurcation phenotype could be investigated in future studies [18,124,125]. Interestingly, cGKI-LZM mice exhibit an error in their DRG axon bifurcation phenotype. While bifurcation is all but absent in cGKI-KO mice [5] it is reduced in embryos of cGKI-LZM animals. This indicates at least a partial involvement of a substrate that interacts with cGKI via its LZ domain, hinting at a possible bigger complex of proteins that could regulate the bifurcation process of DRG neurons at this specific spatiotemporal point.

3.5 Interactome studies of GC-B

A possible point of regulation for cGMP signaling during DRG axon bifurcation lies with cGMP generator and CNP receptor GC-B. The GC activity of this enzyme depends not only on the extracellular binding of its ligand CNP, but also on the phosphorylation state of its KHD. Thus, identifying kinases or phosphatases that regulate GC-B could be important in understanding the signaling pathway leading to a single bifurcation event of DRG neurons at the DREZ. As transmembrane protein, GC-B also represents a prime candidate in anchoring a hypothetical protein complex including downstream components to the membrane and cytoskeleton in the growth cone of developing DRG axons. Thus, to screen for putative GC-B interactors I performed pulldown studies with subsequent MS analysis in collaboration with the CFMB (University of Tübingen). Anti-HA pulldowns were performed on both murine adult heart tissue and embryonic DRG tissue of GC-B-HA and WT animals, allowing for several potential interacting proteins to be identified in both screens.

3.5.1 Adult heart

In a WB analysis, anti-HA staining detected a double band at ~117/130 kDa corresponding to HA-GC-B in whole lysate of heart tissue from GC-B-HA mice which was absent in lysates from WT mice (Figure 3-9E). Additionally, an unspecific band was detected in lysates from both WT and GC-B-HA mice which is in accordance with previous results [91].

An anti-HA pulldown was performed with the lysates of GC-B-HA and WT tissue using different total protein amounts (1 mg, 0.5 mg, and 0.25 mg), henceforth referred to as experiments a, b, and c, respectively. For each experiment, n = 4 technical replicates were performed. In the eluates 755, 770, and 762 individual proteins for experiments a, b, and c, respectively, were found in an MS analysis of the GC-B-HA tissue versus the WT control (Figure 3-9A-C). For each experiment, several putative interactors were consistently and significantly enriched in the GC-B-HA pulldown, with Δ(HA-WT) ≥ 2, t-test p-value ≤ 0.05, and significance A ≤ 0.05 (Figure 3-9F, Table 3-5). The bait protein GC-B was significantly enriched in all three experiments, with a difference of medians of 25.22 (experiment a), 24.01 (experiment b), and 24.03 (experiment c) (red stars in Figure 3-9A-C). Additionally, the cytoskeletal protein Map1a was significantly enriched at all investigated protein amounts with differences of medians of 23.67 ($p = 1.62*10^{-14}$, A<0.001; experiment a), 24.29 (p = 0.02, A<0.001; experiment b), and 24.60 (p = 0.02, A<0.001; experiment c). Interestingly, there were two additional results overlapping with the multifunctional methyltransferase subunit TRM112-like protein (Trmt112) that showed significant interaction in experiments a and c, and the mitochondrial 39S ribosomal protein L1 (Mrpl1), which was found as interactor in experiments b and c (Figure 3-9F, Table 3-5).

Table 3-5 ***Putative GC-B interactors found in proteome analysis of heart lysates.*** *Proteins are listed alphabetically.*

Gene names	Protein ID (UniProt)	Compartments[1]	Δ(HA-WT)[2] Experiment a (1 mg)	Experiment b (0.5 mg)	Experiment c (0.25 mg)
Asrgl1	Q8C0M9	C	(0.97)	23.23	--
Cbr1	P48758	C, M, N, O	24.00	--	--
Chchd1	Q9CQA6	C, N, O	-24.57	--	24.85
Ckap4	Q8BMK4	C, CS, M, O	25.47	(0.12)	--
Eloa	Q8CB77	N	22.63	(0.38)	(1.34)
Igkv12-41	P01635	E	26.47	(1.02)	(-0.68)
Macf1	Q9QXZ0	C, CS, M, O	--	22.36	--
Map1a	Q9QYR6	C, CS	23.67	24.29	24.60
Mrpl1	Q99N96	O	--	23.91	23.83
Mrpl28	Q9D1B9	C, O	(1.28)	--	23.74
Mrps31	Q61733	O	25.00	--	(0.19)
Ngdn	Q9DB96	C, N, O	23.89	(-1.42)	--
Qars	Q8BML9	C	(1.23)	--	22.14
Reep5	Q60870	O	21.41	(-21.18)	--
Sept2	P42208	C, CS, E, M, N, O	(1.32)	24.00	--
Serpinh1	P19324	C, E, O	--	23.26	--
Srrm1	Q52KI8	N	(0.56)	(1.06)	23.70
Tom1	O88746	C, M, O	--	--	23.42
Trmt112	Q9DCG9	C, N	25.38	(0.12)	23.83
Ywhaq	P68254	C	--	--	23.43

[1] *Compartments: C: cytosol, CS: cytoskeleton, E: extracellular, M: membrane, N: nucleus, O: organelles*
[2] *Values in brackets are not significant.*

3.5.2 Embryonic DRGs

In accordance with tissue lysates of adult murine hearts, E13.5 DRG tissue contained a relatively high amount of GC-B, as shown in a WB analysis of the HA-tagged protein in WT and GC-B-HA tissue. In addition to the expected unspecific protein band, only anti-HA probing of E13.5 DRG tissue lysates of GC-B-HA mice yielded the double band at ~117/130 kDa (Figure 3-9E).

An MS analysis of anti-HA pulldown eluates from E13.5 DRG tissue lysates of GC-B-HA mice versus WT controls yields 1027 detected proteins quantified in at least 50 % of samples (Figure 3-9D). Of those, 35 proteins were significant (t-test p-value ≤ 0.05 and significance A ≤ 0.05), 24 of which were specifically pulled down with anti-HA magnetic beads (difference of medians ≥ 2). Among those proteins was the bait protein GC-B with the highest difference of medians at 30.33 ($p = 2.82*10^{-14}$, A<0.001; red star in Figure 3-9D). The 23 putative interactors of GC-B found in this experiment are listed in Table 3-6.

Surprisingly, none of the putative GC-B interactors found in heart tissue proteome analysis could be confirmed in E13.5 DRG tissue. Indeed, the proteins Map1a and Mrpl1 were not detected in the samples at all, while Trmt112 was identified but was not specifically pulled down with anti-HA magnetic beads in the GC-B-HA samples (Δ(HA-WT) = -0.04; p = 0.39; A = 0.59).

However, 8 of 23 putative GC-B interactors found in E13.5 DRG tissue are annotated by UniProt to be found in the membrane compartment, and 6 are part of the cytoskeleton (marked in green in Figure 3-9D+G). Indeed, Mapt was not only found as putative interactor of GC-B in this experiment (Δ(HA-WT) = 29.32, p = 0.012, A<0.001), but a significant downregulation of the phosphorylation site pT112-Mapt after treatment with CNP was also found in the E13.5 DRG phosphoproteome screen (mean CNP/control = 0.56; Figure 3-9G). Aside from the interaction with Mapt, additional direct links to the cytoskeleton were made via clathrin heavy chain 1 (Cltc), cytoplasmic dynein 1 heavy chain 1 (Dync1h1), tubulin alpha-1B chain (Tuba1b), TAO serine/threonine-protein kinase 2 (Taok2), and tubulin beta-6 chain (Tubb6). A similar overlap of putative GC-B interactors was found with the B16F10 phosphoproteome screen, as the phosphorylation site pS495-Hmgcs1 of the cytoplasmic protein hydroxymethylglutaryl-CoA synthase (Hmgcs1) was significantly downregulated there (mean 8Br-

cGMP/control = 0.21; Figure 3-9G). The only potential GC-B interactor with a kinase domain found in the present study is Taok2.

3.5.3 Summary

While no proteins containing an LZ domain nor phosphatases were identified in the screens for putative GC-B interactors in murine adult heart and embryonic DRG tissue samples described above, one protein with kinase activity was detected as possible interactor of GC-B in embryonic DRGs. Additionally, a connection to the cytoskeleton was found in both screens. Map1a was consistently pulled down with GC-B in lysates of adult murine heart tissue at three tested total protein amounts. In DRG samples of E13.5 mouse embryos, not only Mapt but two different tubulin monomers (Tuba1b and Tubb6) were found to interact with GC-B. This lends itself to the idea that GC-B is physically connected to the cytoskeleton. Especially in DRG axon growth cones, where it could be part of a bigger protein complex that regulates the bifurcation process.

Table 3-6 ***Putative GC-B interactors found in proteome analysis of E13.5 DRG tissue.*** *Proteins are listed alphabetically.*

Gene names	Protein ID (UniProt)	Δ(HA-WT)	Compartments[1]
--	P01787	27.47	E
Abcd3	P55096	23.86	O
Asph	Q8BSY0	23.42	C, M, O
Ccdc47	Q9D024	23.27	O
Cltc	Q68FD5	24.00	C, CS, M, O
Ddost	O54734	23.93	O
Dync1h1	Q9JHU4	24.25	C, CS, M, N
Gabbr1	Q9WV18	23.44	C, E, M
Hmgcs1	Q8JZK9[2]	22.75	C
Mapt	P10637[3]	29.32	C, CS, E, M, N
Mrpl50	Q8VDT9	23.48	C, O
Pabpn1	Q8CCS6	25.29	C, N
Pgrmc1	O55022	23.97	O
Prkar2b	P31324	24.55	C, M
Rbx1	P62878	24.03	C, N
Rfc3	Q8R323	23.24	N
Rit1	P70426	24.36	M
Sec16a	E9QAT4	24.55	C, O
Taok2	Q6ZQ29	22.87	C, CS, N, O
Tuba1b	P05213	27.07	C, CS, M
Tubb6	Q922F4	24.35	C, CS, E
Ubap2	Q91VX2	23.44	C, N
Znf652	Q5DU09	24.18	N

[1] Compartments: C: cytosol, CS: cytoskeleton, E: extracellular, M: membrane, N: nucleus, O: organelles
[2] Significantly downregulated phosphorylation of pS495-Hmgcs1 after treatment with 8Br-cGMP was found in B16F10 phosphoproteome screen.
[3] Significantly downregulated phosphorylation of pT112-Mapt after treatment with CNP was found in E13.5 DRG phosphoproteome screen.

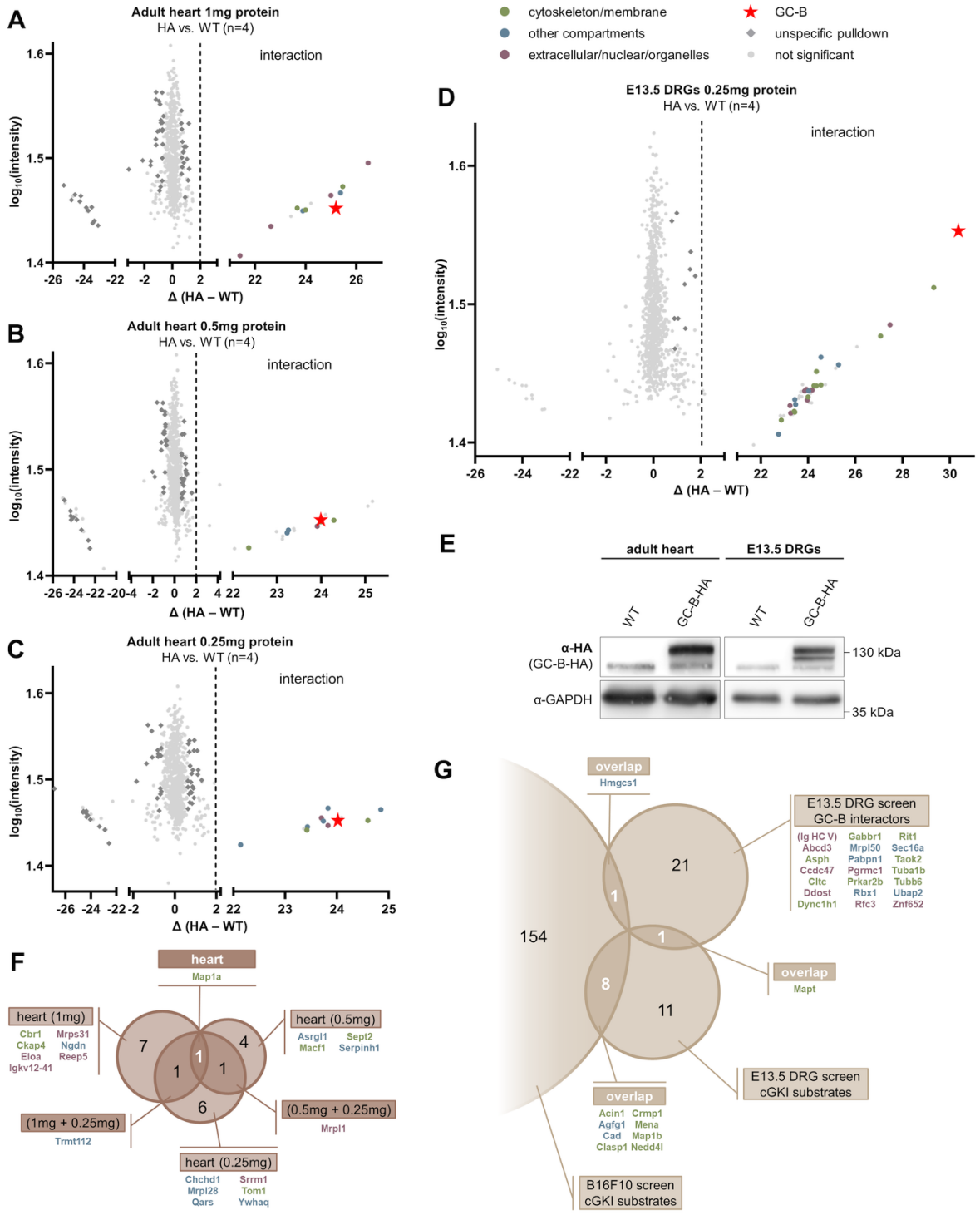

Figure 3-9 ***Proteomic screen for GC-B interactors in adult heart and E13.5 DRG lysates of GC-B-HA mice.***

A-D: *MS analysis of enriched proteins in lysates of GC-B-HA mice versus WT mice. Heart tissue lysates of adult mice (P95 WT, P75 GC-B-HA) were analyzed at different total protein amounts with 4 technical replicates each containing 0.25mg (**A**), 0.5mg (**B**), and 1mg of protein (**C**). Embryonic DRG were analyzed with lysates of 4 litters each of GC-B-HA mice and WT mice, containing 0.25mg total protein (**D**). Interaction is considered significant if both t-test p-value ≤ 0.05 and significance A ≤ 0.05. All other events are considered not significant (light grey circle). Interactions are defined with a difference of medians of at least 2. Interactors located only in the nucleus, other organelles, or the extracellular space are shown in purple. Those occurring in the cytoskeletal compartment, and/or the membrane are shown in green. All others are marked in blue. GC-B is marked with a red star. All remaining events are considered as unspecific pull-down (dark grey diamonds).* ***E:*** *WB analysis of heart tissue lysates used in the MS analysis and one representative lysate each of the E13.5 DRG lysates. Membranes were probed for HA-tag. GAPDH is shown as loading control. Molecular mass markers indicated on the right.* ***F:*** *Venn diagram of the 20 putative GC-B interactors found in heart lysates.* ***G:*** *Venn diagram of the 175 peptides with significant change in phosphorylation found in phosphoproteomic screens of B16F10 cells and E13.5 DRGs and the 23 putative GC-B interactors found in E13.5 DRG tissue.* ***F, G:*** *Results are listed as gene name colored according to compartment group as above.*

4 DISCUSSION

The work presented in this thesis aimed for the discovery of novel components of a cGMP-dependent signaling pathway that mediates axon bifurcation of somatosensory neurons during embryonic development. Specifically, putative phosphorylation substrates of cGKI and interactors of GC-B were investigated to gain further insight into the mechanism of axon bifurcation.

The network of neurons that builds up the mature nervous system is laid out during the embryonic and early postnatal stages. During this time, neurons establish connections with each other via their outgrowing axons, led by growth cones. Axon navigation and growth cone dynamics are based in large part on the cytoskeletal rearrangement and are mediated by vast groups of microtubule- and actin-associated proteins. Regulation of this system by extracellular guidance cues has been studied extensively. However, intracellular mechanisms that affect specific changes in the growth cone remain poorly understood. A big field of study in this regard deals with different patterns of axon branching. The somatosensory system is used as a model system to study those patterns, as bifurcation, interstitial branching, and terminal arborization occur in a stereotyped manner in its first-order neurons. Indeed, it has been found that a cGMP-dependent signaling pathway mediates an axon bifurcation event of somatosensory neurons during development of mouse embryos. When outgrowing axons of DRG neurons arrive at the DREZ of the spinal cord extracellular CNP – released by cells in the dorsal spinal cord – binds to the transmembrane receptor GC-B on DRG neurons. In turn, the activated enzymatic domain of GC-B starts to convert GTP molecules to cGMP. Subsequently, binding of cGMP molecules to cGKIα results in the activation of the enzyme, which then phosphorylates yet to be identified substrates. Eventually, this leads to a restructuring of the growth cone that facilitates its splitting into two stem axons that extend along the rostro-caudal axis. To allow a better mechanistic understanding, this work aimed to identify those cGKIα phosphorylation substrate(s) that mediate(s) axon bifurcation.

The process of axon bifurcation in DRG neurons during embryonic development is spatiotemporally specific. Exactly one bifurcation occurs when the axon enters the oval bundle of His at the DREZ. The resulting two stem axons experience no more bifurcations but instead – after a waiting period – develop collaterals via interstitial branching. Thus, the signaling pathway leading to axon bifurcation needs to be tightly regulated. As CNP is present in the surrounding spinal cord tissue for several days, the hypothesis of a negative feedback loop of the pathway inhibiting itself after initial activation is suggested. A possible switch in this regard is GC-B, as dephosphorylation of seven regulatory S/T residues in its KHD deactivates the enzymatic activity regardless of the presence of CNP, a process which has been termed desensitization. This work investigated GC-B interactors with possible phosphatase or kinase activity and a link to cGKI substrates via downstream kinases or phosphatases.

Considering the precise necessary rearrangements in the structure of the growth cone that would have to precede a split opens many possibilities of spatially distinct changes affected by the CNP-induced cGMP signaling pathway mediating sensory axon bifurcation. For example, the cascade might result in the inactivation or even removal of cytoskeletal components from the center of the growth cone, or it might promote the growth of actin filaments or microtubules on both sides of the growth cone, or it might regulate membrane dynamics. If the cascade indeed has a spatially constricted effect, the transmembrane receptor GC-B could be at the center of a membrane-bound complex that integrates cytoskeletal compounds and guides cGKI to its target substrates. Indeed, cGKI might interact with such a complex via its LZ domain.

In order to identify novel components of the cGMP-dependent signaling pathway that engage in the process of axon bifurcation of somatosensory neurons during embryonic development (Section 1.4; Figure 1-7), putative substrates of cGKI and GC-B interactors were screened. The screening of potential cGKI substrates took into account the consensus sequence of this kinase, its interactions via the LZ domain, possible downstream effects via kinases and phosphatases, as well as subcellular compartments such as the membrane and cytoskeleton. Furthermore, the investigation of GC-B interactors focused on

putative regulators of its KHD phosphorylation state, crosslinks with putative cGKI substrates or LZ domain interactors, and a hypothetical membrane anchoring complex that integrates cytoskeletal components in the growth cone.

This work successfully identified several novel putative elements of a cGMP-dependent signaling cascade in embryonic DRG neurons and other tissues. Substrates of cGKI that could be detected in both a murine melanoma cell line and E13.5 DRG tissue include Acin1, Cad, Clasp1, and Crmp1 with concordant phosphorylation sites in both analyses. Additionally, Mena, Map1b, and Nedd4l were identified as potential substrates in both studies with differing specific phosphorylation sites (Section 3.2). The expression analysis of those putative cGKI substrates largely confirmed their presence in embryonic DRG tissue (Section 3.3.1). Additionally, the cGKIα-mediated phosphorylation of the known substrate Vasp and the identified candidate substrate Mena – both members of the Ena/Vasp-family of actin regulators – could be verified *in vitro* (Section 3.3.2).

Axon tracing studies revealed that a lack of the established cGKI substrates Vasp or Mlk3 does not affect the bifurcation of somatosensory neurons at the DREZ (Section 3.4.1). A mutation in the LZ domain of cGKIα disrupting the enzyme's substrate interaction but not its kinase activity resulted in a loss of axon bifurcation in 77 % of DRG neurons, indicating the involvement of LZ domain interactors of cGKI in the process of growth cone splitting (Section 3.4.2).

The investigation of GC-B interactors revealed candidates that might be of interest in adult heart tissue as well as embryonic DRGs. While no phosphatases or kinases could be detected in the present studies, several links to the cytoskeleton and cytoskeleton-associated proteins have been detected, e.g., MAPs and tubulin monomer isoforms. Map1a consistently interacted with GC-B-HA in adult heart tissue (Section 3.5.1). Tuba1b and Tubb6 could be pulled down with GC-B-HA in E13.5 DRG tissue in addition to Mapt (Section 3.5.2), which was also identified as potential cGKI substrate in the same tissue.

As a means to perform future verification experiments for the found putative components of a cGMP-dependent signaling cascade in DRG neurons, chick embryos might be used as an alternative model system to mice to analyze the contribution of identified candidate proteins in sensory axon bifurcation. Therefore, this work began to investigate the involvement of cGMP signaling cascade components and functions in chick DRGs. Here, the expression of cGKI in E8 chick DRGs could be shown (Section 3.1.2).

4.1 Putative novel cGKI phosphorylation substrates

To investigate novel substrates of cGKI, it was necessary to first confirm the presence and activity of the enzyme in the tissues and models that were used. In B16F10 cells, cGKI was present throughout the cytosol independent of stimulation with membrane permeable 8Br-cGMP or extracellular ligand CNP. An IF staining of cGKI in DRG neurons of transversal embryo sections could also be replicated. A biochemical screen for phosphorylation substrates of cGKI was performed both in the cell line and in acutely dissected DRGs of E13.5 mouse embryos. The stimulation of cGKI was achieved with 8Br-cGMP in B16F10 cells and a phosphoproteome analysis revealed 125 significantly upregulated phosphorylation sites, while 59 were significantly downregulated. The E13.5 DRGs of WT and cGKI-KO mice were stimulated with CNP. Analysis of the phosphoproteome revealed 19 significantly upregulated and 6 significantly downregulated phosphopeptides in WT tissue after subtracting the cGKI independent hits detected in the sample of cGKI-KO mice. Seven proteins (Acin1, Cad, Clasp1, Crmp1, Map1b, Mena, Nedd4l) were selected for further verification as direct cGKI phosphorylation substrates, as their modification was detected in both screening experiments. In an expression analysis, their transcription could be confirmed in E13.5 DRG tissue. With the use of specific antibodies, the expression of five candidates (Acin1, Clasp1, Crmp1, Map1b, Mena) could be confirmed in the cytosolic fraction of E13.5 DRG lysates as well as their presence in cGKIα positive DRG neurons and their projection to the DREZ to varying degrees. In an *in vitro* assay, the phosphorylation of Vasp and Mena by cGKIα could be

confirmed and the detected phosphorylation site of Mena at S637 was verified. While the results for Clasp1 indicate a phosphorylation by cGKI, the results for Map1b have been inconclusive.

4.1.1 B16F10 cell line

A pilot experiment using SILAC to identify novel cGKI substrates in general as opposed to those involved specifically in DRG axon bifurcation was performed on the murine melanoma cell line B16F10. The use of a cell line ensures fast and easily obtained substantial amounts of samples. It is also suited for the metabolic SILAC labeling technique that requires dividing cells for the successful incorporation of isotopes into the proteome.

Before B16F10 cells were used in a phosphoproteome study, WB analysis of subcellular fractions and IF staining of fixed cultured cells revealed the presence of cGKI in the cytosol of these cells. This localization remained unchanged after indirect and direct stimulation of cGKI activity by CNP or 8Br-cGMP, respectively (Figure 3-1). Putative phosphorylation substrates should thus also be located in this subcellular compartment.

For the phosphoproteome analysis, the cells were treated with 8Br-cGMP (0.5 mM, 5 min, 37 °C) to reach a strong consistent activation of cGKI throughout. The administration of this relatively high concentration of membrane permeable cGMP analog, however, can also lead to unspecific stimulation of PKA activity. Therefore, the specificity of phosphorylation substrates to cGKI in this experiment is not entirely certain, representing a major limitation of the study.

MS analysis of 8Br-cGMP-treated cells compared to an unstimulated control condition identified 125 significantly upregulated and 59 significantly downregulated phosphopeptides (Section 3.2.1; Figure 3-3). These include 14 significantly regulated sites of several proteins that contain kinase domains. Some of them were modified at a known regulatory position. Cdk16 was found to be increasingly phosphorylated at S153 in 8Br-cGMP stimulated B16F10 cells, which is known to inhibit its kinase activity [126]. Phosphorylation of Cdk7 at T170 on the other hand, is required for this enzyme's activity and known to be dependent on Cdk2 [127]. This coincides with the downregulated Cdk2-Y15 phosphorylation found here, as this corresponds with a known regulatory site as well. Notably though, this must be an indirect effect, as the S/T-kinase cGKI does not modify Y residues. Phosphorylation of Cdk2-T14 and -Y15 inactivates the enzyme, while phosphorylation at T160 has the opposite effect [128]. While significantly regulated phosphopeptides of Mark3 were detected in the present experiment (S419 and S469), they do not correspond to its established sites of activation (T211) or inhibition (T564) [129]. Ikbkb is documented to auto-phosphorylate on a C-terminal S cluster including Ikbkb-S672 (detected in the present experiment) after activation by S177 and S181 phosphorylation. This decreases activity and prevents prolonged activation of the inflammatory response [130].

As several kinases seem to be affected by the activation of cGKI, it is possible that this screen also includes indirect targets of cGKI that are either more or less phosphorylated by kinases that might be (in-)activated via phosphorylation by cGKI. Alternatively, other kinases like PKA [131] might have been activated in an unspecific manner by 8Br-cGMP. One possibility to limit the results to those phosphorylation sites that are direct targets of cGKI is to look for the consensus sequence of cGKI (R/K-R/K-X-S*/T*). This, however, might also filter out some true positive results, as cGKI can phosphorylate substrates outside of its consensus sequence rather determined by higher order protein structures than merely the amino acid sequence. Additionally, the consensus sequence of cGKI overlaps with that of PKA (R-R/K-X-S*/T*), inviting false positive results. 123 of the significantly regulated phosphopeptides found in this study did not include the consensus sequence. Another filter that can be applied to the results is the annotated subcellular compartment(s) of their corresponding proteins. As cGKI was found to be specifically localized in the cytosol of B16F10 cells, all proteins that are not annotated to be present in this subcellular compartment can be excluded as direct targets of cGKI. These 47 phosphopeptides belong to proteins that are exclusively present in the extracellular space, the nucleus, or inside other organelles, but also those that did not have an annotation for subcellular compartment in the

UniProt database. Filtering out results from either of these categories leaves 54 phosphopeptides (of 49 proteins) that, interestingly, were all significantly upregulated.

While most of the specific sites found in this analysis conform with modified residues found in databases like UniProt, citing large scale phosphoproteome mapping studies like [132], only few are phosphorylation events described in the literature. For example, cAMP-regulated phosphoprotein 19 is modified by PKA at S104 [133]. Cad is likewise phosphorylated by PKA at the residue found in the phosphoproteome screen of DRG tissue presented here, S1406 [119]. Cdk16 was found to be increasingly phosphorylated at S153 in 8Br-cGMP stimulated B16F10 cells, which is known to inhibit kinase activity [126]. Clip1-pS347 is one of several confirmed phosphorylation sites of this CLIP that affects its microtubule binding ability [134]. Phosphorylation of splicing factor 1 on S20 by cGKI regulates spliceosome assembly [135]. Mitogen-activated protein kinase-activated protein kinase 2 phosphorylates the mRNA decay activator protein ZFP36L1 at S54 and other sites, thus leading to its inactivation [136].

Two proteins, Ikbkb and Tsc22d4, of significantly changed phosphopeptides detected in this study contain an LZ domain. While neither of these were phosphorylated at a cGKI consensus sequence, the specificity and interaction with the kinase might be driven by the LZ domain instead. Ikbkb additionally contains a kinase domain, as described above, making it a possible candidate for being part of a hypothetical enzyme complex guiding kinases to downstream targets of the appropriate cascade. A specific non-transient interaction of Ikbkb or Tsc22d4 with cGKI at the LZ domain could be tested in a Co-IP with both WT cGKI and an LZM of cGKI if appropriate ways to identify the candidates via antibodies are available or produced.

4.1.2 Embryonic DRGs

In order to achieve conditions that are closer to the physiology in which the axons of DRG neurons bifurcate after entering the spinal cord at the DREZ, acutely dissected DRG tissue of E13.5 mouse embryos was treated with CNP (0.25 µM, 10 min, 37 °C) to stimulate cGKI activity. In this experimental setup, cGMP is produced by GC-B and thus might reach cGKI on a similar route within the organization of the cytosol as in an *in vivo* situation. This makes unspecific activations of other kinases less likely, if not impossible. The effective activation of cGKIα due to administration of CNP was determined by WB analysis of the phosphorylation of the established substrate Vasp (Figure 3-4A). To further rule out false positive results, an analogous experiment was performed on DRG tissue of cGKI-KO mice. Phosphorylations found there can be declared as independent of cGKI and thus ruled out as a direct substrate of this kinase (Figure 3-4C). Thereby, five phosphorylation sites that were found to be significantly regulated in stimulated WT DRG tissue could be excluded.

Interestingly, there are three phosphorylation sites found in the phosphoproteome analysis of 8Br-cGMP stimulated B16F10 cells that also appear in the exclusion condition analysis of CNP stimulated DRG tissue of cGKI-KO mouse embryos. Those are S93 of chromobox protein homolog 5 (UniProt ID: Q61686) with significantly upregulated phosphorylation, as well as Agfg1-S181 and T143 of myristoylated alanine-rich C-kinase substrate (UniProt ID: P26645) both with significantly downregulated phosphorylation. The significant change in those sites can thus be considered as independent of cGKI activity.

Because the dissection of DRG tissue requires separating the DRGs from the spinal cord, the outgrowing axons are severed between the growth cone and soma. Thus, the growth cones and associated specialized intracellular structures from a considerable fraction of DRG neurons are not included in the acutely prepared tissue samples. All data is generated from DRGs and stumps of projections, meaning mostly the neurons' somata with only short axonal segments are investigated. The likely consequence is that a slightly different protein environment than that of the growth cone is investigated. However, while a small fraction of translation takes place in the growth cone itself [137] the soma is the main site of protein production, so potential substrates of cGKI should still be present in samples. Investigating acutely excised tissue has the advantage of mimicking physiological conditions more closely than cultured primary cells or cell lines. However, this also results in a longer timeline for the experiment,

considering breeding and gestation periods. Additionally, a non-metabolic isotope labeling technique was used – the chemical SIDL method – in which labeling occurs after treatment and digestion.

In the phosphoproteome analysis of CNP-stimulated and unstimulated E13.5 DRG tissue, 19 significantly upregulated and 6 significantly downregulated phosphopeptides were detected (Section 3.2.2; Figure 3-4). Of these significantly regulated phosphopeptides, one is of a protein that contains a kinase domain. The kinase Dclk1 was found to be phosphorylated at S332, which is a phosphorylation site that has not been described before. Conversely, a self-regulatory mechanism that influences this MAPs binding affinity to microtubules has been suggested by auto-phosphorylation at a C-terminal T residue [138].

As described above, phosphorylation at the cGKI consensus sequence is an additional indication of a direct substrate of cGKI. Of the 25 significantly regulated phosphorylation sites, 8 are at a cGKI consensus sequence. In this experiment, the considered subcellular compartment annotations were not limited to the cytosol, but also included the cytoskeleton and the membrane as they are likely involved in growth cone dynamics. An overview of the proteins of all significantly regulated phosphopeptides found in E13.5 DRG tissue after stimulation with CNP is given in Table 4-1, marking the specific phosphorylation sites with the direction of regulation and the presence of cGKI consensus sequence, as well as indicating the annotation of the protein in cytosol, cytoskeleton, or membrane compartment, the presence of a kinase domain, and significantly regulated sites found in the B16F10 screen. Known phosphorylation sites and protein functions are also indicated.

Table 4-1 ***Overview of significantly regulated proteins in E13.5 DRG tissue after stimulation with CNP.*** *Proteins are sorted in alphabetical order.*

Protein	Phosphorylation site(s)	Regulation	Consensus sequence	Cytosol	Cytoskeleton	Membrane	Kinase domain	Sites found in B16F10 screen	Known phosphorylation site	Known function	Selected for verification
Acin1	pS825	↑	✓	✓		✓		pS68 ↑, pS71 ↑, pS825 ↑	S1179 [139]	RNA processing, apoptosis [140]	✓
Agfg1	pS293	↑		✓				pS181 ↓		Spermatogenesis [112]	
Bcl2l13	pS302	↓								Apoptosis [141]	
Cad	pS1406	↑	✓	✓				pS1406 ↑	T456, S1406, S1859 [119]	Pyrimidine biosynthesis [142]	✓
Canx	pS563	↑		✓		✓			S553, S563, S582 [143]	ER function coordination, chaperone [144]	
Clasp1	pS646 pS1088	↑ ↓	✓	✓	✓			pS646 ↑		Neuronal development, microtubule dynamics [28]	✓
Crmp1	pS8	↑		✓	✓			pS8 ↑	T101, T102, S522 [121,145]	Axon guidance, neuronal development [22]	✓
Dclk1	pS332	↑					✓		C-terminal T residue [138]	Neuronal development, tumorigenesis [146,147]	
Hmgb3	pS135	↑		✓					Unknown S residue [148]	Stem cell differentiation [111]	
Huwe1	pS3818	↓		✓						Ubiquitination and protein degradation, neuronal development [149]	
Map1b	pS561 pT1928 pS1307 pT1277	↑ ↑ ↑ ↓	✓	✓	✓	✓		pS1422 ↑	S1260, T1265, and others [150,151]	Axon guidance, neuronal development [151,152]	✓

Protein	Phosphorylation site(s)	Regulation	Consensus sequence	Cytosol	Cytoskeleton	Membrane	Kinase domain	Sites found in B16F10 screen	Known phosphorylation site	Known function	Selected for verification
Mapt	pT112	↓		✓	✓	✓			27 S/T/Y sites [153]	Neuronal development [10]	
Mena	pS637	↑	✓	✓	✓	✓		pS643 ↑, pT721 ↓	S255, Y557 [122,154]	Filopodia formation, neuronal development, cell motility [122,155,156]	✓
Nedd4l	pS477	↑		✓		✓		pS567 ↑	S371, S477 [114]	Ubiquitination and protein degradation [114]	✓
Rpl34	pS12	↓	✓	✓						Ribosome component [157]	
Rps6	pS236	↑							S235, S236, S240, S244, S247 [158,159]	Ribosome component [157]	
	pS235	↑	✓	✓							
Stmn1	pS63	↑	✓	✓	✓				S16, S25, S38, S63 [160]	Neuronal development [10]	
Tmx1	pS245	↑							S245 [161]	Unknown function, associated with Canx [161]	
Tpr	pS2223	↑		✓	✓				Several C-terminal residues [162]	Nucleocytoplasmic transport of proteins [109]	
Tra2a	pT200	↑								RNA processing [163]	

The known cGKI phosphorylation substrate Vasp is notably absent from the significantly regulated proteins of both the B16F10 screen and the E13.5 DRG screen. In the cell line a significant phosphorylation of Vasp-S235 was detected in only one of three samples, leaving the site below the significance requirements of at least 50 % detection rate. In the screen of DRG tissue, Vasp was absent from the phosphoproteome as well as the proteome dataset that was used to normalize the phosphoproteome data. While the absence of a peptide containing the S235 phosphorylation site might be explained by the use of trypsin for digestion, the same cannot be said for the proteome dataset. The absence of Vasp from the E13.5 DRG proteome datasets of all three samples indicates that it might be below the detection threshold for this method. Interestingly, when investigating the IF and IHC staining of Vasp on transversal sections of E13.5 and E12.5 mouse embryos, respectively, the protein seems to be present in structures in and around the DRGs and spinal cord rather than in DRG neurons themselves (Figure 3-5H and N). Vasp is named for its function in the cardiovascular system and is expressed in the smooth muscle cells of blood vessels as well as in platelets [164,165]. This indicates that the structures visible in the staining are indeed blood vessels. The lack of staining of DRG neurons supports the idea that Vasp expression here is too low for detection in MS analysis at the used tissue amount. The detection of Vasp in the cytosolic fraction of E13.5 DRG lysates could stem from the dissection of vessels around the DRGs along with the DRGs themselves. To confirm the tissue distribution of Vasp detected by the utilized antibody, transversal sections of Vasp-KO mice should be stained likewise to rule out an unspecific staining of the antibody.

Likewise, none of the antibodies used in this work that were purchased could be tested on respective KO tissue due to time constraints or lack of such tissue. They were used as indicated by the manufacturer. This represents a limitation of the staining and WB experiments and conclusions drawn from them, as possible unspecific stainings or bands cannot be disregarded.

4.1.3 Verification

Seven putative cGKI phosphorylation substrates were selected for validation experiments, as they were found in both screening experiments described above with significantly regulated phosphorylation at the same or different sites on the protein. However, Agfg1 was excluded, as the significant downregulation at S181 was also detected in the exclusion condition of CNP stimulated DRG tissue of cGKI-KO mice. Table 4-2 shows a current progress for the selected candidates Acin1, Cad, Clasp1, Crmp1, Map1b, Mena, and Nedd4l. Verification experiments include expression analysis, *in vitro* analysis of phosphorylation by cGKIα, and axon tracing analysis of respective KO mouse models to investigate the bifurcation phenotype.

Table 4-2 ***Progress of verification experiments for cGKI substrate candidates.*** *Proteins are listed in alphabetical order.*

Protein	Transcription	Compartments[1]	Tissue distribution	*In vitro* phosphorylation	Bifurcation phenotype
Acin1	E13.5 DRG tissue confirmed	(C, M), N	Universally in nuclei	--	--
Cad	E13.5 DRG tissue confirmed	--	--	--	--
Clasp1	E13.5 DRG tissue confirmed	C, (M)	DRG neurons, DRG projections, DREZ, dorsal spinal cord	Phosphorylation by cGKIα likely	--
Crmp1	E13.5 DRG tissue confirmed	C, (M)	DRG neurons, DRG projections, DREZ, edges of spinal cord	--	--
Map1b	E13.5 DRG tissue confirmed	C, M, (N)	DRG neurons, DRG projections, DREZ, edges of spinal cord	Inconclusive	KO mouse model shows normal bifurcation [H. Schmidt, unpublished]
Mena	E13.5 DRG tissue confirmed	C, (M)	DRG neurons, DRG projections, DREZ, spinal cord	Phosphorylation by cGKIα at S637 confirmed, additional other sites likely	KO mouse model shows normal bifurcation [H. Schmidt, unpublished]
Nedd4l	E13.5 DRG tissue confirmed	--	--	--	--

[1] *Compartments: C: cytosol, M: membrane, N: nucleus; faint bands in WB analysis of subcellular fractions in brackets*

All seven candidates are transcribed in E13.5 DRG tissue as confirmed by RT-PCR (Figure 3-5A). Of the tested five proteins, all could be found via WB analysis in the cytosolic fraction of E13.5 DRG lysates (Figure 3-5B). However, Acin1 was only faintly detectable there and instead predominantly present in the nuclear fraction. This could be confirmed in IF and IHC staining, where this protein was detected in nuclei throughout the whole section (Figure 3-5C and I). Clasp1, Crmp1, Map1b, and Mena on the other hand were all detectable mainly in the cytosolic fraction and to some extent in the membrane fraction. Their tissue distribution includes the DRG neuron projections and DREZ, as well as some presence in additional structures of the spinal cord (Figure 3-5D-G and J-M). The *in vitro* phosphorylation by cGKIα with an ASK mutant was tested for Clasp1, Map1b, and Mena. The direct phosphorylation of Mena by cGKIα could be confirmed (Figure 3-6). Additionally, an ASK assay performed with an S637A mutant of Mena indicated that this specific site is indeed among the phosphorylation sites of the kinase. The ASK assay of Clasp1 strongly indicates a direct phosphorylation by the kinase, but no conclusions could be made about the putative phosphorylation site at Clasp1-S646 (Figure 3-7C). The results for Map1b were entirely inconclusive, as the WB analysis of the ASK assay did not reveal a TPE band corresponding with the candidate that could be distinguished from the background (Figure 3-7D).

4.1.3.1 CLIP-associating protein 1

Clasp1 is a MAP with an approximate size of 170 kDa and was detected in DRG tissue mostly in the cytosolic fraction (Figure 3-5B), which overlaps with the UniProt annotated compartments of cytosol,

cytoskeleton, and the Golgi apparatus. Both IF and IHC staining techniques detected Clasp1 in DRG neurons and their projections to the spinal cord at the DREZ (Figure 3-5D). Additionally, a weaker universal background was recorded, especially in the IHC staining (Figure 3-5J).

In an ASK assay, a 3xFLAG-tagged analog sensitive mutant of cGKIα thio-phosphorylated 3xFLAG-tagged Clasp1 that was transiently expressed in COS7 cells (Figure 3-7C). While weak, a TPE band is visible at the expected size of 170 kDa in the reaction mix that corresponds to the candidate. The same band is weaker in the reaction mix lacking the ASK, which represents the background. Considering this single initial assay, it can be said that Clasp1 is likely a direct substrate of cGKIα. However, repetitions of the assay are necessary to draw conclusions with statistical evidence. Additionally, to ensure the measured TPE band indeed corresponds to Clasp1, an ASK assay with purified protein after anti-FLAG pull-down could be performed. To investigate the validity of the found cGKI phosphorylation site at Clasp-S646, an ASK assay was performed with an A-mutant for this site. If the kinase indeed only modifies this specific residue, the TPE band should not be present in this reaction mix. Here however, it could be detected the same as in the assay with WT Clasp1. This suggests that Clasp1-S646A could still be thio-phosphorylated by cGKIα-ASK in this assay, indicating further phosphorylation sites. Additionally, it is possible that endogenously expressed Clasp1 in the COS7 cell lysate was targeted by the kinase leading to a detectable TPE band in this reaction mix. An analogous assay with purified Clasp1-S646A might be useful to clarify this scenario as well.

The potential role of Clasp1 in axon bifurcation of DRG neurons remains unknown. Axon tracing studies of a KO mouse model would be a possible future experiment to address this question. However, no such mouse model is commercially available and thus it would have to be generated, for example by CRISPR/Cas9 technology. A more time- and resource-efficient method would be an axon tracing study in chick after *in ovo* knock down of the gene. A more elaborate description of chick embryos as a possible future alternate model system is given in section 4.4 below.

The roles of the two mammalian Clasps 1 and 2 as MAPs are not well understood yet and opposing effects in axon growth have been described for the two proteins as well as for different microtubule binding locations. Phosphorylation state might play a role in the functions of these proteins, but no specific phosphorylation sites have been found [28].

4.1.3.2 Microtubule-associated protein 1b

With a combined size of ~270 kDa of its heavy and light chains, Map1b is the largest of the candidate proteins investigated here. For WB analysis, this proved problematic as both the ideal gel running time and blotting time are increased. Detection of Map1b and smaller proteins (e.g., GAPDH at 36 kDa) on the same blot repeatedly posed a challenge. In E13.5 DRG tissue Map1b was detected in all prepared fractions of cytosolic, membrane, and nuclear proteins with similar amounts in the former two fractions and less in the latter (Figure 3-5B). This partly reflects the UniProt compartment annotations of cytosol, cytoskeleton, and membrane. Markedly, there is no annotation of a nuclear localization of Map1b in this database. The tissue distribution of Map1b in transversal sections of mouse embryos determined with IF staining largely overlaps with that of cGKIα (Figure 3-5F). As a prominent MAP however, this protein can also be found in most neurons throughout the spinal cord, which can be prominently observed in an IHC staining of this protein (Figure 3-5L).

To verify the *in vitro* phosphorylation of Map1b by cGKI, an ASK assay was performed with 3xFLAG-tagged proteins of native Map1b and an analog sensitive mutant of cGKIα. This experiment's results, however, remain inconclusive, as the weak TPE band at the expected size that could be observed in the reaction mix of this assay are indistinguishable from the background of the mix lacking the ASK (Figure 3-7D). Again, the size of this protein might be the reason for the difficulty of detection on a blot along with the much smaller kinase (~76 kDa). To better enable the separation of bigger proteins, a lower concentration separating gel (7.5 % acrylamide) was prepared for SDS-PAGE. Gel running time as well as blotting time might be increased in future such attempts to optimize separation and transfer conditions. While no conclusions can be drawn from the present assay as to the direct *in vitro* phosphorylation

of Map1b by cGKIα nor about the modification specifically at Map1b-S561, optimized experimental procedures might make them possible in future experiments. However, several additional putative phosphorylation sites of Map1b were detected in the screening experiments described above, leaving the verification of single specific sites in this setup not feasible.

While Map1b might still be involved in the process of axon bifurcation in DRG neurons, its presence is not essential, as an axon tracing study in E12.5 Map1b-KO mice has shown a normal bifurcation phenotype [H. Schmidt, unpublished]. As Map1b is one of many MAPs involved in growth cone dynamics, it is feasible that other related proteins fulfill compensatory functions in the KO mouse model. This complexity of the growth cone and the intricate interplay of components that potentially work in concert to mediate axon bifurcation renders the identification of specific elements downstream of cGKI a challenging task.

4.1.3.3 Mammalian enabled protein

Three isoforms of Mena, including the neuronal isoform, were detected in the cytosolic and membrane fractions of E13.5 DRG lysates (Figure 3-5B). This matches the UniProt compartment annotations of cytosol, cytoskeleton, and membrane. Like the other cytoskeleton-interacting proteins analyzed in this way, an IF staining of Mena revealed colocalization with cGKIα in DRG neurons and projections to the DREZ (Figure 3-5G). An additional IHC staining confirmed the presence of this protein in DRG neurons, spinal cord neurons and some surrounding cells (Figure 3-5M). Due to the specificity of the antibody used, no distinction can be made between the specific tissue distribution patterns of the different isoforms.

Two versions of an ASK assay were performed to investigate the *in vitro* phosphorylation of Mena by cGKIα. First, the 3xFLAG-tagged Mena variants (WT and S637A-mutant) were purified from lysates of transiently transfected COS7 cells via an anti-FLAG pull-down with magnetic beads. The thus produced proteins were added as template to the ASK reaction mix with equally purified 3xFLAG-cGKIα-ASK, 6-PheEt-ATPγS, and PNBM. In the subsequent WB analysis, a TPE band corresponding to thio-phosphorylated Mena was detected for both variants (Figure 3-6A). Notably, the use of 3xFLAG-Mena-S637A as compared to 3xFLAG-Mena resulted in a weaker TPE band. Comparable results were obtained in the second assay when adding lysates of transiently transfected COS7 cells as template to the ASK reaction mix (Figure 3-6C). The TPE band of thio-phosphorylated WT neural variant of Mena was distinguishable from the background of the reaction lacking cGKIα-ASK. Less so for the respective S637A-mutant. Indeed, quantification of densitometric analysis of 3xFLAG-Mena and 3xFLAG-Mena-S637A showed a significant difference ($Mena = 0.583 \pm 0.034$, $MenaS637A = 0.190 \pm 0.051$, mean ± SEM; $n = 4$; $p = 0.0011$, t-test; Figure 3-6D). Consequently, it was confirmed that the neural variant of Mena is directly phosphorylated by cGKIα *in vitro* and that Mena-S637 is one of its phosphorylation sites. While endogenously expressed Mena could account for some of the modified protein in the S637A-mutant template mix in the latter assay, this was not the case when purified proteins were used as in the first assay. The detected thio-phosphorylation of Mena-S637A must therefore stem from additional phosphorylation sites. Indeed, several such sites should be considered, as Mena-S643 was detected with a significantly increased phosphorylation in the screen of B16F10 cells described in this thesis. Additionally, Mena includes a phosphorylation site at S255 that is analogous to S153, found in Mena's protein family member Vasp [122]. This is usually phosphorylated by PKA, but for Vasp it has been shown that cGKI can also modify this site [19–21]. The phosphorylation of the established cGKI substrate Vasp could be confirmed in this thesis with a respective ASK assay using purified 3xFLAG-Vasp as template for the reaction with 3xFLAG-cGKIα-ASK construct (Figure 3-7B). Phosphorylation at specific sites of Vasp was not tested here, but respective constructs of A-mutants could be produced and used accordingly in future experiments.

To investigate which proteins are specifically modified by cGKIα, a respective ASK assay could be performed with a subsequent MS analysis of the reaction mix to detect peptides with thio-phosphorylated S and T residues. A negative control with a reaction mix lacking the ASK would be instrumental

in the exclusion of cGKIα-independent modifications. This assay would thus enable the identification of only direct *in vitro* substrates of the kinase. Performing such an experiment with DRG tissue could be an additional step of verification for the putative phosphorylation substrates of cGKI found in the screening experiments described above.

Looking towards a potential function of Mena in DRG axon bifurcation, it is of note that this protein, like other members of the Ena/Vasp family, interacts with the cytoskeleton. Indeed, most research does not differentiate between functions of the single family members, as their functions overlap and the deletion of one family member might be compensated for by the others [18]. Indeed, a triple KO mouse model with deletions of all three vertebrate Ena/Vasp proteins (Mena, Vasp, and Evl) was generated to investigate the functions of this family [125]. Ena/Vasp proteins are deeply involved in filopodia dynamics, as they promote their formation via actin filament interactions that lead to their bundling and elongation. Specifically in cortical neurons, Ena/Vasp proteins are critical to form actin bundles and filopodia, which are required for neurite formation. Interestingly, these proteins also affect microtubule behavior as actin bundles are required to guide pioneering microtubules into filopodia, directing growth cone dynamics. As other mechanisms can also initiate filopodia formation, Ena/Vasp proteins are not critical for neurite formation in all neuronal subtypes. However, they might instead be involved in axon guidance processes via their influence on filopodia dynamics in general. Here, their phosphorylation status might be crucial, and differential modulation by PKA and cGKI could be a converging point of the ratio between cAMP and cGMP concentrations [15,17,125]. Notably, neither a KO of Mena [H. Schmidt, unpublished] nor a KO of Vasp (Figure 3-8) nor a double KO of Mena and Vasp [166] have led to a bifurcation error in axons of DRG neurons after reaching the DREZ. Axon tracing studies of these mouse models revealed a normal bifurcation phenotype in mouse embryos that persisted into adulthood. Considering the overlapping functions of Ena/Vasp proteins and possible compensation mechanisms in single and double KO mouse models, respective axon tracing studies should be performed on a triple KO of Mena, Vasp, and Evl. A previous study of this triple KO mouse model indeed describes DRG axon guidance defects, but no statement is made about axon bifurcation at the DREZ [167].

Beside Clasp1, Map1b, and Mena, other putative cGKI substrates found in the phosphoproteome screening experiments described here are cytoskeletal interactors that play a part in growth cone dynamics. Specifically, Crmp1, Dclk1, Mapt, and Stmn1 are among the proteins with significantly regulated phosphorylation sites in E13.5 DRG tissue after stimulation with CNP. The effect of CNP on the localization of these proteins in growth cones of DRG neurons can be investigated in cultured primary cells. Provided that appropriate antibodies are available, subcellular location can be detected under different stimulation conditions by IF staining. Alternatively, primary cells could be transiently transfected with vectors of fluorescently tagged constructs and live cell imaging can be performed to detect translocation and possible restructuring of the growth cone *in vitro*. While no cGMP-dependent bifurcation of DRG neurons can be observed in culture, treatment with cGMP-inducing substances induces consistent structural changes of the growth cone leading to its enlargement [35].

4.2 A FUNCTIONING LZ DOMAIN IN CGKI IS INTEGRAL TO AXON BIFURCATION IN DRG NEURONS

Next to Vasp-KO and Mlk3-KO, the bifurcation phenotype of DRG neurons of a third mouse model was studied in the present work. In the cGKI-LZM mouse line, the first four leucine and isoleucine residues of the cGKIα LZ domain are replaced by A residues. This renders the kinase unable to interact with partners via the LZ domain and thus unable to phosphorylate substrates dependent on this interaction while leaving the kinase activity domain itself functional *in vitro* [90]. However, the LZ domain is additionally involved in the homodimerization of cGKI and a lack of dimerization in this mutant could have other effects as well. The ability of the cGKI-LZM to phosphorylate substrates *in vivo* or *ex vivo* has not been shown yet. To verify normal kinase function of cGKI in DRG tissue of the LZM mouse model, a stimulation with CNP could be performed on acutely dissected tissue, followed by a WB analysis of pS235-Vasp. As Vasp does not contain an LZ domain, its phosphorylation should not depend on

the interaction of this substrate with the LZ domain of cGKI, a functioning kinase domain should still lead to phosphorylation.

An axon tracing study was performed with E13.5 cGKI-LZM mouse embryos to investigate the axon bifurcation phenotype of DRG neurons in these animals. At E13.5, only 23 % of the central afferents of DRG neurons in cGKI-LZM mouse embryos displayed a proper axon bifurcation. The remaining 77 % exhibited R- or C-turns (Figure 3-8A and B). This represents a noticeable if not complete bifurcation error as exhibited by cGKI-KO mice [5]. Some phosphorylation substrates of cGKI (e.g., Mlk3) depend on the LZ domain for interaction and cannot be modified by the mutant cGKI [168]. Another such substrate might be involved in the bifurcation process. Considering a lack of evidence for the kinase function in the tissue in question of mutant mice, the bifurcation error could stem from a disrupted dimerization in the kinase that affects its activity in general rather than a lack of LZ domain interactions with substrates. Another hypothesis as to the involvement of the LZ domain of cGKI could be interactions with scaffolding proteins; interactors that are not phosphorylated by the kinase but instead anchor it to a protein complex or guide it to phosphorylation targets. This might be an explanation for the greatly reduced but not fully abolished number of bifurcations in DRG neurons of cGKI-LZM mice, as the kinase can still perform its main function of phosphorylation but displays an impaired subcellular location. An anti-cGKI Co-IP assay with DRG samples of WT and cGKI-LZM mouse embryos could be performed followed by MS analysis of the LZ domain interactors.

To confirm the bifurcation phenotype of cGKI-LZM mice, they could be crossbred with the Thy1-YFP-H reporter line [94]. Subsequently, axon tracing could be performed on P15 mice to check for a possible rectification of the aberrant phenotype postnatally. Another way to examine the extent of the axon bifurcation error in cGKI-LZM mice would be to determine the area of the oval bundle of His in embryos or the dorsal funiculus and compare these to WT animals. A deletion of cGKI in a KO model and the resulting lack of bifurcation results in a decreased area due to the decreased number of stem axons [5]. A less dramatic decrease would be expected in cGKI-LZM mice, as some axons still bifurcate. It is also possible that this is compensated for in some way during later stages of development.

4.3 Putative novel GC-B interactors

In GC-B-HA mice, an extracellular HA-tag on endogenously expressed GC-B [91] makes this protein easily detectable as opposed to the WT form. An anti-HA pull-down can be performed to purify GC-B-HA or to do a Co-IP study of interactors. Such a screen for GC-B interactors was done in the present work with two different tissues: heart tissue of adult mice and DRG tissue of E13.5 mouse embryos. Anti-HA Co-IP eluates of GC-B-HA mouse samples were compared to WT mice. Three experiments were performed on heart tissue samples with differing total protein amounts to determine the lowest amount necessary for valid MS analysis results. All three experiments resulted in comparable MS analyses with 9, 6, and 9 significantly enriched proteins, respectively, validating all three protein amounts as suitable. Since the collection of sufficient E13.5 DRG tissue is time and cost intensive and in order to reduce the number of animals that must be sacrificed, the lowest protein amount per sample was chosen to perform the experiment on this tissue. The proteome analysis of DRG tissue resulted in the detection of 23 significantly enriched proteins in GC-B-HA mouse samples compared to the WT control. No putative GC-B interactors were found consistently in both tissues. One protein, Map1a, was found as a GC-B interactor in all three experiments with murine heart tissue but was not detected in the DRG samples. Instead, Mapt was detected in the Co-IP and in the phosphoproteome analysis of E13.5 DRG tissue as potential interactor of GC-B and putative cGKI substrate, respectively. If a GC-B interactor also contained an LZ domain, this might represent a crosslink to cGKI thus integrating the kinase into a hypothetical membrane-bound protein complex. Interestingly, when annotating characteristics of the putative GC-B interactors found in both investigated tissues, none contained an LZ domain. Screening for possible regulatory interactors, phosphatase and kinase activity domains were also annotated. None of the candidate interactors contained a phosphatase activity domain, and only one contained a kinase activity domain. However, many are found in the cytoskeletal subcellular compartment.

4.3.1 Heart tissue

Three experiments were performed on heart tissue with four technical replicates, each comprised of lysates from one P95 WT mouse and a pooled lysate originating from three P75 GC-B-HA mice. The samples of each experiment were adjusted so each contained different total protein amounts (experiment a: 1 mg; experiment b: 0.5 mg; experiment c: 0.25 mg) to determine the lowest viable lysate amount still producing a post-pull-down eluate measurable via MS analysis. With 0.25 mg the lowest tested input protein amount could be confirmed as viable option for this set up, as heart tissue of adult mice and DRG tissue of embryonic mice both have a high level of GC-B expression (Figure 3-9E).

The results of the proteome analysis of the anti-HA pull-down eluates varied greatly between the three experiments (Table 3-5), even though the input originated from the same samples adjusted to different protein amounts. A single hit, Map1a, was present throughout all experiments (Figure 3-9F). In the case of Trmt112, there is a lack of significance in experiment b as the protein in question is pulled down equally in the GC-B-HA tissue sample and in the WT control, likely due to an unspecific interaction with the anti-HA beads used in the pull-down. In the case of Mrpl1, however, there is no value for the protein in experiment a, indicating that the interaction with GC-B-HA was not strong enough to prevent the removal of the protein during washing steps.

Map1a belongs to the same MAP family as Map1b and is present mostly in neurons. While Map1b expression reaches a peak during neuronal development, Map1a is expressed mainly in adult stages. Both Map1a and Map1b show interaction with microtubules as well as actin filaments thus representing excellent candidates for anchoring other proteins to the cytoskeleton [152].

Interestingly, the characteristics screened for to identify possible modulators of the KHD or links to cGKI substrates were negative, as none of the proteins identified in any of the three pull-downs included a kinase or phosphatase activity domain nor an LZ domain. Next to Map1a however, three additional candidates are also part of the cytoskeletal compartment, representing a possible anchoring point of the cytoskeleton to the membrane via GC-B in heart tissue.

4.3.2 DRG tissue

The GC-B-HA distribution in DRG neurons of GC-B-HA-mice is comparable to cGKI in NFH positive cells, but not detectable via anti-HA antibody in WT mice (Figure 3-2A and B). In WT mice, IHC staining of transversal sections of E12.5 mice with antibodies specific to GC-B and cGKIα, respectively, shows an overlapping distribution of both proteins in DRG neurons (Figure 3-5O). Additionally, the detection of GC-B-HA by anti-HA and GC-B by anti-GC-B demonstrated a colocalized staining pattern. The detection of GC-B-HA by anti-HA antibody is specific since no unspecific binding of the antibody on WT tissue was observed. The utilization of this anti-HA antibody in WB analyses in of DRG lysates from GC-B-HA mice revealed an additional unspecific band below the double band of the GC-B-HA protein, which also appears in lysates from WT tissue (Figure 3-9E), as previously reported [91]. The HA-tag renders GC-B easily identifiable by antibody in many ways, making the GC-B-HA mouse model a valuable tool for analysis of this hard-to-detect transmembrane protein.

One experiment was performed to identify putative GC-B interactors in embryonic DRG tissue with four biological replicates per genotype, investigating tissues dissected form GC-B-HA mice in comparison to tissue from a WT control. Each replicate originates from a lysate of the collected DRGs of one litter of embryos with identical genotypes. After performing an anti-HA pull-down on the lysates, an MS analysis was performed on the resulting eluates. Here, in addition to GC-B itself, 23 proteins were found to be significantly enriched in the GC-B-HA samples compared to the WT (Table 3-6). None of these putative GC-B interactors were found in the previous pull-downs with heart tissue. None of the pulled down proteins in embryonic DRG tissue included a phosphatase or LZ domain. One kinase, Taok2, was identified.

In addition to Taok2, five other cytoskeleton components were identified in this experiment: Cltc, Dync1h1, Mapt, Tubb6, and Tuba1b. Interestingly, these include isoforms of both α-tubulin and β-

tubulin monomers, so GC-B might directly anchor microtubules to the cell membrane in DRG neurons. Notably, Mapt was identified as a putative cGKI substrate with a significantly decreased phosphorylation site at T112 in the DRG phosphoproteome screen described above (Figure 3-9G).

According to these results, Mapt might provide a link not only between GC-B and a cytoskeleton anchoring complex, but also between GC-B and cGKI. This represents an interesting hypothesis about regulation of axon bifurcation in DRG neurons, as the phosphorylation of Mapt by cGKI could change its interaction with other cytoskeletal proteins as well as GC-B. This raises an interesting question: Do the interaction partners of GC-B in DRG neurons change after treatment with CNP and stimulation of cGKI activity? Further pull-downs with respective treatment groups could be a first step in answering this question. Nevertheless, Mapt itself seems not to be an essential part of the axon bifurcation process, as axon tracing studies revealed a normal DRG neuron bifurcation phenotype in Mapt KO mice [169]. As the functions of Map1b and Mapt are somewhat overlapping, the investigation of sensory axon bifurcation in a double KO mouse model could yield further insights as well.

The interaction between the candidates found in the experiments described above and GC-B should be verified in future experiments. Some biochemical assays that could be performed with proper antibodies are IF co-staining of transversal embryo sections or a Co-IP of DRG tissue with subsequent WB analysis of the eluate. To investigate colocalization in DRG growth cones, cultures of primary cells can be analyzed by IF staining as well. Here, the HA-tagged GC-B reporter mouse line will be of use again, as different HA antibodies are readily available to pair with respective specific antibodies for the candidates.

Regarding the search for phosphatases or kinases that regulate the phosphorylation status and thus activity of GC-B, the present study has found no such candidates that interact with GC-B in embryonic DRG tissue. This is likely the case due to the transient nature of kinase- and phosphatase-substrate interactions. Future studies to investigate components that regulate GC-B activity could be performed with cultured primary DRG neurons that are transiently transfected with a cGMP biosensor that can be used for live imaging of cellular cGMP levels. One such biosensor, the fluorescence resonance energy transfer-based cGi500, undergoes conformational changes upon cGMP binding, thus changing wavelength of emitted light after excitation [170]. Treatment of DRG neurons containing the cGi500 cGMP-biosensor with activators or inhibitors of specific phosphatases and observing the effect of CNP on cGMP production will reveal the role of those phosphatases in regulating GC-B activity. Performing axon tracing studies on respective phosphatase KO models and evaluating their bifurcation phenotype will then illuminate their role in the bifurcation process.

4.4 Chick embryos as an alternative system for future studies

As the generation of a large number of KO mouse models, while theoretically possible with the CRISPR/Cas method, is time and cost intensive, other model systems to investigate axon bifurcation of DRG neurons are preferable. Additionally, the reduction in use of mice or other animals protected in the EU directive 2010/63/EU is a desirable goal of future studies. Chick embryos could be used as such an alternative model, as only “foetal forms of mammals” are protected under this directive due to their proposed ability to experience “pain, suffering and distress”. Extensive research must be done to ensure the CNP-induced cGMP pathway that regulates axon bifurcation in somatosensory neurons at the DREZ shown in mice is also present and functioning in the chick *in ovo*. First steps have been taken in the present work by showing the presence of cGKI in NFH-positive cells in transversal sections of E8 chick embryos. The tissue distribution of cGKI in DRG neurons and projections, including the oval bundle of His at the DREZ, is comparable between WT E13.5 mice and E8 chick (Figure 3-2). However, the timepoint of sensory axon bifurcation in chick embryos could be much earlier (E1-E2).

Next steps to further verify the presence of this cGMP-dependent pathway should include an IHC staining of GC-B, as well as CNP if possible. Alternatively, the translation of CNP, GC-B, and cGKI might be verified on the mRNA level by in situ hybridization experiments. Subsequently, DRG explants of

chick embryos should be cultured to test for cGMP signaling. This can be achieved by transiently transfecting primary cells with a cGMP-biosensor like cGi500. Thus, the reaction to CNP stimulation can be determined. Axon tracing of DRG neurons by DiI staining can be performed to determine the presence of axon bifurcation in somatosensory neurons under basal conditions at different ages to verify the presence of the process and characterize its developmental timeline.

Once chick embryos are verified as an alternative model system to investigate the CNP-induced cGMP signaling pathway that regulates axon bifurcation in somatosensory neurons, this system can be utilized to answer further research questions. Elucidating the essential downstream phosphorylation substrates of cGKI could be achieved in an *in ovo* setup without creating novel genotypes. Specific genes can be knocked down *in ovo* by introducing mutations via electroporation. The resulting embryo with non-functioning versions of proteins in question can be studied for its bifurcation phenotype, e.g., by DiI labeling or even live cell imaging of *ex vivo* spinal cords [171]. Before investigating the role of putative cGKI substrates or GC-B interactors in DRG axon bifurcation, this setup should be used to verify that CNP, GC-B, and cGKI are equally essential components of this process in chick as in mouse embryos.

4.5 Conclusions and outlook

4.5.1 Conclusions

In B16F10 cells, cGKI is located in the cytosol, so direct substrates will likely be present in the same compartment. Of 184 significantly regulated phosphorylation sites in 8Br-cGMP stimulated B16F10 cells, 54 map to a cGKI consensus sequence in cytosolic proteins. All of them were significantly upregulated and represent promising putative novel cGKI substrates, which might be of interest to the field of cGMP research in general.

Several putative direct cGKI substrates were found that might be relevant for axon bifurcation of somatosensory neurons. Of the 25 significantly regulated phosphorylation sites in CNP stimulated DRG tissue, 8 were also detected in the B16F10 screen (Table 4-1). However, the downregulation of Agfg1-S181 was not only detected in the B16F10 cell screen, but also in the analysis of CNP stimulated DRG tissue of cGKI-KO mice. Therefore, Agfg1 was excluded from the list of putative direct cGKI substrates that were selected for verification experiments. The results of those experiments for the candidates Acin1, Cad, Clasp1, Crmp1, Map1b, Mena, and Nedd4l are summarized in Table 4-2. The transcription in embryonic DRG tissue could be verified for all candidates. The protein expression of Acin1 was found here to be mostly constricted to nuclei. This localization of Acin1 decreases the likelihood of a direct involvement in sensory axon bifurcation *in vivo*. While the detected site at S8 of Crmp1 is not within a consensus sequence of cGKI, protein expression of this MAP in DRG neurons and projections to the DREZ could be confirmed in the present work. The phosphorylation of these proteins could still be tested in an ASK assay and its role in DRG axon bifurcation might be explored in the future.

Clasp1 and Map1b showed a similar tissue distribution pattern as Crmp1, being present in DRG neurons and their projections as well as some regions of the spinal cord. While the *in vitro* phosphorylation assay of Clasp1 showed promising results for a direct interaction with cGKIα, the results for Map1b were inconclusive. Both proteins should not be ruled out as cGKI substrates and further testing is necessary. A KO mouse model of Map1b has already been analyzed for the axon bifurcation phenotype of DRG neurons, which was found to be unaltered [H. Schmidt, unpublished], leading to the conclusion, that this protein is not essential for somatosensory axon bifurcation. However, there might be compensatory effects of other MAPs with overlapping functions, like Mapt. Since an axon tracing study has similarly shown a normal bifurcation in DRG neurons of Mapt-KO mice [169], it could be of interest to study double KO models or utilize an *in ovo* knock down method to visualize bifurcation phenotype in a chick embryo model. This approach could also be used to investigate the role of Clasps in DRG neurons. This work has taken first steps in establishing the presence of an analogous cGMP-dependent pathway mediating somatosensory axon bifurcation in chick embryos.

Ena/Vasp proteins have been shown to be involved in cGMP-dependent pathways in several contexts [15,16,122,172,173]. Here, tissue distribution and subcellular expression patterns of Mena indicate its localization in DRG neurons during embryonic development. Additionally, a direct phosphorylation by cGKIα could be verified *in vitro* at S637 among other residues. Detection of Vasp in embryonic murine tissue showed its presence mostly in vessels in and around DRGs as well as the spinal cord. An *in vitro* phosphorylation of Vasp by cGKIα could also be shown. However, neither protein seems to play a critical role for axon bifurcation of DRG neurons at the DREZ, as shown by several axon tracing studies of single [this work; H. Schmidt, unpublished] and double [166] KO mouse models.

Mena, Clasp1, Map1b, Crmp1, and other putative substrates of cGKI found in this work represent several possible points of integration for the cGMP-dependent signaling pathway mediating somatosensory axon bifurcation and the cytoskeleton. Additionally, novel putative GC-B interactors were identified in this work, which built another link to components of the cytoskeleton. Map1a was found to interact with GC-B in heart tissue samples. In embryonic DRG tissue, 6 of the 23 detected GC-B interactors were part of the cytoskeletal compartment. Among them were two tubulin monomer isoforms, indicating a possible direct interaction of GC-B with microtubules. This supports the hypothesis that GC-B might be a membrane anchor for a protein complex that modulates the cytoskeleton during axon bifurcation in a CNP-induced manner. While no putative GC-B interactors with an LZ domain were identified in the present work, cGKI might be part of such a protein complex via LZ domain dependent substrates.

A functioning LZ domain of cGKIα is integral for the process of somatosensory axon bifurcation in murine DRG neurons. Specific LZ dependent substrates of cGKI that play a role in this context remain to be identified. Pull-down assays with samples of cGKI-LZM mice have been performed to identify such interactors in heart tissue [168,174] and analogous experiments could be carried out using DRG tissue.

Overall, this work has led to the discovery of novel components in the cGMP-dependent signaling pathways. Several cytoskeleton-associated elements could be identified in both phosphoproteomic screens for cGKI substrates and GC-B interactome studies. The verification of direct phosphorylation by cGKI remains to be investigated. To elucidate the mechanistic involvement in sensory axon bifurcation of the components discovered here additional research needs to be conducted. Another point of focus for future studies might be substrates of cGKI that contain an LZ domain as they appear to play a critical role *in vivo*.

4.5.2 Outlook

Remarkably, KO mouse models of any putative phosphorylation substrate of cGKI that have been investigated to date show a normal bifurcation phenotype. These include KO models of the following proteins: Mapt [169], Vasp [this study and H. Schmidt, unpublished], Mena [H. Schmidt unpublished], Mena-Vasp double KO [166], Map1b [H. Schmidt, unpublished], Myosin IIb [166]. As many cytoskeleton-associated proteins might have redundant functionality and could compensate for loss-of-function mutations, it is necessary to visualize growth cones in an *in vitro* or *ex vivo* setting to observe the process and involved components. IF stainings of proposed components could give information about their subcellular location under different conditions of cGKI stimulation. A specific and reproducible growth cone change that can be observed under those circumstances might serve as read-out in lieu of axon bifurcation [35].

Interestingly, recent recordings of biomechanical growth cone characteristics in cultivated DRG neurons from embryonic mice has also hinted to a cGMP-mediated regulation of cytoskeletal elements that might be involved in the process of sensory axon bifurcation as well. The stiffness as well as actin filament intensity in dissociated DRG neurons from E12.5 mouse embryos were decreased in response to CNP and 8Br-cGMP treatment *in vitro* [A. Balmes and A. Böttcher et al., in preparation, experiments by A. Balmes]. This might be occurring in concert with change in DRG neuron growth cone calcium levels and filopodia number. It has been found that ATP induces calcium signals, which is dovetailed by an increased average number of filopodia. Both of those effects were attenuated by CNP-induced cGMP

signaling neurons [A. Balmes and A. Böttcher et al., in preparation, experiments by S. Peters and E. Streit-Morsch]. It will be of interest to test possible involvements of the putative novel cGKI substrates found in this work in such dynamics. Additionally, the structural role of GC-B interactors integrating the cGMP-dependent pathway to cytoskeletal dynamics might be investigated in future studies (e.g., via bifurcation phenotype characterizations of models lacking putative GC-B interactors). This could lead to the identification of a membrane anchoring complex that guides components to a specific location within the growth cone. As a cGKIα variant with a mutant LZ domain but functional kinase activity leads to near abolition of axon bifurcation of DRG neurons, it should be considered that cGKI activation can not only lead to phosphorylation of substrates but might also exert its function in the process of axon bifurcation via S-palmitoylation of substrates [35].

A major point of interest going forward will be the regulation of GC-B activity in DRG neurons. The enzyme can be reversibly shut off by dephosphorylation of regulatory S/T-residues in its KHD, thus stopping cGMP production even in the presence of extracellular CNP. This represents an important molecular switch that might be responsible for regulating growth cone splitting of DRG neurons. The work of finding potential phosphatases and kinases that might modulate the phosphorylation status of GC-B is ongoing.

Lastly, the possibility of a transcriptional effect of CNP-induced cGMP signaling in DRG neurons should not be disregarded, especially considering the reported presence of nuclear localized cGKI [175]. In the present work, several putative cGKI substrates (e.g., Acin1 and splicing factor 1) that are implicated in RNA processing have been identified. Even with an absence of cGKI from the nucleus, the kinase could have indirect effects via substrates that travel to and from the nucleus or via transmembrane proteins located in the nuclear membrane.

Overall, the identification of novel components of the cGMP-dependent signaling cascade that mediates bifurcation in sensory neurons during embryonic development should promote a better mechanistic understanding of axonal branching. It is of great importance to understand downstream processes of cGKI activation and modulation of the novel cytoskeletal substrates identified here, especially in view of the role that the cytoskeleton plays in processes like cell migration and contraction, the formation of cell-cell contacts, and many others. Furthermore, considering the known role of cGMP-dependent pathways in many (patho-)physiological contexts, the discovery of novel putative components is also of more general interest in the field of cGMP research even beyond the process of somatosensory axon bifurcation.

LIST OF ABBREVIATIONS

+TIP	plus-end tracking protein
6-PhEt-ATPγS	N6-(2-phenylethyl) adenosine-5'-O-(3-thiotriphosphate)
8Br-cGMP	8-bromo-cyclic guanosine monophosphate
8pCPT-cGMP	8-(4-chlorophenylthio)-cyclic guanosine monophosphate
A	alanine
A*TPγS	bulky ATP with an additional gamma-thiol
Acin1	apoptotic chromatin condensation inducer in the nucleus
ADP	adenosine diphosphate
Agfg1	Arf-GAP domain and FG repeat-containing protein 1
AMDM	acromesomelic dysplasia type maroteaux
ANP	atrio-natriuretic peptide
APS	ammonium peroxydisulphate
ASK	analogue-sensitive kinase
ATP	adenosine triphosphate
BCA	bicinchoninic acid
BNP	B-type natriuretic peptide
BSA	bovine serum albumin
Cad	glutamine-dependent carbamoyl-phosphate synthase-aspartate carbamoyltransferase-dihydroorotase fusion protein
cAMP	cyclic adenosine monophosphate
CAMSAP	calmodulin-regulated spectrin-associated protein
Canx	Calnexin
Cdk	cyclin-dependent kinase
C-domain	central domain
CFMB	Core Facility for Medical Bioanalytics
cGK	cGMP-dependent protein kinase
cGMP	cyclic guanosine monophosphate
Clasp	CLIP-associating protein
Cltc	clathrin heavy chain 1
CLIP	cytoplasmic linker protein
CNG	cyclic nucleotide-gated
CNP	C-type natriuretic peptide
CNS	central nervous system
cOmplete	cOmplete Mini, EDTA-free
Crmp	collapsin response mediator protein
CSG	cranial sensory ganglion
DAB	3, 3'-diaminobenzidine
DAPI	4,6-diamidine-2-phenylindole
Dclk1	doublecortin-like kinase 1
DEPC	diethyl pyrocarbonate
DiI	1,1'-dioctadecyl-3,3,3',3'-tetramethylindocarbocyanine perchlorate
DMEM	Dulbecco's modified eagle's medium
DMSO	dimethyl sulfoxide
dNTP	deoxynucleotide triphosphate
DOC	sodium deoxycholate
DREZ	dorsal root entry zone
DRG	dorsal root ganglion
DTT	dithiothreitol
Dync1h1	cytoplasmic dynein 1 heavy chain 1
E	glutamate
E#	embryonic day number #
EB	end-binding protein
ECL	enhanced chemiluminescence
EDTA	ethylenediaminetetraacetic acid
ER	endoplasmic reticulum
Erk1	extracellular signal-regulated kinase 1
EtOH	ethanol
EVH	Ena/Vasp homology
Evl	Ena-Vasp-like protein
FBS	fetal bovine serum
FGFR3	fibroblast growth factor receptor 3
G2P	glycerol-2-phosphate
GAPDH	glyceraldehyde 3-phosphate dehydrogenase
GC	guanylyl cyclase
GDP	guanosine diphosphate
GMP	guanosine monophosphate
GSK3	glycogen synthase kinase 3
GTP	guanosine triphosphate
HA	hemagglutinin
HBSS	Hanks' balanced salt solution
HEPES	N-2-hydroxyethylpiperazine-N'-2-ethane sulphonic acid

Hmgb3	high mobility group protein B3
Hmgcs1	hydroxymethylglutaryl-CoA synthase
HRP	horse radish peroxidase
IF	immunofluorescent
IHC	immunohistochemical
Ikbkb	inhibitor of nuclear factor kappa-B kinase subunit beta
IP	immunoprecipitation
K	lysine
KHD	kinase homology domain
KO	knock-out
LSM	laser scanning microscope
LZ	leucine zipper
LZM	leucine zipper mutant
MAP	microtubule-associated protein
Mapt	microtubule-associated protein tau
Mark3	MAP/microtubule affinity-regulating kinase 3
Mena	mammalian enabled protein
MeOH	methanol
Mlk3	mixed lineage kinase 3
Mrpl1	mitochondrial 39S ribosomal protein L1
MS	mass spectrometry/spectrometric
MTN	mesencephalic trigeminal neuron
nanoLC-MS/MS	nano-liquid chromatography with tandem mass spectrometry
Nedd4l	E3 ubiquitin-protein ligase NEDD4-like
NFH	neurofilament H
NGS	normal goat serum
NOG	n-octyl β-D-glucopyranoside
NP40	Nonidet P40
P#	postnatal day number #
PBS	phosphate-buffered saline
PCR	polymerase chain reaction
PDE	phosphodiesterase
PDL	poly-D-lysine
P-domain	peripheral domain
PEP	posterior error probability
PFA	paraformaldehyde
pGC	particulate guanylyl cyclase
PhI	phosphatase inhibitor cocktail
PKA	protein kinase A
PMSF	phenylmethyl sulphonyl fluoride
PNBM	p-nitrobenzyl mesylate
PVDF	polyvinylidene fluoride
R	arginine
Rps6	ribosomal protein S6
RT	room temperature
S	serine
SDS	sodium dodecyl sulphate
SDS-PAGE	SDS polyacrylamide gel electrophoresis
SF	sodium fluoride
sGC	soluble guanylyl cyclase
Sgk1	serum/glucocorticoid-regulated kinase 1
SIDL	stable isotope dimethyl labeling
SILAC	stable isotope labeling by amino acid in cell culture
SOV	sodium orthovanadate
Stmn	stathmin
T	threonine
TAE	tris-acetate-EDTA buffer
Taok2	TAO serine/threonine-protein kinase 2
TBS	tris-buffered saline
TBS-T	tris-buffered saline with Tween20
TEMED	N,N,N',N'-tetramethylethylenediamine
Tmx1	thioredoxin-related transmembrane protein 1
TPE	thio-phosphate ester
Tpr	translocated promoter region
Tra2a	transformer-2 protein homolog alpha
Trmt112	TRM112-like protein
Tsc22d4	TSC22 domain family protein 4
Tuba1b	tubulin alpha-1B chain
Tubb6	tubulin beta-6 chain
TX100	Triton® X-100
T-zone	transition zone
UV	ultraviolet
Vasp	vasodilator-stimulated phosphoprotein
WB	western blot
WT	wildtype
Y	tyrosine
YFP	yellow fluorescent protein

LIST OF FIGURES

LIST OF TABLES

REFERENCES

[1] A. Friebe, J.R. Kraehling, M. Russwurm, P. Sandner, A. Schmidtko, The 10th International Conference on cGMP 2022: recent trends in cGMP research and development—meeting report, Naunyn Schmiedebergs Arch Pharmacol. 396 (2023) 1669–1686. https://doi.org/10.1007/s00210-023-02484-8.

[2] P. Sandner, M. Follmann, E. Becker-Pelster, M.G. Hahn, C. Meier, C. Freitas, L. Roessig, J. Stasch, Soluble GC stimulators and activators: Past, present and future, Br J Pharmacol. (2021). https://doi.org/10.1111/bph.15698.

[3] F. Hofmann, The cGMP system: components and function, Biol Chem. 401 (2020) 447–469. https://doi.org/10.1515/hsz-2019-0386.

[4] R. Lukowski, R. Feil, Recent developments in cGMP research: From mechanisms to medicines and back, Br J Pharmacol. 179 (2022) 2321–2327. https://doi.org/10.1111/bph.15824.

[5] H. Schmidt, M. Werner, P.A. Heppenstall, M. Henning, M.I. Moré, S. Kühbandner, G.R. Lewin, F. Hofmann, R. Feil, F.G. Rathjen, cGMP-mediated signaling via cGKIα is required for the guidance and connectivity of sensory axons, Journal of Cell Biology. 159 (2002) 489–498. https://doi.org/10.1083/jcb.200207058.

[6] H. Schmidt, A. Stonkute, R. Jüttner, S. Schäffer, J. Buttgereit, R. Feil, F. Hofmann, F.G. Rathjen, The receptor guanylyl cyclase Npr2 is essential for sensory axon bifurcation within the spinal cord, J Cell Biol. 179 (2007) 331–340. https://doi.org/10.1083/jcb.200707176.

[7] H. Schmidt, A. Stonkute, R. Jüttner, D. Koesling, A. Friebe, F.G. Rathjen, C-type natriuretic peptide (CNP) is a bifurcation factor for sensory neurons, Proceedings of the National Academy of Sciences. 106 (2009) 16847–16852. https://doi.org/10.1073/pnas.0906571106.

[8] B. Alberts, D. Bray, K. Hopkin, A. Johnson, J. Lewis, M. Raff, K. Roberts, P. Walter, Das Cytoskelett, in: Lehrbuch Der Molekularen Zellbiologie, 4th ed., Wiley-VCH, 2012: pp. 613–652.

[9] L.A. Lowery, D. Van Vactor, The trip of the tip: understanding the growth cone machinery, Nat Rev Mol Cell Biol. 10 (2009) 332–343. https://doi.org/10.1038/nrm2679.

[10] H. V. Goodson, E.M. Jonasson, Microtubules and Microtubule-Associated Proteins, Cold Spring Harb Perspect Biol. 10 (2018) a022608. https://doi.org/10.1101/cshperspect.a022608.

[11] A. Akhmanova, C.C. Hoogenraad, K. Drabek, T. Stepanova, B. Dortland, T. Verkerk, W. Vermeulen, B.M. Burgering, C.I. De Zeeuw, F. Grosveld, N. Galjart, CLASPs Are CLIP-115 and -170 Associating Proteins Involved in the Regional Regulation of Microtubule Dynamics in Motile Fibroblasts, Cell. 104 (2001) 923–935. https://doi.org/10.1016/S0092-8674(01)00288-4.

[12] N. Galjart, CLIPs and CLASPs and cellular dynamics, Nat Rev Mol Cell Biol. 6 (2005) 487–498. https://doi.org/10.1038/nrm1664.

[13] J. Al-Bassam, F. Chang, Regulation of microtubule dynamics by TOG-domain proteins XMAP215/Dis1 and CLASP, Trends Cell Biol. 21 (2011) 604–614. https://doi.org/10.1016/j.tcb.2011.06.007.

[14] M. Atkins, X. Nicol, C. Fassier, Microtubule remodelling as a driving force of axon guidance and pruning, Semin Cell Dev Biol. 140 (2023) 35–53. https://doi.org/10.1016/j.semcdb.2022.05.030.

[15] F. Drees, F.B. Gertler, Ena/VASP: proteins at the tip of the nervous system, Curr Opin Neurobiol. 18 (2008) 53–59. https://doi.org/10.1016/j.conb.2008.05.007.

[16] M. Krause, E.W. Dent, J.E. Bear, J.J. Loureiro, F.B. Gertler, Ena/VASP Proteins: Regulators of the Actin Cytoskeleton and Cell Migration, Annu Rev Cell Dev Biol. 19 (2003) 541–564. https://doi.org/10.1146/annurev.cellbio.19.050103.103356.

[17] L. Armijo-Weingart, G. Gallo, It takes a village to raise a branch: Cellular mechanisms of the initiation of axon collateral branches, Molecular and Cellular Neuroscience. 84 (2017) 36–47. https://doi.org/10.1016/j.mcn.2017.03.007.

[18] L.M. Lanier, M.A. Gates, W. Witke, A.S. Menzies, A.M. Wehman, J.D. Macklis, D. Kwiatkowski, P. Soriano, F.B. Gertler, Mena Is Required for Neurulation and Commissure Formation, Neuron. 22 (1999) 313–325. https://doi.org/10.1016/S0896-6273(00)81092-2.

[19] F.B. Gertler, K. Niebuhr, M. Reinhard, J. Wehland, P. Soriano, Mena, a Relative of VASP and Drosophila Enabled, Is Implicated in the Control of Microfilament Dynamics, Cell. 87 (1996) 227–239. https://doi.org/10.1016/S0092-8674(00)81341-0.

[20] E. Butt, K. Abel, M. Krieger, D. Palm, V. Hoppe, J. Hoppe, U. Walter, cAMP- and cGMP-dependent protein kinase phosphorylation sites of the focal adhesion vasodilator-stimulated phosphoprotein (VASP) in vitro and in intact human platelets., J Biol Chem. 269 (1994) 14509–17. http://www.ncbi.nlm.nih.gov/pubmed/8182057.

[21] M. Halbrügge, C. Friedrich, M. Eigenthaler, P. Schanzenbächer, U. Walter, Stoichiometric and reversible phosphorylation of a 46-kDa protein in human platelets in response to cGMP- and cAMP-elevating vasodilators., Journal of Biological Chemistry. 265 (1990) 3088–3093. https://doi.org/10.1016/S0021-9258(19)39737-6.

[22] F. Nakamura, T. Ohshima, Y. Goshima, Collapsin Response Mediator Proteins: Their Biological Functions and Pathophysiology in Neuronal Development and Regeneration, Front Cell Neurosci. 14 (2020). https://doi.org/10.3389/fncel.2020.00188.

[23] H.-C. Yu-Kemp, J.P. Kemp, W.M. Brieher, CRMP-1 enhances EVL-mediated actin elongation to build lamellipodia and the actin cortex, Journal of Cell Biology. 216 (2017) 2463–2479. https://doi.org/10.1083/jcb.201606084.

[24] G.M. Cammarata, E.A. Bearce, L.A. Lowery, Cytoskeletal social networking in the growth cone: How +TIPs mediate microtubule-actin cross-linking to drive axon outgrowth and guidance, Cytoskeleton. 73 (2016) 461–476. https://doi.org/10.1002/cm.21272.

[25] Y.-W. Kuo, J. Howard, Cutting, Amplifying, and Aligning Microtubules with Severing Enzymes, Trends Cell Biol. 31 (2021) 50–61. https://doi.org/10.1016/j.tcb.2020.10.004.

[26] K. Kalil, E.W. Dent, Branch management: mechanisms of axon branching in the developing vertebrate CNS, Nat Rev Neurosci. 15 (2014) 7–18. https://doi.org/10.1038/nrn3650.

[27] C. Sánchez-Huertas, E. Herrera, With the Permission of Microtubules: An Updated Overview on Microtubule Function During Axon Pathfinding, Front Mol Neurosci. 14 (2021). https://doi.org/10.3389/fnmol.2021.759404.

[28] C.L. Sayas, S. Basu, M. van der Reijden, E. Bustos-Morán, M. Liz, M. Sousa, W.F.J. van IJcken, J. Avila, N. Galjart, Distinct Functions for Mammalian CLASP1 and -2 During Neurite and Axon Elongation, Front Cell Neurosci. 13 (2019) 5. https://doi.org/10.3389/fncel.2019.00005.

[29] R. Pinto-Costa, M.M. Sousa, Microtubules, actin and cytolinkers: how to connect cytoskeletons in the neuronal growth cone, Neurosci Lett. 747 (2021) 135693. https://doi.org/10.1016/j.neulet.2021.135693.

[30] S.C. Leite, R. Pinto-Costa, M.M. Sousa, Actin dynamics in the growth cone: a key player in axon regeneration, Curr Opin Neurobiol. 69 (2021) 11–18. https://doi.org/10.1016/j.conb.2020.11.015.

[31] S. Averaimo, X. Nicol, Intermingled cAMP, cGMP and calcium spatiotemporal dynamics in developing neuronal circuits, Front Cell Neurosci. 8 (2014). https://doi.org/10.3389/fncel.2014.00376.

[32] R.J. Gasperini, M. Pavez, A.C. Thompson, C.B. Mitchell, H. Hardy, K.M. Young, J.K. Chilton, L. Foa, How does calcium interact with the cytoskeleton to regulate growth cone motility during axon pathfinding?, Molecular and Cellular Neuroscience. 84 (2017) 29–35. https://doi.org/10.1016/j.mcn.2017.07.006.

[33] H. Akiyama, T. Fukuda, T. Tojima, V.O. Nikolaev, H. Kamiguchi, Cyclic Nucleotide Control of Microtubule Dynamics for Axon Guidance, The Journal of Neuroscience. 36 (2016) 5636–5649. https://doi.org/10.1523/JNEUROSCI.3596-15.2016.

[34] K. Togashi, M.J. von Schimmelmann, M. Nishiyama, C.-S. Lim, N. Yoshida, B. Yun, R.S. Molday, Y. Goshima, K. Hong, Cyclic GMP-Gated CNG Channels Function in Sema3A-Induced Growth Cone Repulsion, Neuron. 58 (2008) 694–707. https://doi.org/10.1016/j.neuron.2008.03.017.

[35] A. Dumoulin, A. Dagane, G. Dittmar, F.G. Rathjen, S-palmitoylation Is Required for the Control of Growth Cone Morphology of DRG Neurons by CNP-Induced cGMP Signaling, Front Mol Neurosci. 11 (2018) 345. https://doi.org/10.3389/fnmol.2018.00345.

[36] K.M. Jacobs, Somatosensory System, in: J.S. Kreutzer, J. DeLuca, B. Caplan (Eds.), Encyclopedia of Clinical Neuropsychology, Springer International Publishing, Cham, 2018: pp. 3218–3223. https://doi.org/10.1007/978-3-319-57111-9_359.

[37] A. Chédotal, Roles of axon guidance molecules in neuronal wiring in the developing spinal cord, Nat Rev Neurosci. 20 (2019) 380–396. https://doi.org/10.1038/s41583-019-0168-7.

[38] D.D.M. O'Leary, A.R. Bicknese, J.A. De Carlos, C.D. Heffner, S.E. Koester, L.J. Kutka, T. Terashima, Target Selection by Cortical Axons: Alternative Mechanisms to Establish Axonal Connections in the Developing Brain, Cold Spring Harb Symp Quant Biol. 55 (1990) 453–468. https://doi.org/10.1101/SQB.1990.055.01.045.

[39] A.A. Nugent, A.L. Kolpak, E.C. Engle, Human disorders of axon guidance, Curr Opin Neurobiol. 22 (2012) 837–843. https://doi.org/10.1016/j.conb.2012.02.006.

[40] A.G. Brown, Organization in the Spinal Cord, 1st ed., Springer London, London, 1981. https://doi.org/10.1007/978-1-4471-1305-8.

[41] S. Ozaki, W.D. Snider, Initial trajectories of sensory axons toward laminar targets in the developing mouse spinal cord, J Comp Neurol. 380 (1997) 215–229. https://doi.org/10.1002/(SICI)1096-9861(19970407)380:2<215::AID-CNE5>3.0.CO;2-6.

[42] H. Schmidt, A. Böttcher, T. Gross, A. Schmidtko, cGMP signalling in dorsal root ganglia and the spinal cord: Various functions in development and adulthood, Br J Pharmacol. 179 (2022) 2361–2377. https://doi.org/10.1111/bph.15514.

[43] D. Koesling, E. Mergia, M. Russwurm, Physiological Functions of NO-Sensitive Guanylyl Cyclase Isoforms, Curr Med Chem. 23 (2016) 2653–2665. https://doi.org/10.2174/0929867323666160812145050.

[44] A. Friebe, P. Sandner, A. Schmidtko, cGMP: a unique 2nd messenger molecule – recent developments in cGMP research and development, Naunyn Schmiedebergs Arch Pharmacol. 393 (2020) 287–302. https://doi.org/10.1007/s00210-019-01779-z.

[45] M. Kuhn, Molecular Physiology of Membrane Guanylyl Cyclase Receptors, Physiol Rev. 96 (2016) 751–804. https://doi.org/10.1152/physrev.00022.2015.

[46] L.R. Potter, Guanylyl cyclase structure, function and regulation, Cell Signal. 23 (2011) 1921–1926. https://doi.org/10.1016/j.cellsig.2011.09.001.

[47] L.R. Potter, Regulation and therapeutic targeting of peptide-activated receptor guanylyl cyclases, Pharmacol Ther. 130 (2011) 71–82. https://doi.org/10.1016/j.pharmthera.2010.12.005.

[48] J.W. Robinson, J.R. Egbert, J. Davydova, H. Schmidt, L.A. Jaffe, L.R. Potter, Dephosphorylation is the mechanism of fibroblast growth factor inhibition of guanylyl cyclase-B, Cell Signal. 40 (2017) 222–229. https://doi.org/10.1016/j.cellsig.2017.09.021.

[49] J.R. Egbert, L.C. Shuhaibar, A.B. Edmund, D.A. Van Helden, J.W. Robinson, T.F. Uliasz, V. Baena, A. Geerts, F. Wunder, L.R. Potter, L.A. Jaffe, Dephosphorylation and inactivation of NPR2 guanylyl cyclase in granulosa cells contributes to the LH-induced decrease in cGMP that causes resumption of meiosis in rat oocytes, Development. 141 (2014) 3594–3604. https://doi.org/10.1242/dev.112219.

[50] J.R. Egbert, I. Silbern, T.F. Uliasz, K.M. Lowther, S.-P. Yee, H. Urlaub, L.A. Jaffe, Phosphatases modified by LH signaling in ovarian follicles: testing their role in regulating the NPR2 guanylyl cyclase, Biol Reprod. (2023). https://doi.org/10.1093/biolre/ioad130.

[51] L.C. Shuhaibar, J.W. Robinson, G. Vigone, N.P. Shuhaibar, J.R. Egbert, V. Baena, T.F. Uliasz, D. Kaback, S.-P. Yee, R. Feil, M.C. Fisher, C.N. Dealy, L.R. Potter, L.A. Jaffe, Dephosphorylation of the NPR2 guanylyl cyclase contributes to inhibition of bone growth by fibroblast growth factor, Elife. 6 (2017). https://doi.org/10.7554/eLife.31343.

[52] C.F. Bartels, H. Bükülmez, P. Padayatti, D.K. Rhee, C. van Ravenswaaij-Arts, R.M. Pauli, S. Mundlos, D. Chitayat, L.-Y. Shih, L.I. Al-Gazali, S. Kant, T. Cole, J. Morton, V. Cormier-Daire, L. Faivre, M. Lees, J. Kirk, G.R. Mortier, J. Leroy, B. Zabel, C.A. Kim, Y. Crow, N.E. Braverman, F. van den Akker, M.L. Warman, Mutations in the Transmembrane Natriuretic Peptide Receptor NPR-B Impair Skeletal Growth and Cause Acromesomelic Dysplasia, Type Maroteaux, The American Journal of Human Genetics. 75 (2004) 27–34. https://doi.org/10.1086/422013.

[53] R. Bocciardi, R. Giorda, J. Buttgereit, S. Gimelli, M.T. Divizia, S. Beri, S. Garofalo, S. Tavella, M. Lerone, O. Zuffardi, M. Bader, R. Ravazzolo, G. Gimelli, Overexpression of the C-type natriuretic peptide (CNP) is associated with overgrowth and bone anomalies in an individual with balanced t(2;7) translocation, Hum Mutat. 28 (2007) 724–731. https://doi.org/10.1002/humu.20511.

[54] A. Moncla, C. Missirian, P. Cacciagli, E. Balzamo, L. Legeai-Mallet, J.-L. Jouve, B. Chabrol, M. Le Merrer, G. Plessis, L. Villard, N. Philip, A cluster of translocation breakpoints in 2q37 is associated with overexpression of NPPC in patients with a similar overgrowth phenotype, Hum Mutat. 28 (2007) 1183–1188. https://doi.org/10.1002/humu.20611.

[55] S. Duggan, Vosoritide: First Approval, Drugs. 81 (2021) 2057–2062. https://doi.org/10.1007/s40265-021-01623-w.

[56] L.A. Jaffe, J.R. Egbert, Regulation of Mammalian Oocyte Meiosis by Intercellular Communication Within the Ovarian Follicle, Annu Rev Physiol. 79 (2017) 237–260. https://doi.org/10.1146/annurev-physiol-022516-034102.

[57] M. Biel, S. Michalakis, Cyclic Nucleotide-Gated Channels, in: H.H.H.W. Schmidt, F. Hofmann, J.-P. Stasch (Eds.), CGMP: Generators, Effectors and Therapeutic Implications, Springer Berlin Heidelberg, Berlin, Heidelberg, 2009: pp. 111–136. https://doi.org/10.1007/978-3-540-68964-5_7.

[58] S. Michalakis, E. Becirovic, M. Biel, Retinal Cyclic Nucleotide-Gated Channels: From Pathophysiology to Therapy, Int J Mol Sci. 19 (2018) 749. https://doi.org/10.3390/ijms19030749.

[59] R. Feil, T. Kleppisch, NO/cGMP-Dependent Modulation of Synaptic Transmission, in: T.C. Südhof, K. Starke (Eds.), Pharmacology of Neurotransmitter Release, Springer Berlin Heidelberg, 2008: pp. 529–560. https://doi.org/10.1007/978-3-540-74805-2_16.

[60] A. Roy, J. Groten, V. Marigo, T. Tomar, R. Hilhorst, Identification of Novel Substrates for cGMP Dependent Protein Kinase (PKG) through Kinase Activity Profiling to Understand Its Putative Role in Inherited Retinal Degeneration, Int J Mol Sci. 22 (2021) 1180. https://doi.org/10.3390/ijms22031180.

[61] A. Roy, A. Tolone, R. Hilhorst, J. Groten, T. Tomar, F. Paquet-Durand, Kinase activity profiling identifies putative downstream targets of cGMP/PKG signaling in inherited retinal neurodegeneration, Cell Death Discov. 8 (2022) 93. https://doi.org/10.1038/s41420-022-00897-7.

[62] P.J. Kennelly, E.G. Krebs, Consensus sequences as substrate specificity determinants for protein kinases and protein phosphatases, Journal of Biological Chemistry. 266 (1991) 15555–15558. https://doi.org/10.1016/S0021-9258(18)98436-X.

[63] T. Krieg, R. Lukowski, eds., Guanylate Cyclase and Cyclic GMP, Humana Press, Totowa, NJ, 2013. https://doi.org/10.1007/978-1-62703-459-3.

[64] F. Hofmann, J.W. Wegener, cGMP-Dependent Protein Kinases (cGK), in: T. Krieg, R. Lukowski (Eds.), Guanylate Cyclase and Cyclic GMP: Methods and Protocols, Humana Press, Totowa, NJ, 2013: pp. 17–50. https://doi.org/10.1007/978-1-62703-459-3_2.

[65] J.R. Burgoyne, M. Madhani, F. Cuello, R.L. Charles, J.P. Brennan, E. Schröder, D.D. Browning, P. Eaton, Cysteine Redox Sensor in PKGIa Enables Oxidant-Induced Activation, Science (1979). 317 (2007) 1393–1397. https://doi.org/10.1126/science.1144318.

[66] C. Luo, V. Gangadharan, K.K. Bali, R.-G. Xie, N. Agarwal, M. Kurejova, A. Tappe-Theodor, I. Tegeder, S. Feil, G. Lewin, E. Polgar, A.J. Todd, J. Schlossmann, F. Hofmann, D.-L. Liu, S.-J. Hu, R. Feil, T. Kuner, R. Kuner, Presynaptically Localized Cyclic GMP-Dependent Protein Kinase 1 Is a Key Determinant of Spinal Synaptic Potentiation and Pain Hypersensitivity, PLoS Biol. 10 (2012) e1001283. https://doi.org/10.1371/journal.pbio.1001283.

[67] H. Uchida, S. Matsumura, T. Katano, M. Watanabe, J. Schlossmann, S. Ito, Two isoforms of cyclic GMP-dependent kinase-I exhibit distinct expression patterns in the adult mouse dorsal root ganglion, Mol Pain. 14 (2018). https://doi.org/10.1177/1744806918796409.

[68] J.E. Lorenz, W. Kallenborn-Gerhardt, R. Lu, K.M.J. Syhr, P. Eaton, G. Geisslinger, A. Schmidtko, Oxidant-Induced Activation of cGMP-Dependent Protein Kinase Iα Mediates Neuropathic Pain After Peripheral Nerve Injury, Antioxid Redox Signal. 21 (2014) 1504–1515. https://doi.org/10.1089/ars.2013.5585.

[69] A. Schmidtko, W. Gao, M. Sausbier, I. Rauhmeier, U. Sausbier, E. Niederberger, K. Scholich, A. Huber, W. Neuhuber, H.-D. Allescher, F. Hofmann, I. Tegeder, P. Ruth, G. Geisslinger, Cysteine-Rich Protein 2, a Novel Downstream Effector of cGMP/cGMP-Dependent Protein Kinase I-Mediated Persistent Inflammatory Pain, The Journal of Neuroscience. 28 (2008) 1320–1330. https://doi.org/10.1523/JNEUROSCI.5037-07.2008.

[70] M. Piper, F. van Horck, C. Holt, The Role of Cyclic Nucleotides in Axon Guidance, in: D. Bagnard (Ed.), Axon Growth and Guidance, Springer New York, 2007: pp. 134–143. https://doi.org/10.1007/978-0-387-76715-4_10.

[71] R.W. Gundersen, J.N. Barrett, Characterization of the turning response of dorsal root neurites toward nerve growth factor., Journal of Cell Biology. 87 (1980) 546–554. https://doi.org/10.1083/jcb.87.3.546.

[72] A.J. Murray, A.G. Peace, D.A. Shewan, cGMP promotes neurite outgrowth and growth cone turning and improves axon regeneration on spinal cord tissue in combination with cAMP, Brain Res. 1294 (2009) 12–21. https://doi.org/10.1016/j.brainres.2009.07.071.

[73] K.T. Nguyen-Ba-Charvet, K. Brose, V. Marillat, C. Sotelo, M. Tessier-Lavigne, A. Chédotal, Sensory Axon Response to Substrate-Bound Slit2 Is Modulated by Laminin and Cyclic GMP, Molecular and Cellular Neuroscience. 17 (2001) 1048–1058. https://doi.org/10.1006/mcne.2001.0994.

[74] H. Song, G. Ming, Z. He, M. Lehmann, L. McKerracher, M. Tessier-Lavigne, M. Poo, Conversion of Neuronal Growth Cone Responses from Repulsion to Attraction by Cyclic Nucleotides, Science (1979). 281 (1998) 1515–1518. https://doi.org/10.1126/science.281.5382.1515.

[75] T. Tojima, R. Itofusa, H. Kamiguchi, The Nitric Oxide-cGMP Pathway Controls the Directional Polarity of Growth Cone Guidance via Modulating Cytosolic Ca2+ Signals, Journal of Neuroscience. 29 (2009) 7886–7897. https://doi.org/10.1523/JNEUROSCI.0087-09.2009.

[76] M. Nishiyama, A. Hoshino, L. Tsai, J.R. Henley, Y. Goshima, M. Tessier-Lavigne, M. Poo, K. Hong, Cyclic AMP/GMP-dependent modulation of Ca2+ channels sets the polarity of nerve growth-cone turning, Nature. 423 (2003) 990–995. https://doi.org/10.1038/nature01751.

[77] T. Kobayashi, F. Nagase, K. Hotta, K. Oka, Crosstalk between Second Messengers Predicts the Motility of the Growth Cone, Sci Rep. 3 (2013) 3118. https://doi.org/10.1038/srep03118.

[78] H. Schmidt, S. Peters, K. Frank, L. Wen, R. Feil, F.G. Rathjen, Dorsal root ganglion axon bifurcation tolerates increased cyclic GMP levels: the role of phosphodiesterase 2A and scavenger receptor Npr3, European Journal of Neuroscience. 44 (2016) 2991–3000. https://doi.org/10.1111/ejn.13434.

[79] Z. Zhao, L. Ma, Regulation of axonal development by natriuretic peptide hormones, Proceedings of the National Academy of Sciences. 106 (2009) 18016–18021. https://doi.org/10.1073/pnas.0906880106.

[80] Z. Zhao, Z. Wang, Y. Gu, R. Feil, F. Hofmann, L. Ma, Regulate Axon Branching by the Cyclic GMP Pathway via Inhibition of Glycogen Synthase Kinase 3 in Dorsal Root Ganglion Sensory Neurons, The Journal of Neuroscience. 29 (2009) 1350–1360. https://doi.org/10.1523/JNEUROSCI.3770-08.2009.

[81] P. Tröster, J. Haseleu, J. Petersen, O. Drees, A. Schmidtko, F. Schwaller, G.R. Lewin, G. Ter-Avetisyan, Y. Winter, S. Peters, S. Feil, R. Feil, F.G. Rathjen, H. Schmidt, The Absence of Sensory Axon Bifurcation Affects Nociception and Termination Fields of Afferents in the Spinal Cord, Front Mol Neurosci. 11 (2018) 19. https://doi.org/10.3389/fnmol.2018.00019.

[82] G. Ter-Avetisyan, F.G. Rathjen, H. Schmidt, Bifurcation of Axons from Cranial Sensory Neurons Is Disabled in the Absence of Npr2-Induced cGMP Signaling, The Journal of Neuroscience. 34 (2014) 737–747. https://doi.org/10.1523/JNEUROSCI.4183-13.2014.

[83] G. Ter-Avetisyan, A. Dumoulin, A. Herrel, H. Schmidt, J. Strump, S. Afzal, F.G. Rathjen, Loss of Axon Bifurcation in Mesencephalic Trigeminal Neurons Impairs the Maximal Biting Force in Npr2-Deficient Mice, Front Cell Neurosci. 12 (2018). https://doi.org/10.3389/fncel.2018.00153.

[84] H. Schmidt, D.M. Dickey, A. Dumoulin, M. Octave, J.W. Robinson, R. Kühn, R. Feil, L.R. Potter, F.G. Rathjen, Regulation of the Natriuretic Peptide Receptor 2 (Npr2) by Phosphorylation of Juxtamembrane Serine and Threonine Residues Is Essential for Bifurcation of Sensory Axons, The Journal of Neuroscience. 38 (2018) 9768–9780. https://doi.org/10.1523/JNEUROSCI.0495-18.2018.

[85] L.C. Shuhaibar, J.R. Egbert, A.B. Edmund, T.F. Uliasz, D.M. Dickey, S.-P. Yee, L.R. Potter, L.A. Jaffe, Dephosphorylation of juxtamembrane serines and threonines of the NPR2 guanylyl cyclase is required for rapid resumption of oocyte meiosis in response to luteinizing hormone, Dev Biol. 409 (2016) 194–201. https://doi.org/10.1016/j.ydbio.2015.10.025.

[86] C. Xia, M. Nguyen, A.K. Garrison, Z. Zhao, Z. Wang, C. Sutherland, L. Ma, CNP/cGMP signaling regulates axon branching and growth by modulating microtubule polymerization, Dev Neurobiol. 73 (2013) 673–687. https://doi.org/10.1002/dneu.22078.

[87] I.J. Fidler, Biological behavior of malignant melanoma cells correlated to their survival in vivo., Cancer Res. 35 (1975) 218–24. http://www.ncbi.nlm.nih.gov/pubmed/1109790.

[88] Y. Gluzman, SV40-transformed simian cells support the replication of early SV40 mutants., Cell. 23 (1981) 175–82. https://doi.org/10.1016/0092-8674(81)90282-8.

[89] J.W. Wegener, H. Nawrath, W. Wolfsgruber, S. Kühbandner, C. Werner, F. Hofmann, R. Feil, cGMP-dependent protein kinase I mediates the negative inotropic effect of cGMP in the murine myocardium, Circ Res. 90 (2002) 18–20. https://doi.org/10.1161/hh0102.103222.

[90] S.K. Michael, H.K. Surks, Y. Wang, Y. Zhu, R. Blanton, M. Jamnongjit, M. Aronovitz, W. Baur, K. Ohtani, M.K. Wilkerson, A.D. Bonev, M.T. Nelson, R.H. Karas, M.E. Mendelsohn, High blood pressure arising from a defect in vascular function, Proceedings of the National Academy of Sciences. 105 (2008) 6702–6707. https://doi.org/10.1073/pnas.0802128105.

[91] V. Baena, C.M. Owen, T.F. Uliasz, K.M. Lowther, S.-P. Yee, M. Terasaki, J.R. Egbert, L.A. Jaffe, Cellular heterogeneity of the luteinizing hormone receptor and its significance for cyclic GMP signaling in mouse preovulatory follicles, Endocrinology. 161 (2020). https://doi.org/10.1210/endocr/bqaa074.

[92] D. Brancho, J.-J. Ventura, A. Jaeschke, B. Doran, R.A. Flavell, R.J. Davis, Role of MLK3 in the regulation of mitogen-activated protein kinase signaling cascades, Mol Cell Biol. 25 (2005) 3670–3681. https://doi.org/10.1128/MCB.25.9.3670-3681.2005.

[93] S. Weber, D. Bernhard, R. Lukowski, P. Weinmeister, R. Wörner, J.W. Wegener, N. Valtcheva, S. Feil, J. Schlossmann, F. Hofmann, R. Feil, Rescue of cGMP kinase I knockout mice by smooth muscle-specific expression of either isozyme, Circ Res. 101 (2007) 1096–1103. https://doi.org/10.1161/CIRCRESAHA.107.154351.

[94] G. Feng, R.H. Mellor, M. Bernstein, C. Keller-Peck, Q.T. Nguyen, M. Wallace, J.M. Nerbonne, J.W. Lichtman, J.R. Sanes, Imaging neuronal subsets in transgenic mice expressing multiple spectral variants of GFP, Neuron. 28 (2000) 41–51. https://doi.org/10.1016/S0896-6273(00)00084-2.

[95] W. Hauser, K.-P. Knobeloch, M. Eigenthaler, S. Gambaryan, V. Krenn, J. Geiger, M. Glazova, E. Rohde, I. Horak, U. Walter, M. Zimmer, Megakaryocyte hyperplasia and enhanced agonist-induced platelet activation in vasodilator-stimulated phosphoprotein knockout mice, Proceedings of the National Academy of Sciences. 96 (1999) 8120–8125. https://doi.org/10.1073/pnas.96.14.8120.

[96] H. Schmidt, F.G. Rathjen, DiI-labeling of DRG neurons to study axonal branching in a whole mount preparation of mouse embryonic spinal cord, Journal of Visualized Experiments. (2011) e3667. https://doi.org/10.3791/3667.

[97] M. Schmitt, T. Sinnberg, N.C. Nalpas, A. Maass, B. Schittek, B. Macek, Quantitative proteomics links the intermediate filament nestin to resistance to targeted BRAF inhibition in melanoma cells, Molecular & Cellular Proteomics. 18 (2019) 1096–1109. https://doi.org/10.1074/mcp.RA119.001302.

[98] J.-L. Hsu, S.-H. Chen, Stable isotope dimethyl labelling for quantitative proteomics and beyond, Philosophical Transactions of the Royal Society A: Mathematical, Physical and Engineering Sciences. 374 (2016) 20150364. https://doi.org/10.1098/rsta.2015.0364.

[99] P.J. Boersema, R. Raijmakers, S. Lemeer, S. Mohammed, A.J.R. Heck, Multiplex peptide stable isotope dimethyl labeling for quantitative proteomics, Nat Protoc. 4 (2009) 484–494. https://doi.org/10.1038/nprot.2009.21.

[100] P. Spät, B. Maček, K. Forchhammer, Phosphoproteome of the cyanobacterium Synechocystis sp. PCC 6803 and its dynamics during nitrogen starvation, Front Microbiol. 6 (2015) 248. https://doi.org/10.3389/fmicb.2015.00248.

[101] J. Cox, M. Mann, MaxQuant enables high peptide identification rates, individualized p.p.b.-range mass accuracies and proteome-wide protein quantification., Nat Biotechnol. 26 (2008) 1367–72. https://doi.org/10.1038/nbt.1511.

[102] UniProt Consortium, UniProt: the universal protein knowledgebase in 2023., Nucleic Acids Res. 51 (2023) D523–D531. https://doi.org/10.1093/nar/gkac1052.

[103] J.J. Allen, M. Li, C.S. Brinkworth, J.L. Paulson, D. Wang, A. Hübner, W.-H. Chou, R.J. Davis, A.L. Burlingame, R.O. Messing, C.D. Katayama, S.M. Hedrick, K.M. Shokat, A semisynthetic epitope for kinase substrates, Nat Methods. 4 (2007) 511–516. https://doi.org/10.1038/nmeth1048.

[104] S.M. Carlson, F.M. White, Labeling and identification of direct kinase substrates, Sci Signal. 5 (2012) 1–16. https://doi.org/10.1126/scisignal.2002568.

[105] K. Shokat, M. Velleca, Novel chemical genetic approaches to the discovery of signal transduction inhibitors, Drug Discov Today. 7 (2002) 872–879. https://doi.org/10.1016/S1359-6446(02)02391-7.

[106] C. Ruschil, G. Gabernet, C.L. Kemmerer, M.A. Jarboui, F. Klose, S. Poli, U. Ziemann, S. Nahnsen, M.C. Kowarik, Cladribine treatment specifically affects peripheral blood memory B cell clones and clonal expansion in multiple sclerosis patients, Front Immunol. 14 (2023). https://doi.org/10.3389/fimmu.2023.1133967.

[107] T.A.S. Deuel, J.S. Liu, J.C. Corbo, S.-Y. Yoo, L.B. Rorke-Adams, C.A. Walsh, Genetic interactions between doublecortin and doublecortin-like kinase in neuronal migration and axon outgrowth, Neuron. 49 (2006) 41–53. https://doi.org/10.1016/j.neuron.2005.10.038.

[108] Y. Liu, H. Nie, C. Liu, X. Zhai, Q. Sang, Y. Wang, D. Shi, L. Wang, Z. Xu, Angulin proteins ILDR1 and ILDR2 regulate alternative pre-mRNA splicing through binding to splicing factors TRA2A, TRA2B, or SRSF1, Sci Rep. 7 (2017) 7466. https://doi.org/10.1038/s41598-017-07530-z.

[109] E.J. Tran, S.R. Wente, Dynamic nuclear pore complexes: life on the edge, Cell. 125 (2006) 1041–1053. https://doi.org/10.1016/j.cell.2006.05.027.

[110] Z. Zhao, Y. Wu, J. Zhou, F. Chen, A. Yang, D.W. Essex, The transmembrane protein disulfide isomerase TMX1 negatively regulates platelet responses, Blood. 133 (2019) 246–251. https://doi.org/10.1182/blood-2018-04-844480.

[111] M.J. Nemeth, M.R. Kirby, D.M. Bodine, Hmgb3 regulates the balance between hematopoietic stem cell self-renewal and differentiation, Proceedings of the National Academy of Sciences. 103 (2006) 13783–13788. https://doi.org/10.1073/pnas.0604006103.

[112] N. Kang-Decker, G.T. Mantchev, S.C. Juneja, M.A. McNiven, J.M.A. van Deursen, Lack of acrosome formation in Hrb-deficient mice, Science (1979). 294 (2001) 1531–1533. https://doi.org/10.1126/science.1063665.

[113] L. Cui, J. Zheng, Q. Zhao, J.-R. Chen, H. Liu, G. Peng, Y. Wu, C. Chen, Q. He, H. Shi, S. Yin, R.A. Friedman, Y. Chen, M.-X. Guan, Mutations of MAP1B encoding a microtubule-associated phosphoprotein cause sensorineural hearing loss, JCI Insight. 5 (2020). https://doi.org/10.1172/jci.insight.136046.

[114] C. Debonneville, S.Y. Flores, E. Kamynina, P.J. Plant, C. Tauxe, M.A. Thomas, C. Münster, A. Chraïbi, J.H. Pratt, J.D. Horisberger, D. Pearce, J. Loffing, O. Staub, Phosphorylation of Nedd4-2 by Sgk1 regulates epithelial Na(+) channel cell surface expression., EMBO J. 20 (2001) 7052–9. https://doi.org/10.1093/emboj/20.24.7052.

[115] Y. Kwon, Y.W. Jeon, M. Kwon, Y. Cho, D. Park, J.E. Shin, βPix-d promotes tubulin acetylation and neurite outgrowth through a PAK/Stathmin1 signaling pathway, PLoS One. 15 (2020) e0230814. https://doi.org/10.1371/journal.pone.0230814.

[116] E. Chevet, J. Smirle, P.H. Cameron, D.Y. Thomas, J.J.M. Bergeron, Calnexin phosphorylation: Linking cytoplasmic signalling to endoplasmic reticulum lumenal functions, Semin Cell Dev Biol. 21 (2010) 486–490. https://doi.org/10.1016/j.semcdb.2009.12.005.

[117] S. Ferrari, H.R. Bandi, J. Hofsteenge, B.M. Bussian, G. Thomas, Mitogen-activated 70K S6 kinase. Identification of in vitro 40 S ribosomal S6 phosphorylation sites., Journal of Biological Chemistry. 266 (1991) 22770–22775. https://doi.org/10.1016/S0021-9258(18)54634-2.

[118] Y.-C. Lin, Y.-H. Lu, Y.-C. Lee, C.-S. Hung, J.-C. Lin, Altered expressions and splicing profiles of Acin1 transcripts differentially modulate brown adipogenesis through an alternative splicing mechanism, Biochimica et Biophysica Acta (BBA) - Gene Regulatory Mechanisms. 1863 (2020) 194601. https://doi.org/10.1016/j.bbagrm.2020.194601.

[119] F.D. Sigoillot, D.H. Kotsis, E.M. Masko, M. Bame, D.R. Evans, H.I.G. Evans, Protein kinase C modulates the up-regulation of the pyrimidine biosynthetic complex, CAD, by MAP kinase., Front Biosci. 12 (2007) 3892–8. https://doi.org/10.2741/2358.

[120] E.-M. Hur, Saijilafu, B.D. Lee, S.-J. Kim, W.-L. Xu, F.-Q. Zhou, GSK3 controls axon growth via CLASP-mediated regulation of growth cone microtubules, Genes Dev. 25 (2011) 1968–1981. https://doi.org/10.1101/gad.17015911.

[121] F. Nakamura, K. Kumeta, T. Hida, T. Isono, Y. Nakayama, E. Kuramata-Matsuoka, N. Yamashita, Y. Uchida, K. Ogura, K. Gengyo-Ando, S. Mitani, T. Ogino, Y. Goshima, Amino- and carboxyl-terminal domains of Filamin-A interact with CRMP1 to mediate Sema3A signalling, Nat Commun. 5 (2014) 5325. https://doi.org/10.1038/ncomms6325.

[122] C. Lebrand, E.W. Dent, G.A. Strasser, L.M. Lanier, M. Krause, T.M. Svitkina, G.G. Borisy, F.B. Gertler, Critical role of Ena/VASP proteins for filopodia formation in neurons and in function downstream of Netrin-1, Neuron. 42 (2004) 37–49. https://doi.org/10.1016/S0896-6273(04)00108-4.

[123] T.D. Calamaras, R.A. Baumgartner, M.J. Aronovitz, A.L. McLaughlin, K. Tam, D.A. Richards, C.W. Cooper, N. Li, W.E. Baur, X. Qiao, G.-R. Wang, R.J. Davis, N.K. Kapur, R.H. Karas, R.M. Blanton, Mixed lineage kinase-3 prevents cardiac dysfunction and structural remodeling with pressure overload, American Journal of Physiology-Heart and Circulatory Physiology. 316 (2019) H145–H159. https://doi.org/10.1152/ajpheart.00029.2018.

[124] A.S. Menzies, A. Aszodi, S.E. Williams, A. Pfeifer, A.M. Wehman, K.L. Goh, C.A. Mason, R. Fassler, F.B. Gertler, Mena and Vasodilator-Stimulated Phosphoprotein Are Required for Multiple Actin-Dependent Processes That Shape the Vertebrate Nervous System, The Journal of Neuroscience. 24 (2004) 8029–8038. https://doi.org/10.1523/JNEUROSCI.1057-04.2004.

[125] A. V. Kwiatkowski, D.A. Rubinson, E.W. Dent, J. Edward van Veen, J.D. Leslie, J. Zhang, L.M. Mebane, U. Philippar, E.M. Pinheiro, A.A. Burds, R.T. Bronson, S. Mori, R. Fässler, F.B. Gertler, Ena/VASP Is Required for Neuritogenesis in the Developing Cortex, Neuron. 56 (2007) 441–455. https://doi.org/10.1016/j.neuron.2007.09.008.

[126] X.-Y. Chen, X.-T. Gu, H. Saiyin, B. Wan, Y.-J. Zhang, J. Li, Y.-L. Wang, R. Gao, Y.-F. Wang, W.-P. Dong, S.M. Najjar, C.-Y. Zhang, H.-F. Ding, J.O. Liu, L. Yu, Brain-selective Kinase 2 (BRSK2) Phosphorylation on PCTAIRE1 Negatively Regulates Glucose-stimulated Insulin Secretion in Pancreatic β-Cells, Journal of Biological Chemistry. 287 (2012) 30368–30375. https://doi.org/10.1074/jbc.M112.375618.

[127] S. Garrett, W.A. Barton, R. Knights, P. Jin, D.O. Morgan, R.P. Fisher, Reciprocal Activation by Cyclin-Dependent Kinases 2 and 7 Is Directed by Substrate Specificity Determinants outside the T Loop, Mol Cell Biol. 21 (2001) 88–99. https://doi.org/10.1128/MCB.21.1.88-99.2001.

[128] Y. Gu, J. Rosenblatt, D.O. Morgan, Cell cycle regulation of CDK2 activity by phosphorylation of Thr160 and Tyr15., EMBO J. 11 (1992) 3995–4005. https://doi.org/10.1002/j.1460-2075.1992.tb05493.x.

[129] J.M. Lizcano, O. Göransson, R. Toth, M. Deak, N.A. Morrice, J. Boudeau, S.A. Hawley, L. Udd, T.P. Mäkelä, D.G. Hardie, D.R. Alessi, LKB1 is a master kinase that activates 13 kinases of the AMPK subfamily, including MARK/PAR-1, EMBO J. 23 (2004) 833–843. https://doi.org/10.1038/sj.emboj.7600110.

[130] M. Delhase, M. Hayakawa, Y. Chen, M. Karin, Positive and Negative Regulation of IκB Kinase Activity Through IKKβ Subunit Phosphorylation, Science (1979). 284 (1999) 309–313. https://doi.org/10.1126/science.284.5412.309.

[131] E. Butt, cGMP-Dependent Protein Kinase Modulators, in: H.H.H.W. Schmidt, F. Hofmann, J.-P. Stasch (Eds.), CGMP: Generators, Effectors and Therapeutic Implications, Springer Berlin Heidelberg, Berlin, Heidelberg, 2009: pp. 409–421. https://doi.org/10.1007/978-3-540-68964-5_17.

[132] E.L. Huttlin, M.P. Jedrychowski, J.E. Elias, T. Goswami, R. Rad, S.A. Beausoleil, J. Villén, W. Haas, M.E. Sowa, S.P. Gygi, A Tissue-Specific Atlas of Mouse Protein Phosphorylation and Expression, Cell. 143 (2010) 1174–1189. https://doi.org/10.1016/j.cell.2010.12.001.

[133] I. Dulubova, A. Horiuchi, G.L. Snyder, J.-A. Girault, A.J. Czernik, L. Shao, R. Ramabhadran, P. Greengard, A.C. Nairn, ARPP-16/ARPP-19: a highly conserved family of cAMP-regulated phosphoproteins, J Neurochem. 77 (2008) 229–238. https://doi.org/10.1046/j.1471-4159.2001.00191.x.

[134] H.-S. Lee, Y.A. Komarova, E.S. Nadezhdina, R. Anjum, J.G. Peloquin, J.M. Schober, O. Danciu, J. van Haren, N. Galjart, S.P. Gygi, A. Akhmanova, G.G. Borisy, Phosphorylation Controls Autoinhibition of Cytoplasmic Linker Protein-170, Mol Biol Cell. 21 (2010) 2661–2673. https://doi.org/10.1091/mbc.e09-12-1036.

[135] X. Wang, S. Bruderer, Z. Rafi, J. Xue, P.J. Milburn, A. Krämer, P.J. Robinson, Phosphorylation of splicing factor SF1 on Ser20 by cGMP-dependent protein kinase regulates spliceosome assembly., EMBO J. 18 (1999) 4549–59. https://doi.org/10.1093/emboj/18.16.4549.

[136] S. Maitra, C.-F. Chou, C.A. Luber, K.-Y. Lee, M. Mann, C.-Y. Chen, The AU-rich element mRNA decay-promoting activity of BRF1 is regulated by mitogen-activated protein kinase-activated protein kinase 2, RNA. 14 (2008) 950–959. https://doi.org/10.1261/rna.983708.

[137] Y. Sasaki, Local Translation in Growth Cones and Presynapses, Two Axonal Compartments for Local Neuronal Functions, Biomolecules. 10 (2020) 668. https://doi.org/10.3390/biom10050668.

[138] R.L. Agulto, M.M. Rogers, T.C. Tan, A. Ramkumar, A.M. Downing, H. Bodin, J. Castro, D.W. Nowakowski, K.M. Ori-McKenney, Autoregulatory control of microtubule binding in doublecortin-like kinase 1, Elife. 10 (2021). https://doi.org/10.7554/eLife.60126.

[139] S.-W. Jang, S. Yang, A. Ehlén, S. Dong, H. Khoury, J. Chen, J.L. Persson, K. Ye, Serine/Arginine Protein–Specific Kinase 2 Promotes Leukemia Cell Proliferation by Phosphorylating Acinus and Regulating Cyclin A1, Cancer Res. 68 (2008) 4559–4570. https://doi.org/10.1158/0008-5472.CAN-08-0021.

[140] C. Schwerk, J. Prasad, K. Degenhardt, H. Erdjument-Bromage, E. White, P. Tempst, V.J. Kidd, J.L. Manley, J.M. Lahti, D. Reinberg, ASAP, a Novel Protein Complex Involved in RNA Processing and Apoptosis, Mol Cell Biol. 23 (2003) 2981–2990. https://doi.org/10.1128/MCB.23.8.2981-2990.2003.

[141] M. Fujiwara, L. Tian, P.T. Le, V.E. DeMambro, K.A. Becker, C.J. Rosen, A.R. Guntur, The mitophagy receptor Bcl-2–like protein 13 stimulates adipogenesis by regulating mitochondrial oxidative phosphorylation and apoptosis in mice, Journal of Biological Chemistry. 294 (2019) 12683–12694. https://doi.org/10.1074/jbc.RA119.008630.

[142] D.R. Evans, H.I. Guy, Mammalian Pyrimidine Biosynthesis: Fresh Insights into an Ancient Pathway, Journal of Biological Chemistry. 279 (2004) 33035–33038. https://doi.org/10.1074/jbc.R400007200.

[143] H.N. Wong, M.A. Ward, A.W. Bell, E. Chevet, S. Bains, W.P. Blackstock, R. Solari, D.Y. Thomas, J.J.M. Bergeron, Conserved in VivoPhosphorylation of Calnexin at Casein Kinase II Sites as Well as a Protein Kinase C/Proline-directed Kinase Site, Journal of Biological Chemistry. 273 (1998) 17227–17235. https://doi.org/10.1074/jbc.273.27.17227.

[144] T. Paskevicius, R.A. Farraj, M. Michalak, L.B. Agellon, Calnexin, More Than Just a Molecular Chaperone, Cells. 12 (2023) 403. https://doi.org/10.3390/cells12030403.

[145] T.-C. Chen, S.-A. Lee, T.-M. Hong, J.-Y. Shih, J.-M. Lai, H.-Y. Chiou, S.-C. Yang, C.-H. Chan, C.-Y. Kao, P.-C. Yang, C.-Y.F. Huang, From Midbody Protein−Protein Interaction Network Construction to Novel Regulators in Cytokinesis, J Proteome Res. 8 (2009) 4943–4953. https://doi.org/10.1021/pr900325f.

[146] D. Chhetri, S. Vengadassalapathy, S. Venkadassalapathy, V. Balachandran, V.R. Umapathy, V.P. Veeraraghavan, S. Jayaraman, S. Patil, A. Iyaswamy, K. Palaniyandi, D. Gnanasampanthapandian, Pleiotropic effects of DCLK1 in cancer and cancer stem cells, Front Mol Biosci. 9 (2022). https://doi.org/10.3389/fmolb.2022.965730.

[147] J.M. Weimer, E.S. Anton, Doubling Up on Microtubule Stabilizers: Synergistic Functions of Doublecortin-like Kinase and Doublecortin in the Developing Cerebral Cortex, Neuron. 49 (2006) 3–4. https://doi.org/10.1016/j.neuron.2005.12.016.

[148] J.H. Youn, J.-S. Shin, Nucleocytoplasmic Shuttling of HMGB1 Is Regulated by Phosphorylation That Redirects It toward Secretion, The Journal of Immunology. 177 (2006) 7889–7897. https://doi.org/10.4049/jimmunol.177.11.7889.

[149] X. Zhao, J.I.-T. Heng, D. Guardavaccaro, R. Jiang, M. Pagano, F. Guillemot, A. Iavarone, A. Lasorella, The HECT-domain ubiquitin ligase Huwe1 controls neural differentiation and proliferation by destabilizing the N-Myc oncoprotein, Nat Cell Biol. 10 (2008) 643–653. https://doi.org/10.1038/ncb1727.

[150] N. Trivedi, P. Marsh, R.G. Goold, A. Wood-Kaczmar, P.R. Gordon-Weeks, Glycogen synthase kinase-3β phosphorylation of MAP1B at Ser1260 and Thr1265 is spatially restricted to growing axons, J Cell Sci. 118 (2005) 993–1005. https://doi.org/10.1242/jcs.01697.

[151] D. Villarroel-Campos, C. Gonzalez-Billault, The MAP1B case: An old MAP that is new again, Dev Neurobiol. 74 (2014) 953–971. https://doi.org/10.1002/dneu.22178.

[152] S. Halpain, L. Dehmelt, The MAP1 family of microtubule-associated proteins, Genome Biol. 7 (2006) 224. https://doi.org/10.1186/gb-2006-7-6-224.

[153] M. Morris, G.M. Knudsen, S. Maeda, J.C. Trinidad, A. Ioanoviciu, A.L. Burlingame, L. Mucke, Tau post-translational modifications in wild-type and human amyloid precursor protein transgenic mice, Nat Neurosci. 18 (2015) 1183–1189. https://doi.org/10.1038/nn.4067.

[154] K. Tani, S. Sato, T. Sukezane, H. Kojima, H. Hirose, H. Hanafusa, T. Shishido, Abl Interactor 1 Promotes Tyrosine 296 Phosphorylation of Mammalian Enabled (Mena) by c-Abl Kinase, Journal of Biological Chemistry. 278 (2003) 21685–21692. https://doi.org/10.1074/jbc.M301447200.

[155] S. Yun, S.-S. Cha, J.H. Kim, DJ-1 promotes cell migration by interacting with Mena, the mammalian homolog of Drosophila enabled, Adv Biol Regul. 88 (2023) 100943. https://doi.org/10.1016/j.jbior.2022.100943.

[156] L. Ulrich, C. Gliem, D. Groneberg, T. Frömel, K. Schuh, I. Fleming, P.M. Benz, Mena and VASP are required for vascular smooth muscle relaxation, BioRxiv. (2023). https://doi.org/10.1101/2023.04.21.537622.

[157] H. Li, Y. Huo, X. He, L. Yao, H. Zhang, Y. Cui, H. Xiao, W. Xie, D. Zhang, Y. Wang, S. Zhang, H. Tu, Y. Cheng, Y. Guo, X. Cao, Y. Zhu, T. Jiang, X. Guo, Y. Qin, J. Sha, A male germ-cell-specific ribosome controls male fertility, Nature. 612 (2022) 725–731. https://doi.org/10.1038/s41586-022-05508-0.

[158] H.R. Bandi, S. Ferrari, J. Krieg, H.E. Meyer, G. Thomas, Identification of 40 S ribosomal protein S6 phosphorylation sites in Swiss mouse 3T3 fibroblasts stimulated with serum., Journal of Biological Chemistry. 268 (1993) 4530–4533. https://doi.org/10.1016/S0021-9258(18)53642-5.

[159] P.P. Roux, D. Shahbazian, H. Vu, M.K. Holz, M.S. Cohen, J. Taunton, N. Sonenberg, J. Blenis, RAS/ERK Signaling Promotes Site-specific Ribosomal Protein S6 Phosphorylation via RSK and Stimulates Cap-dependent Translation, Journal of Biological Chemistry. 282 (2007) 14056–14064. https://doi.org/10.1074/jbc.M700906200.

[160] L. Beretta, T. Dobránsky, A. Sobel, Multiple phosphorylation of stathmin. Identification of four sites phosphorylated in intact cells and in vitro by cyclic AMP-dependent protein kinase and p34cdc2., Journal of Biological Chemistry. 268 (1993) 20076–20084. https://doi.org/10.1016/S0021-9258(20)80696-6.

[161] Y. Matsuo, Introducing Thioredoxin-Related Transmembrane Proteins: Emerging Roles of Human TMX and Clinical Implications, Antioxid Redox Signal. 36 (2022) 984–1000. https://doi.org/10.1089/ars.2021.0187.

[162] T. Vomastek, M.P. Iwanicki, W.R. Burack, D. Tiwari, D. Kumar, J.T. Parsons, M.J. Weber, V.K. Nandicoori, Extracellular Signal-Regulated Kinase 2 (ERK2) Phosphorylation Sites and Docking Domain on the Nuclear Pore Complex Protein Tpr Cooperatively Regulate ERK2-Tpr Interaction, Mol Cell Biol. 28 (2008) 6954–6966. https://doi.org/10.1128/MCB.00925-08.

[163] R. Tacke, M. Tohyama, S. Ogawa, J.L. Manley, Human Tra2 Proteins Are Sequence-Specific Activators of Pre-mRNA Splicing, Cell. 93 (1998) 139–148. https://doi.org/10.1016/S0092-8674(00)81153-8.

[164] M. Halbrugge, U. Walter, Purification of a vasodilator-regulated phosphoprotein from human platelets, Eur J Biochem. 185 (1989) 41–50. https://doi.org/10.1111/j.1432-1033.1989.tb15079.x.

[165] S. Gambaryan, W. Hauser, A. Kobsar, M. Glazova, U. Walter, Distribution, cellular localization, and postnatal development of VASP and Mena expression in mouse tissues, Histochem Cell Biol. 116 (2001) 535–543. https://doi.org/10.1007/s00418-001-0353-3.

[166] A. Stonkute, cGMP signalling via CNP-NPR2-cGKI, and its role in axonal branching during embryonic development, Dissertation, Freie Universität Berlin, 2010. https://doi.org/10.17169/refubium-15458.

[167] R.E. McConnell, J. Edward van Veen, M. Vidaki, A. V. Kwiatkowski, A.S. Meyer, F.B. Gertler, A requirement for filopodia extension toward Slit during Robo-mediated axon repulsion, Journal of Cell Biology. 213 (2016) 261–274. https://doi.org/10.1083/jcb.201509062.

[168] T.D. Calamaras, S. Pande, R.A.U. Baumgartner, S.K. Kim, J.C. McCarthy, G.L. Martin, K. Tam, A.L. McLaughlin, G. Wang, M.J. Aronovitz, W. Lin, J.I. Aguirre, P. Baca, P. Liu, D.A. Richards, R.J. Davis, R.H. Karas, I.Z. Jaffe, R.M. Blanton, MLK3 mediates impact of PKG1α on cardiac function and controls blood pressure through separate mechanisms, JCI Insight. 6 (2021). https://doi.org/10.1172/jci.insight.149075.

[169] G. Ter-Avetisyan, The receptor guanylyl cyclase Npr2 regulates the bifurcation of cranial sensory axons, Dissertation, Freie Universität Berlin, 2013. https://doi.org/10.17169/refubium-14859.

[170] M. Russwurm, F. Mullershausen, A. Friebe, R. Jäger, C. Russwurm, D. Koesling, Design of fluorescence resonance energy transfer (FRET)-based cGMP indicators: a systematic approach, Biochemical Journal. 407 (2007) 69–77. https://doi.org/10.1042/BJ20070348.

[171] A. Dumoulin, E.T. Stoeckli, Looking for Guidance – Models and Methods to Study Axonal Navigation, Neuroscience. 508 (2023) 30–39. https://doi.org/10.1016/j.neuroscience.2022.08.005.

[172] P.M. Benz, T. Frömel, H. Laban, J. Zink, L. Ulrich, D. Groneberg, R.A. Boon, P. Poley, T. Renne, C. de Wit, I. Fleming, Cardiovascular Functions of Ena/VASP Proteins: Past, Present and Beyond, Cells. 12 (2023) 1740. https://doi.org/10.3390/cells12131740.

[173] M. Reinhard, T. Jarchau, U. Walter, Actin-based motility: stop and go with Ena/VASP proteins, Trends Biochem Sci. 26 (2001) 243–249. https://doi.org/10.1016/S0968-0004(00)01785-0.

[174] R. Thoonen, S. Giovanni, S. Govindan, D.I. Lee, G.-R. Wang, T.D. Calamaras, E. Takimoto, D.A. Kass, S. Sadayappan, R.M. Blanton, Molecular Screen Identifies Cardiac Myosin–Binding Protein-C as a Protein Kinase G-Iα Substrate, Circ Heart Fail. 8 (2015) 1115–1122. https://doi.org/10.1161/CIRCHEARTFAILURE.115.002308.

[175] J. Chen, J.D. Roberts, cGMP-dependent protein kinase I gamma encodes a nuclear localization signal that regulates nuclear compartmentation and function, Cell Signal. 26 (2014) 2633–2644. https://doi.org/10.1016/j.cellsig.2014.08.004.

ACKNOWLEDGEMENTS

First and foremost, my gratitude goes to PD Dr. Hannes Schmidt for giving me the opportunity to pursue a doctoral title under his mentorship and supervising me during my time as doctoral student. Your guidance has been truly integral to the success of my work. Thank you for all the discussions and feedback throughout the last four years.

Thank you as well to Prof. Robert Feil for being my second reviewer and supervisor. Thank you for investing your time in the improvement of all doctoral students in your lab and giving us helpful feedback.

I would like to extend my gratitude to Assoc. Prof. Robert Blanton not only for his co-mentorship during the last years, but also for welcoming me to his lab at Tufts Medical Center for a three-month research stay. It was a pleasure to work with you and your team. Special shout-outs go to Greg and Suchita as well, you guys made it a joy to come to lab, even when we had to fight our way through the Boston snow in winter.

I am deeply grateful to PD Dr. Andrea Wizenmann for agreeing to be the third reviewer for this thesis. Likewise, I would like to extend my thanks to Prof. Peter Ruth for being on my defense committee.

A big thank you goes to all past and present members of the Feil lab who have been integral for my success as doctoral candidate by teaching, helping, discussing, and giving feedback. Thank you to Michael Krämer for lots of instructions and tips to let me land on my feet when I first started out. Thank you to Barbara Birk for always lending a helping hand with all sorts of things. Thanks to you and everyone along the way for making the day-to-day lab work so much fun.

Being a member of the GRK 2381 "cGMP: From Bedside to Bench" made this journey truly unique and rewarding. Thank you to everyone involved.

During the last four years I have met some people who have truly changed my life and who I will always be grateful to. Dr. Maria Teresa Kristina Zaldivia, in you I have found a kindred spirit that will accompany me on my life's journey far beyond our time in Tübingen. Video call soon? Mariagiovanna Barresi and Malte Roeßing, without you two I would not have made it this far. It was a true honor to share these past years with you learning, discussing, commiserating, growing, at times failing but, in the end, succeeding. Sharing this experience with you has made it a pleasure to come to the office every morning (or noon, depending on who you ask).

Last but not least, I want to express my deepest appreciation to my friends and family. To my parents Elisabeth and Frank for their unconditional love and for always encouraging me to do my best and not lose faith. To my brother Sebastian for having my back no matter what and being a calm presence of reassurance in my life. To my partner Morgan, who had to deal with lots of my antics these past months, for being a place of peace and joy to me. Thank you also to my dad, brother, and Morgan for proofreading the draft of this thesis.

DECLARATIONS OF CONTRIBUTIONS

This work was written entirely by the author. The use of artificial intelligence (e.g., ChatGPT) was limited to proofreading some paragraphs of the thesis.

The experiments detailed here were planned, executed, and analyzed by the author with the following exceptions:

- Pre-measure processing (mixing, reduction, alkylation, digestion, purification) of SILAC samples, as well as their phosphopeptide enrichment and MS measurement and analysis were carried out by Prof. Boris Maček and Dr. Ana Velic (Proteome Center Tübingen, University of Tübingen).
- Pre-measure processing (reduction, alkylation, digestion, acidification, desalting, on-column-labeling, mixing) of SIDL samples, as well as their phosphopeptide enrichment and MS measurement and analysis were carried out by Prof. Boris Maček and Dr. Ana Velic (Proteome Center Tübingen, University of Tübingen).
- Pre-measure processing (on-bead-digest, alkylation, desalting) of GC-B Co-IP samples as well as MS measurement and analysis was carried out by Dr. Karsten Boldt and Katrin Junger (CFMB, University of Tübingen).

PUBLICATIONS BY THE AUTHOR

The presented work has contributed to the following publications:

A. Balmes*, A. Böttcher*, A. Botezatu, E. Streit Morsch, S. Peters, A. Velić, B. Maček, F. G. Rathjen, R. M. Blanton, R. Feil, H. Schmidt, T. Schäffer CNP-induced cGMP signaling in embryonic DRG neurons modulates growth cone Ca2+ and stiffness. *In preparation* *Authors contributed equally.

H. Schmidt, A. Böttcher, T. Gross, A. Schmidtko cGMP signalling in dorsal root ganglia and the spinal cord: Variuos functions in development and adulthood. (2021) British journal of pharmacology. DOI: 10.1111/bph.15514

In addition, the author has contributed to the following unrelated publications:

M. Amoroso, A. Böttcher, C. A. Lowry, D. Langgartner, S. O. Reber Subcutaneous Mycobacterium vaccae promotes resilience in a mouse model of chronic psychosocial stress when administered prior to or during psychosocial stress. (2020) Brain Behavior and Immunity. DOI: https://doi.org/10.1016/j.bbi.2019.12.018

The author has also presented her work on the following conferences:

A. Böttcher, R. M. Blanton, B. Macek, A. Velic, R. Feil, H. Schmidt Identification of novel cGKIα substrates mediating axon bifurcation in embryonic DRG neurons. (2022) 10th International Conference on cGMP 2022. DOI: 10.1186/s12967-022-03800-1

A. Böttcher, B. Macek, A. Velic, R. M. Blanton, R. Feil, H. Schmidt Identification of cGKI substrates mediating sensory axon bifurcation. (2021) GRK 2381 conference CanCaN 2021. Link: event.fourwaves.com/cancan